UNIVERSITY OF MINNESOTA

ST. ANTHONY FALLS HYDRAULIC LABORATORY

Project Report No. 350

EXPERIMENTAL DEVELOPMENT OF A NOVEL AERATION DEVICE

by

V.Ramanathan and Roger E. A. Arndt

Prepared for

LEGISLATIVE COMMISSION ON MINNESOTA RESOURCES
St. Paul, Minnesota

and

METROPOLITAN WASTE CONTROL COMMISSION
St. Paul, Minnesota

April 1994
Minneapolis, Minnesota

UNIVERSITY OF MINNESOTA
St. Anthony Falls Hydraulic Laboratory

Project Report No. 350

EXPERIMENTAL DEVELOPMENT OF A NOVEL AERATION DEVICE

by

V.Ramanathan and Roger E. A. Arndt

Prepared for

LEGISLATIVE COMMISSION ON MINNESOTA RESOURCES
St. Paul, Minnesota

and

METROPOLITAN WASTE CONTROL COMMISSION
St. Paul, Minnesota

April 1994

Abstract

Theoretical and experimental studies were carried out with the aim of developing an improved aeration device. Many of the aeration devices currently in use contain fine pores, through which air is pumped to produce small bubbles in the diameter range of 2 to 3 mm in water, the objective being optimum performance in terms of mass transfer. Because of the very small pore size, these devices are often subject to clogging, consequent deterioration of efficiency and escalation of power requirements. The development of the new aeration device, named the SAF diffuser, is an attempt to generate bubbles of the optimum size range using relatively larger orifices so that the diffuser clogging and the energy requirements can be reduced.

The SAF Diffuser comprises a vertical draft tube immersed in the water body to be aerated. A buoyancy induced flow is created within the tube by injecting air through 0.5 mm diameter peripheral orifices located near the inlet end. The induced flow exerts a drag force on the bubbles that are being formed at the peripheral orifices. This drag force causes the bubble to detach from the orifice before it grows to the normal size attained in stagnant water. Utilizing this concept, hole sizes that are larger than (about 15 times) those used in conventional fine pore diffusers are possible. For a given air flowrate, the induced velocity and hence the bubble size depends upon the tube dimensions. This dependence provides a novel technique to control the bubble size.

Theoretical and experimental study of the air–water flow as well as the mass transfer characteristics of the device were undertaken. Simple methods of measuring the two phase flow parameters were developed. Through theoretical analysis and experimentation, non–dimensional correlations to predict the phase velocities within the device as well as the mass transfer characteristics of the device were developed. The studies showed that for medium depth applications, the device can operate with 10 to 20 percent higher aeration efficiencies than conventional designs. Even higher efficiencies are possible in the low depth applications typical in aquaculture.

Acknowledgement

This research work was funded partly by the Legislative Commission on Minnesota Resources and partly by the Metropolitan Waste Control Commission, St. Paul. The authors gratefully acknowledge their assistance.

The authors are also extremely thankful to Dr. Robert C. Polta and Mr. Michael G. Rieth of the Metropolitan Waste Control Commission, St. Paul, for their valuable suggestions and for providing the experimental tank without which such detailed studies would not have been possible

Table of Contents

Nomenclature

A	air–water interfacial area in the bubble column
A_c	air–water interfacial area in an elemental strip of the bubble column
A_{op}	cross sectional area of the tube inlet
A_p	cross sectional area of the tube
A_{pl}	air–water interfacial area in the plume
A_t	air–water interfacial area in the tube
B	buoyancy flux
C	concentration of oxygen in water
C_a	added mass coefficient
C_d	drag coefficient
C_s	saturation concentration of oxygen in water
C_{ss}	saturation concentration of oxygen in water corresponding to standard atmosphere
d_b	bubble diameter at the time of detachment from the orifice
d_{bc}	mean bubble diameter in an elemental strip of the bubble column
D_c	diameter of an elemental strip of the bubble column
d_o	orifice diameter
D_{op}	diameter of the tube inlet
D_{ow}	molecular diffusivity of oxygen in water
D_p	diameter of the tube
D_r	diameter ratio $= (D_p/D_{op})$
F_b	buoyancy force
F_d	drag force
F_i	inertia force
$F\sigma$	surface tension force
F_m	mass flux
F_{ra}	air flow Froude number $= (J_a/(L_e\ g)^{1/2})$
F_{rw}	water flow Froude number $= (V_w/(L_e\ g)^{1/2})$

F_s submergence Froude number = $(J_a/(H_s\ g)^{1/2})$

f friction factor for developing air–water bubbly flow

g gravitational acceleration

G_a Galileo number = (gH_s^3/ν_w^2)

H depth of water

H_r submergence ratio = (H_s/D_p)

H_s diffuser submergence

J_a superficial air velocity = (Q_a/A_p)

J_w superficial water velocity = (Q_w/A_p)

K overall loss term

K_b term representing the losses due to the lateral entry of air bubbles into the tube at the air inlet

k_c appropriate contraction loss coefficient at the bubble entrance region

K_e entrance loss term

K_{ex} expansion loss term

K_f friction loss term

K_l liquid film coefficient

K_la volumetric mass transfer coefficient

K_lA mass transfer coefficient

K_s secondary loss term

L_e effective tube length = $(L_2 + (L_1(A_{op}/A_p))$

L_r length ratio = (L_e/D_p)

L_1 inlet tube length in the entrance region above the air inlet

L_2 tube length

ℓ size of largest eddies

N number of bubbles

N_m number of modules

Q_a air flowrate corresponding to the pressure at the tube centre

Q_{ao} air flowrate through one orifice

Q_{as} air flowrate corresponding to standard atmosphere

Q_w induced water flowrate

R_{ew} Reynolds number based on superficial water velocity = (J_wD_p/ν_w)

S_{tm} modified Stanton number = $(K_lA)/(J_aD_p^2)$

s	vertical distance of bubble centre from the orifice
t_r	formation time of bubble or bubble residence time
u	velocity of large scale eddies
U_c	mean velocity in an elemental strip of the bubble column
V_a	mean air velocity in the tube = (J_a/α)
V_{ao}	air velocity through one orifice
V_o	water velocity in the tube inlet upstream of the orifices (orifice water velocity)
V_r	relative air velocity (slip velocity)
V_w	mean water velocity in the tube = $(J_w/(1-\alpha))$
$\forall$	volume of water
$\forall_b$	volume of bubble
$\forall_c$	volume of air in an elemental strip of the bubble column
w	average velocity of bubble during formation
α	mean void fraction of air in the tube
α_c	mean void fraction of air in an elemental strip of the bubble column
ν_w	kinematic viscosity of water
ρ_a	density of air
ρ_c	density of the air–water mixture in an elemental strip of the bubble column
ρ_m	density of air–water mixture in the tube
ρ_w	density of water
σ	surface tension
τ	characteristic time constant

LIST OF FIGURES

List of Tables

Chapter 1
Introduction

This thesis deals with the research undertaken for the development of a new aeration device named the SAF diffuser. As part of this research, the concept of the new aeration device was conceived, a simplified theoretical analysis and extensive experimental studies in respect of the hydrodynamics of the flow through the device and the mass transfer characteristics of the device were undertaken and experimental correlations to predict the performance characteristics of the device were developed.

The primary application of the new device is for diffused aeration which forms a major energy consuming component in several water quality improvement processes pertaining to aquaculture, wastewater treatment and lake water quality enhancement. The purpose of aeration is to improve the dissolved oxygen content of water. Low dissolved oxygen concentration is a major factor limiting the production of fish and other species in intensive aquaculture operations. Aeration is currently the most effective means of dissolved oxygen enhancement and represents the second largest component cost–wise next to feed cost, in aquaculture. Likewise, wastewater treatment is another example where aeration forms a major energy consuming component. From 50 to 90 per cent of the power requirement of a treatment plant lies within the aeration system (1). A typical large wastewater facility like the Pig's Eye sewage treatment plant at St. Paul, Minnesota, requires at least five million dollars per year for electricity to operate aeration facilities. These examples illustrate the immense energy savings and benefits that can accrue from an improved aeration technology.

Diffused aeration is the process of injecting air under pressure below the liquid surface to form bubbles (see figure 1.1). As the bubbles rise, oxygen diffuses from the bubble surface into the liquid.

The devices producing the bubbles in diffused aeration systems are termed diffusers. For a given air flowrate, the size of the bubbles produced by the diffuser depends on the size and the number of the orifices/pores in the diffuser. In general, for a given air flowrate through the orifice, the smaller the orifice, the smaller the bubble size.

The aeration efficiency (mass of oxygen transferred per unit power input) of an aeration device depends on the bubble size, the bubble rise velocity, the mixing effected by the induced flow and the energy required to compress the air to form bubbles. Barnhart (2) has shown that for an air–water system, maximum oxygen transfer is obtained with bubble diameters

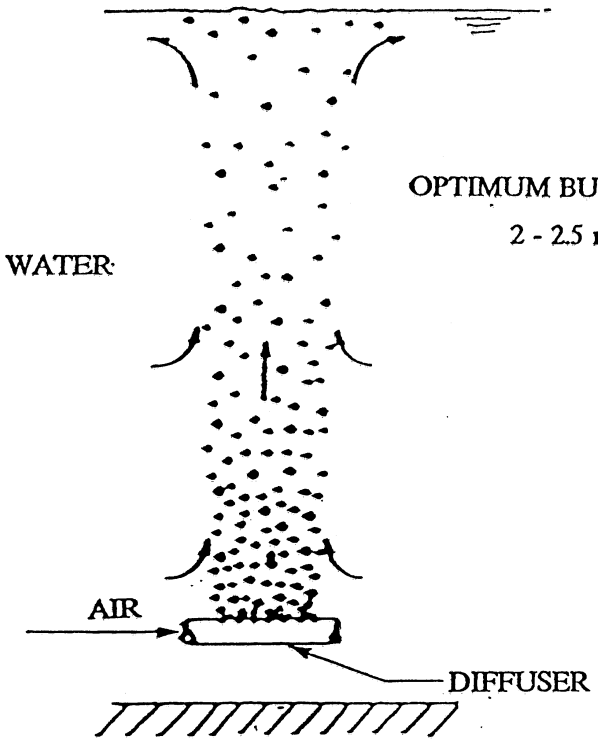

DIFFUSED AERATION

APPLICATIONS: WASTE WATER TREATMENT,
AQUACULTURE,
LAKE AERATION,
CHEMICAL PROCESSES, ETC.

Fig. 1.1 Diffused Aeration – Schematic

on the order of 2.2 mm. Production of bubbles of this size is usually achieved using diffusers having very small pore sizes. Such diffusers are termed "Fine Bubble Diffusers". The fine bubble diffusers which produce small air bubbles (2–3 mm diameter) in water have very small pore sizes (< 40 microns) (3). Because of the very small pore sizes involved, these devices are often subject to severe clogging and consequent deterioration of mass transfer efficiency and escalation of power requirements. One solution to this problem would be to produce small bubbles using larger orifices. With this objective in mind, the development of a new aeration device was undertaken. Before delving into the details of the new device, it is felt appropriate to provide a brief outline of the existing diffused aeration devices.

Diffused aeration devices:

Diffused aeration devices are classified as either fine or coarse bubble diffusers based on the size of the bubbles produced. The coarse bubble diffusers normally produce bubbles in the diameter range of 6–10 mm in clean water whereas the fine bubble diffusers produce bubbles in the diameter range of 2–5 mm in clean water (4). In most of these devices, the main parameter that governs the bubble size is the diameter of the orifice through which the air is injected, a smaller orifice being associated with a smaller bubble.

The diffusers that are commercially available are usually classified by the physical characteristics of the device as outlined below (5, 6):

i) Fine pore diffusers
ii) Nonporous diffusers
iii) Other devices such as jet aerators, aspiring aerators and U–tube aerators

These diffusers are briefly described below.

Fine pore diffusers:

These diffusers are made of ceramic, plastic or rubber material and are available in the form of plates, domes, discs and tubes. Basically the body of the diffuser comprises a network of interconnecting passage ways, a few microns in diameter, through which the compressed air flows. On account of the large number of pores, the air flowrate per pore would be very low. The low air flowrate and the very fine pore size combined result in relatively small bubbles. These devices have the highest aeration efficiencies compared to other devices under water depths of 3 to 8 meters. The air supplied should be clean and free of dust particles to prevent air side clogging of the diffuser. In addition, these devices are also subject to exterior fouling due to the formation of biological slimes or inorganic precipitants. Fouling has been found to considerably reduce the aeration efficiencies of these devices after some use on account of the increased pressure drops and larger bubble sizes resulting from the nonuniformity of air flow through the clogged diffuser.

Cases have been reported where the diffuser clogging has increased the head loss across the ceramic diffuser from 15 cm to 46 cm of water (5). In addition to the reduced aeration efficiency, clogging also increases maintenance costs.

Nonporous diffusers:

These diffusers are available in several types such as perforated piping, spargers, slotted tubes, perforated hoses and static tubes. These devices have much larger orifices (typically 3 mm to 13 mm dia). On account of the large orifice size, these devices produce large bubbles and hence have lower aeration efficiencies. However, they are less subject to clogging problems and thus have lower maintenance costs.

Other devices:

These include jet and U–tube aerators and aspiring devices. Jet aeration combines liquid pumping with air diffusion (5). A pumping system recirculates the liquid in the aeration basin ejecting it with compressed air through a nozzle assembly. U–tube aeration consists of a deep shaft that has central downcomer surrounded by an outer riser tube. Air is added to the influent water in the downcomer, the mixture travels to the bottom of the shaft and then back to the surface. Since the air–water mixture is subject to great depths, the high pressure produces very high oxygen transfer into the solution. The aspiring device comprises a hollow tube with an electric motor on one end and a propeller at the other. The pump draws air from the atmosphere and injects it under water at high velocity creating large scale turbulence and consequent diffusion of the air bubbles into the water.

Figure 1.2 shows a comparison of the aeration efficiencies of the porous and non–porous diffusers. Comparison of the other devices in a similar manner is not productive due to their site–specific aeration efficiencies.

Though the fine pore devices have the highest aeration efficiencies (when new) of all the devices in the water depth range of 3 to 8 meters, these devices have poor aeration efficiencies at low water depths. This is primarily due to the lowering of the contact time of the bubbles with water (on account of the low depth) and the pressure drop across the diffuser, which becomes a larger percent of the water depth.

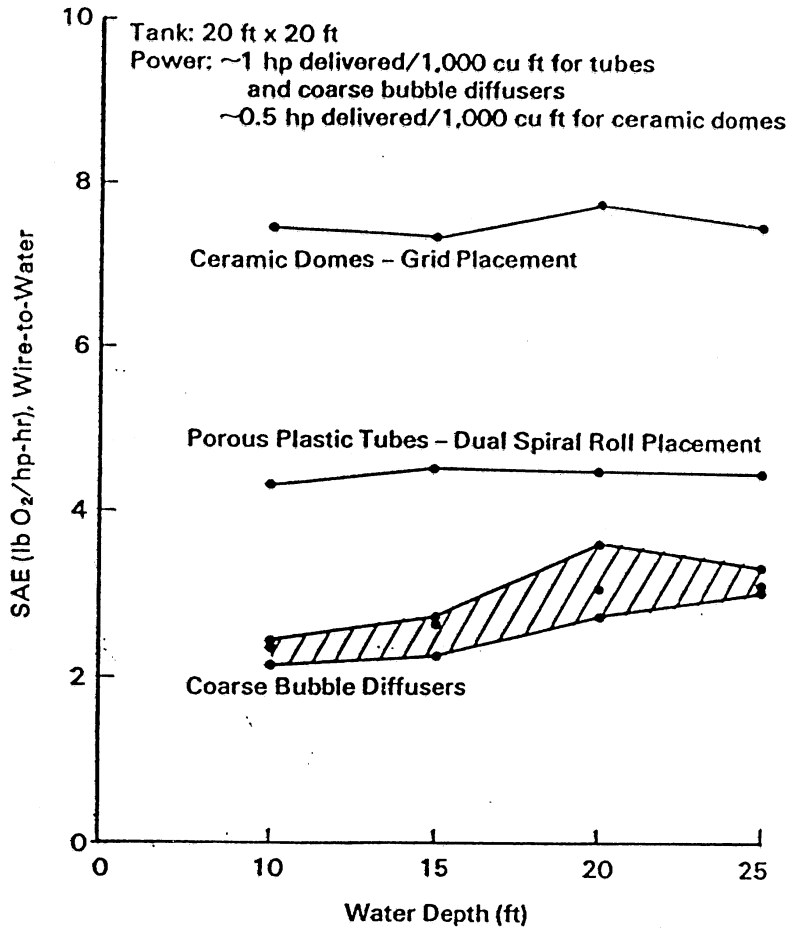

Fig. 1.2 Comparison of Aeration Efficiencies of Diffusers

Source: "Fine Pore Aeration Systems", EPA Report EPA/625/8-85/010, October 1985

The SAF Diffuser:

As already mentioned, the aeration efficiency of an aeration device depends on the bubble size, the bubble rise velocity, the mixing effected by the induced flow and the energy input required to compress the air to produce the bubbles. In order to obtain high transfer efficiencies, it is essential to optimize the combined effect of these parameters. In the SAF diffuser design, this is achieved by controlling the geometric configuration of the device.

The design of the SAF diffuser is based on the *air lift* principle. The diffuser essentially uses a vertical composite draft tube immersed in the body of water to be aerated (see figures 1.3 and 1.4). The term "composite draft tube" is used to denote a tube whose cross sectional area varies along its length in a prescribed manner. A buoyancy induced water flow field is created inside the tube by injecting air through 0.5 mm to 1 mm diameter peripheral orifices located near the inlet end. The induced water velocity exerts a drag on the bubbles that are being formed at the peripheral orifices. This additional drag force causes the bubble to detach from the orifice much before it grows to the normal size which it would have otherwise attained in a stagnant water body. Figures 1.5 and 1.6 show a schematic of this process. Figure 1.5 shows the formation of a bubble in stagnant water. The main forces acting on the bubble are those of buoyancy (a lifting force tending to detach the bubble), and surface tension and inertia (restraining forces which oppose bubble detachment). The bubble size would be determined by the balance of these forces. In the case of bubble formation shown in figure 1.6, a vertical tube has been introduced at the outlet of the nozzle. The bubbles rise through the tube and fill it partly. Introduction of the bubbles into the tube causes a buoyancy induced flow through it. This induced flow exerts a drag force on the bubble forming at the nozzle. Thus in addition to the forces considered in the case of the bubble formation in stagnant water shown in figure 1.5, we have an additional drag force in the case of the bubble formation in the induced flow field shown in figure 1.6. On account of this drag force, the size of the bubble forming in the induced flow field would be smaller than the size of the bubble forming in stagnant water for the same air flowrate. For a given air flowrate, the induced water velocity at the nozzle and hence the bubble size would depend upon the tube dimensions. This dependence provides a unique way of controlling the bubble size. This is the basic idea behind the design of the SAF diffuser. The only difference between the schematic of figure 1.6 and the SAF diffuser is that in the SAF diffuser the orifices are provided on the periphery of the tube near the inlet end. The geometric proportions of the device and the size and the number of the peripheral orifices can be varied to achieve optimal operation in a variety of applications.

Several geometric configurations of the device are possible. For example, the device can be of circular planform or of rectangular planform (see figure 1.7). The transition from the tube inlet (smaller cross section) to the main tube body (larger cross section) can be in the form of a sudden expansion or a gradual one. The size of the orifices can be varied from a few microns (fine

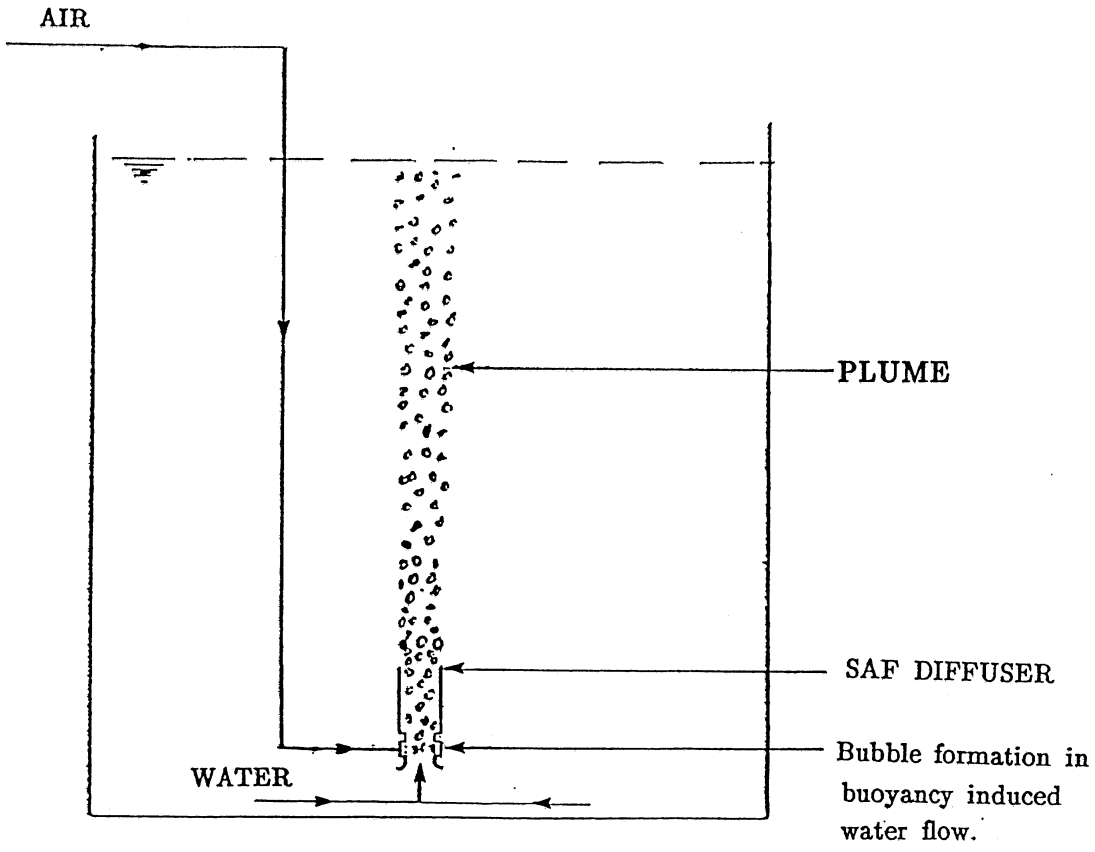

Fig. 1.3 Schematic of the Performance of the SAF Diffuser

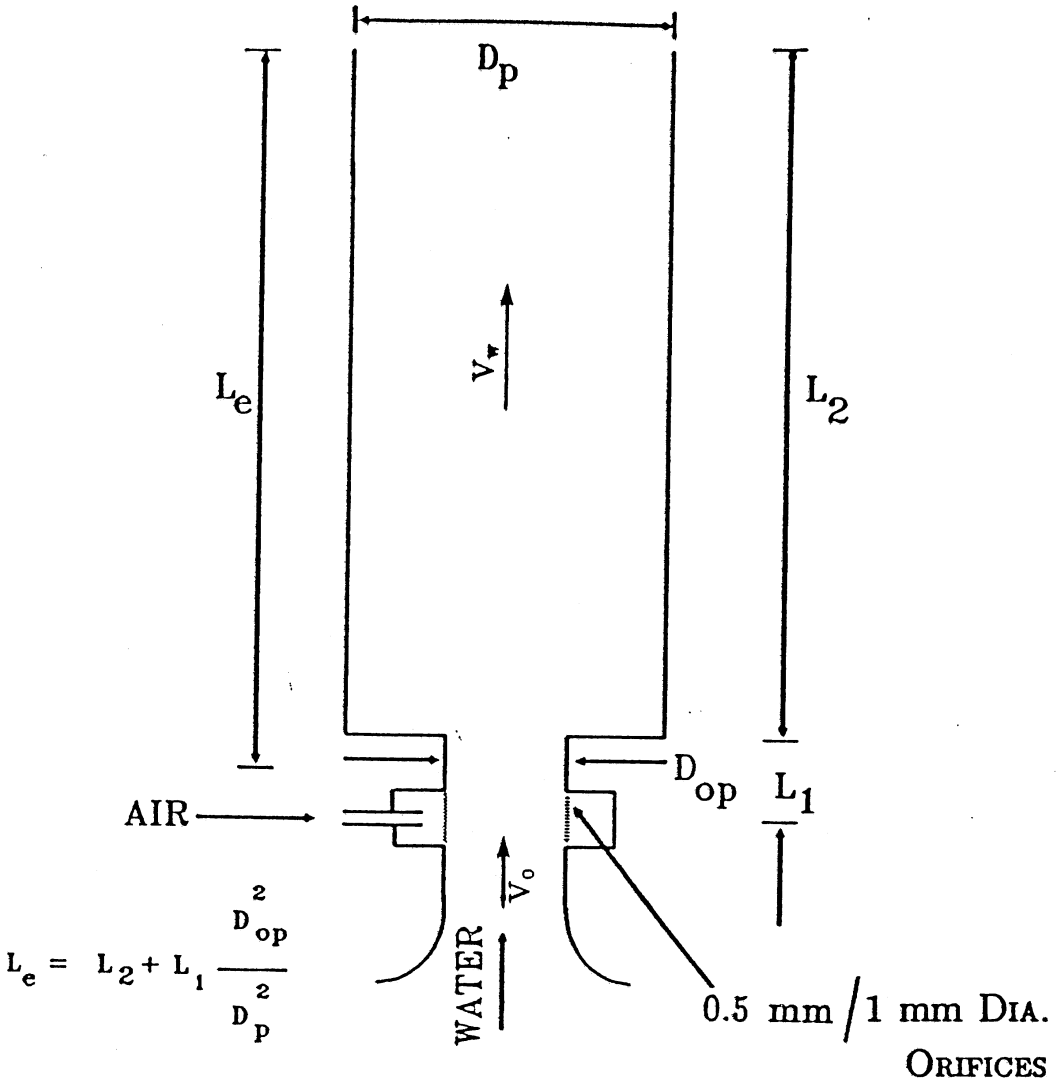

Fig. 1.4 The SAF Diffuser – Cross Section

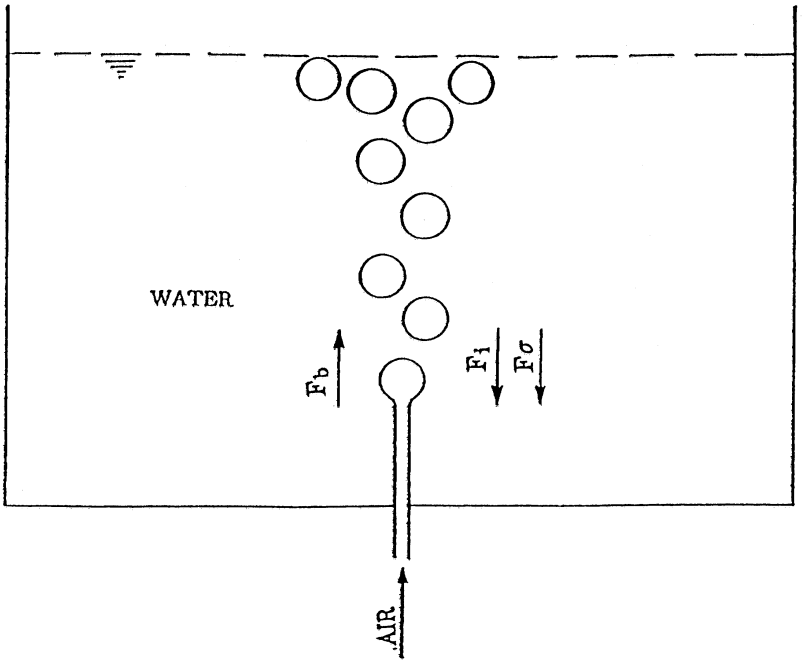

Fig. 1.5 Bubble Formation in Stagnant Water

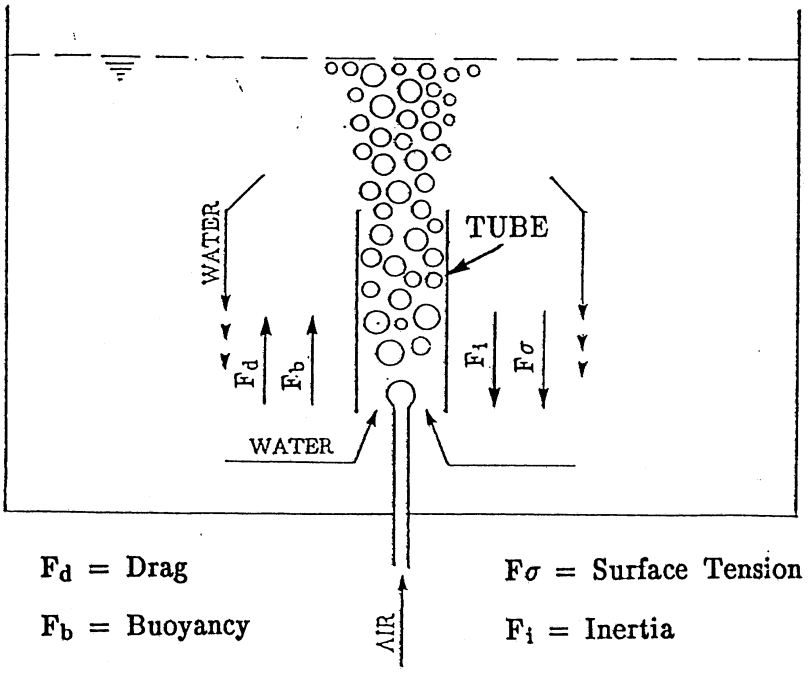

Fig. 1.6 Bubble Formation in Flowing Water

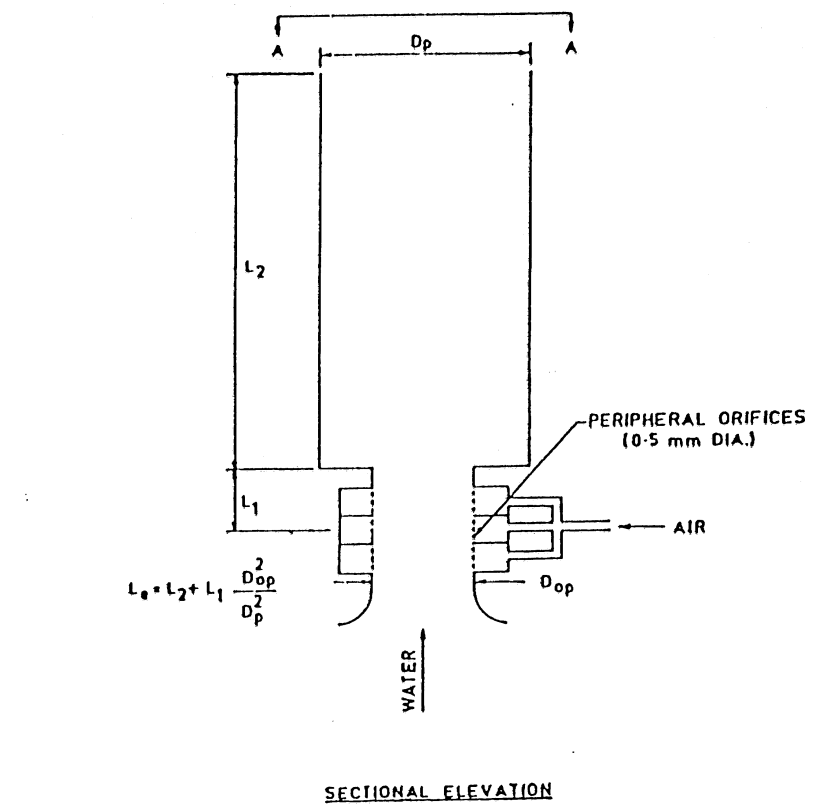

Fig. 1.7 The SAF Diffuser – some possible configurations

pores) to about 0.5 to 1 mm or even higher values depending upon the water quality and the site specific requirements. They can also be non–circular. These orifices can be arranged along the periphery of the inlet tube or along the circumference of a tube placed concentrically within the inlet tube (see figure 1.8). Also, in order to increase the rangeability of the device in respect of air flowrate and to achieve uniformity of air flow, the peripheral orifices are arranged in modules, each module containing a particular number of holes (see figure 1.8). Since the peripheral orifices are arranged in the vertical plane, it would be possible to accommodate more orifices for a given plan area of the diffuser than would be possible with conventional designs, with holes arranged in a horizontal plane. This results in reduced energy losses and increased rangeability for the device.

A detailed experimental study to explore the feasibility of the concept of the SAF diffuser was undertaken. The main processes associated with the performance of the SAF diffuser are the following:

- Creation of a buoyancy induced flow field in the tube (for the sake of simplicity the SAF diffuser is referred to as "tube" hereafter).
- Formation of air bubbles in the buoyancy induced flow field and coalescence/breakup of the bubbles as they rise through the tube.
- Discharge of the air–water mixture from the tube into the water body outside thereby creating a plume.
- Mass transfer from the air bubbles to the water as the bubbles rise through the tube and the plume.

Considering an air–water system, the independent variables that affect the above mentioned processes are the following.

- Air flow rate
- Geometry and dimensions of the diffuser
- Size, number and spacing of the peripheral orifices
- Diffuser submergence below the water surface

The effect of the above parameters on the performance of the SAF diffuser was the main focus of this study. The theoretical considerations, the experimental studies and the results are presented in the following chapters.

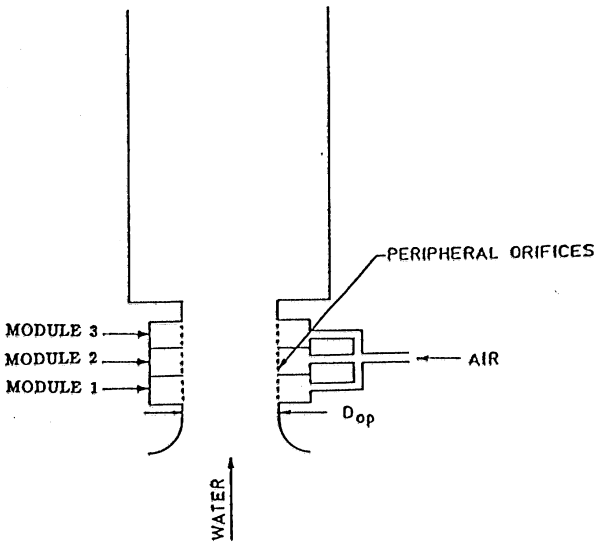

SECTIONAL ELEVATION

a) PERIPHERAL ORIFICES ARRANGED IN MODULES

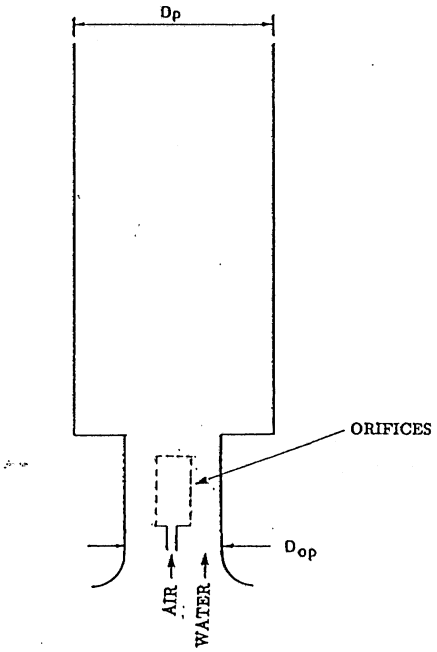

SECTIONAL ELEVATION

b) ORIFICES LOCATED INSIDE THE TUBE INLET

Fig. 1.8 The SAF Diffuser – some possible configurations

Chapter 2

Theoretical Considerations and Experimental Objectives

As outlined in Chapter 1, the SAF diffuser envisages the control of the bubble size and the bubble rise velocities in a plume by generating bubbles in the buoyancy induced flow field inside a vertical composite draft tube. In order to design and optimize such a device, one should be able to predict the induced velocities and the mass transfer characteristics for a given geometry of the device and system characteristics. Since many of the physical processes involved in the functioning of the device are yet poorly understood, experimental studies were planned to understand and assess the effects of various hydrodynamic and geometric parameters that affect the performance of the device. Before that, however, the following simplified analysis was undertaken to identify the significant dynamic and geometric parameters to be considered in the experimental studies.

2.1 BUBBLE SIZE

The bubble size is controlled by the processes of bubble formation, coalescence and breakup. In addition, the effects of the pressure variation and the mass transfer during ascent of the bubble also need consideration. Here only the effect of the induced velocity on the bubble size at formation is analysed. The objective here is to get an idea of the magnitude of the induced water velocities necessary to produce bubbles in the size range of 2 to 3 mm.

Bubble formation over a submerged orifice is influenced by several parameters such as the orifice size, shape and orientation, the gas flowrate through the orifice, the system pressure above the orifice, turbulence in the liquid column, physical properties of the liquid, velocity of the continuous phase and the volume of the gas chamber associated with the orifice.

With regard to the volume of the gas chamber, investigators have classified bubble formation as occurring under any one of the following conditions (7, 8, 9):

i) Constant flow (this corresponds to very small gas chamber volume)
i) Constant pressure (when the gas chamber volume is very large)
iii) Intermediate between (i) and (ii)

For a given air flowrate and orifice diameter, the bubble size increases with the increase in the chamber volume. The bubble formation is affected by both the air pressure within the bubble and the air pressure in the chamber associated with the orifice at any instant during the bubble formation. Davidson and Schuler (7) assume that either the pressure within the chamber is constant, which corresponds to the condition when the chamber volume is very large or that the gas flowrate into the bubble is constant, which corresponds to the situation when the chamber volume is negligible. At intermediate values of the chamber volume, the pressure within the chamber and the bubble and the gas flowrate into the bubble varies. Hence the effect of the chamber volume on the bubble size needs consideration while sizing the plenum chamber which houses the peripheral orifices of the diffuser.

Experimental results of Miyahara et al (10) for orifices of diameters 0.5 mm and 1 mm with chamber volumes of 130 cc have shown that the effect of the chamber volume disappeared when the number of orifices was more than 19. The result could be interpreted as a cut–off below 6.84 cc/orifice. Since the SAF diffuser is also contemplated to be designed with orifices in the size range of 0.5 to 1 mm in diameter, if the plenum chamber of the diffuser is provided with a volume per orifice much lower than that given above, the effect of the chamber volume on the bubble size can be neglected. Also, with a very small chamber volume per orifice, the bubble formation can be assumed to occur under nearly constant flow conditions.

Many theoretical models have been have been proposed to describe bubble formation. Most of them depended on a force balance at the moment of detachment of the bubble, assuming the bubble to be spherical (11, 12, 13, 14). A similar analysis is presented here for air bubbles forming in water. Considering an isolated bubble forming in flowing water, the main forces acting on the bubble at the time of detachment can be grouped as lifting forces and restraining forces as described below (see figure 2.1):

F_i = Inertia Force

F_σ = Surface Tension Force

F_b = Buoyancy Force

F_d = Drag Force

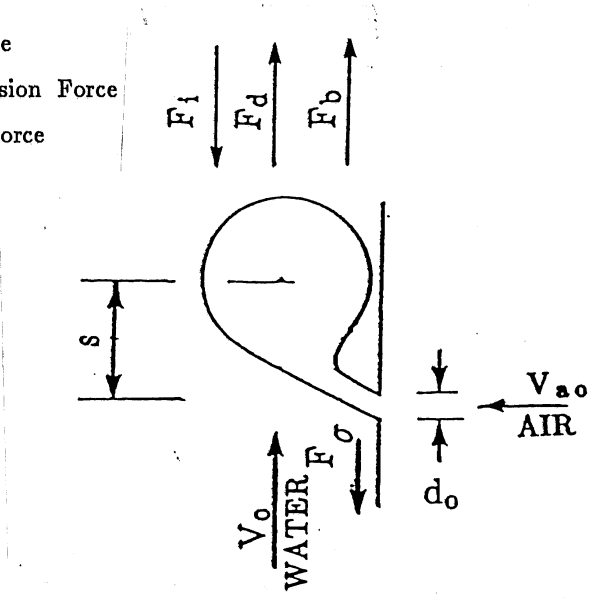

Fig. 2.1 Bubble formation – Definition sketch

Lifting forces:

a) Buoyancy force (F_b):

$$F_b = \rho_w \, g \, \frac{\pi}{6} \, d_b^3 \tag{2.1}$$

where
- ρ_w = density of water
- g = gravitational acceleration
- d_b = bubble diameter at the time of detachment from the orifice

b) Drag force (F_d):

$$F_d = C_d \, \rho_w \left[V_o - \frac{ds}{dt}\right]^2 \frac{1}{2} \, \frac{\pi}{4} \, d_b^2 \tag{2.2}$$

where
- V_o = water velocity in the tube across the orifices
- C_d = drag coefficient
- $\frac{ds}{dt}$ = rise velocity of the center of the bubble

Several studies of bubble formation in water (13, 14) have shown that the contribution of the term $\frac{ds}{dt}$ towards the drag force on the bubble during formation is small compared to the other forces. Hence, neglecting this term, the drag force can be expressed as

$$F_d = C_d \, \rho_w \, \frac{V_o^2}{2} \, \frac{\pi}{4} \, d_b^2 \tag{2.3}$$

Restraining forces:

a) Surface tension force ($F\sigma$):

$$F_\sigma = \pi \, d_o \, \sigma \cos \gamma \tag{2.4}$$

where
- d_o = diameter of the orifice
- σ = surface tension
- γ = contact angle

b) Inertia force (F_i):

$$F_i = (\rho_a \, \forall_b + \rho_w \, \forall_l) \, a \tag{2.5}$$

where

a = acceleration of the bubble

$\forall_l$ = liquid volume associated with the bubble motion

$$= C_a \frac{\pi d_b^3}{6} \tag{2.6}$$

$\forall_b$ = bubble volume at the time of detachment

C_a = added mass coefficient

ρ_a = density of air

While developing expressions for the inertia force associated with bubbles forming in stagnant water, Gaddis et al (13) assumed that the acceleration at the time of the bubble detachment can be expressed in terms of the mean bubble velocity during the bubble formation and the bubble formation time. With this assumption, the expression for the acceleration becomes

$$a = \frac{w}{t_r} \tag{2.7}$$

where

w = average velocity of the bubble during the bubble formation

t_r = formation time of the bubble

The mean velocity w can be expressed in terms of the vertical displacement s of the bubble center from the orifice as

$$w = \frac{s}{t_r} \tag{2.8}$$

Several experimental studies (13, 14) on bubble formation in stagnant liquids have shown that the distance s can be expressed as $s = K_s d_b$ where K_s is a constant.

The bubble formation time t_r is given by

$$t_r = \frac{\forall_b}{Q_{ao}}$$

$$= \frac{\pi d_b^3}{6 Q_{ao}} \tag{2.9}$$

Substituting for the distance s and the bubble formation time t_r in equation (2.8),

$$w = \frac{6 K_s Q_{ao}}{\pi d_b^2} \tag{2.10}$$

Using the expressions for w and t_r in equations (2.7) and (2.5) and neglecting the gas momentum, the inertia term becomes

$$F_i = K_i \frac{Q_{ao}^2}{d_b^2} \tag{2.11}$$

where

$$K_i = \frac{6\ C_a\ K_s\ \rho_w}{\pi}$$

Thus the force balance at the time of bubble detachment gives,

$$\rho_w g \frac{\pi}{6} d_b^3 + C_d\ \rho_w \frac{V_o^2 \pi}{2} \frac{\pi}{4} d_b^2 = \pi\ d_o\ \sigma \cos\ \gamma + K_i(Q_{ao}^2/d_b^2) \tag{2.12}$$

In the above equation, the surface tension force is constant for a given orifice diameter. If we assume that the water velocity is zero, the bubble detachment is governed by the buoyancy, surface tension and inertia forces. For extremely small air flowrates ($Q_{ao} \simeq 0$), the inertia force becomes very small compared to the other two forces and the bubble diameter is determined by the balance of the buoyancy and the surface tension forces. The force balance then becomes

$$\rho_w\ g \frac{\pi}{6} d_b^3 = \pi\ d_o\ \sigma \cos\ \gamma$$

$$d_b = \left[\frac{6\ d_o\ \sigma}{\rho_w\ g} \cos\ \gamma \right]^{1/3} \tag{2.13}$$

As the air flowrate is increased, the buoyancy and the inertia forces increase while the surface tension force remains the same. At large air flowrates, the bubble detachment would then be governed by the balance between the buoyancy and the inertia forces.

The present investigations envisage studies on orifices in the size range of 0.5 mm to 1 mm up to air flowrates of about 5 cc/s per orifice. A comparison of the forces at the time of detachment acting on a bubble forming over a 0.5 mm diameter orifice in stagnant water, under an air flowrate of 5 cc/s, computed from equations (2.1), (2.4) and (2.11) is shown below:

Buoyancy (N)	Surface tension (N)	Inertia (N)
0.083087	0.000114	0.082973

The computations were done with $C_a = 11/16$ and $K_s = 3/4$ based on available literature (12, 13). Also in the computations, cos γ was assumed as unity. This would correspond to maximum surface tension force.

From the above comparison, it is seen that the surface tension force is very small compared to the buoyancy and the inertia forces. Drag forces vary considerably and will be included. Hence, neglecting the surface tension term, the equation (2.12) can be written as

$$\rho_w \, g \, \frac{\pi}{6} \, d_b^3 + C_d \, \rho_w \, \frac{V_o^2}{2} \, \frac{\pi}{4} \, d_b^2 = K_i \, (Q_{ao}^2/d_b^2) \tag{2.14}$$

The air flowrate through the orifice can be expressed in terms of the orifice diameter:

$$Q_{ao} = \frac{\pi}{4} \, d_o^2 \, V_{ao} \tag{2.15}$$

where

d_o = diameter of the orifice

V_{ao} = air velocity through the orifice

In the equation (2.14), the drag coefficient is a function of the Reynolds number. Assuming the bubble to be spherical, the drag coefficient for the bubbles considered in this study, which fall in the Reynolds number range of 250–1200 have values lying in the range 0.4 to 0.6. A mean value of 0.5 is assumed as an approximation in this analysis. Substituting this value in equation (2.14) and combining equations (2.14) and (2.15) and simplifying, we get

$$\frac{d_b}{d_o} = C_1 \left[\frac{V_{ao}^2}{g d_b + C_2 \, V_o^2} \right]^{0.25}$$

$$= C_1 \left[\frac{(V_{ao}/V_o)^2}{(1/F_{rb}^2) + C_2} \right]^{0.25} \tag{2.16}$$

where

F_{rb} = Froude number based on the bubble diameter and the induced water velocity

$$= \frac{V_o}{\sqrt{g \, d_b}}$$

$$C_1 = \frac{9 \, C_a \, K_s}{4}$$

$$C_2 = \frac{C_d \, \pi}{4}$$

$$= 0.38 \text{ (assuming } C_d = 0.5)$$

It appears that equation (2.16) accounts for the effect of the orifice diameter while predicting the bubble size. However, by expressing V_{ao} in terms of the air flowrate as given by equation (2.15), we get an expression for the bubble size independent of the orifice diameter, or

$$d_b = C_1 (4/\pi)^{0.5} \left[\frac{Q_{ao}^2}{gd_b + C_2 V_o^2}\right]^{0.25} \qquad (2.17)$$

Equations of the above form have been proposed by several researchers (13, 15, 16, 17) to predict the bubble size in stagnant water. The bubble size predicted by the above equation is independent of the orifice size. Hence the above equation is only useful for predicting bubble sizes for large air flowrates where the bubble detachment is primarily governed by the forces of buoyancy and inertia. Several experimental results (14, 18) of bubble formation over orifices in the diameter range of 1 mm to 6 mm operating with air flows in the range of 1 to 10 cc/s have shown that in this range of air flowrate, the bubble size is dependent on the orifice diameter, the bubble size increasing with the orifice diameter for a given air flowrate. In the present study, the air flowrates per orifice would be below about 5 cc/s and the orifice diameters will be in the range 0.5 mm to 1mm. Hence the equations of the above form need to be modified for application in the intermediate range of air flowrates where the air flowrate as well as the orifice diameters are important.

Sada et al. (18) have developed an experimental correlation for air bubble formation in flowing water over an orifice placed parallel to the liquid flow. Their relationship is

$$\frac{d_b}{d_o} = 1.55 \left[\frac{V_{ao}^2}{gd_b + 0.33 V_o^2}\right]^{0.2} \qquad (2.18)$$

Equation (2.18) is similar to equation (2.16) except for the exponent of the term on the right hand side of the equation. The correlation predicts the bubble size taking into account the effect of the orifice diameter, with the bubble diameter varying as $d_o^{0.2}$ when the Froude number (F_{rb}) is large enough . The experimental results for orifices in the size range 0.8 mm to 3 mm showed good agreement with the predicted values (18).

Figure 2.2 shows the bubble sizes predicted by the equations (2.16) and (2.18) for orifice diameters of 0.5 mm, 1 mm and 2 mm in the air flowrate range of 1 to 10 cc/s. Equation (2.16) predicts the same bubble size for all the three orifices whereas the equation (2.18) predicts different bubble sizes for the three orifices, the bubble size for a given air flowrate increasing with the increase in the orifice diameter. The trend predicted by equation (2.18) was in agreement with the experimental observations (18).

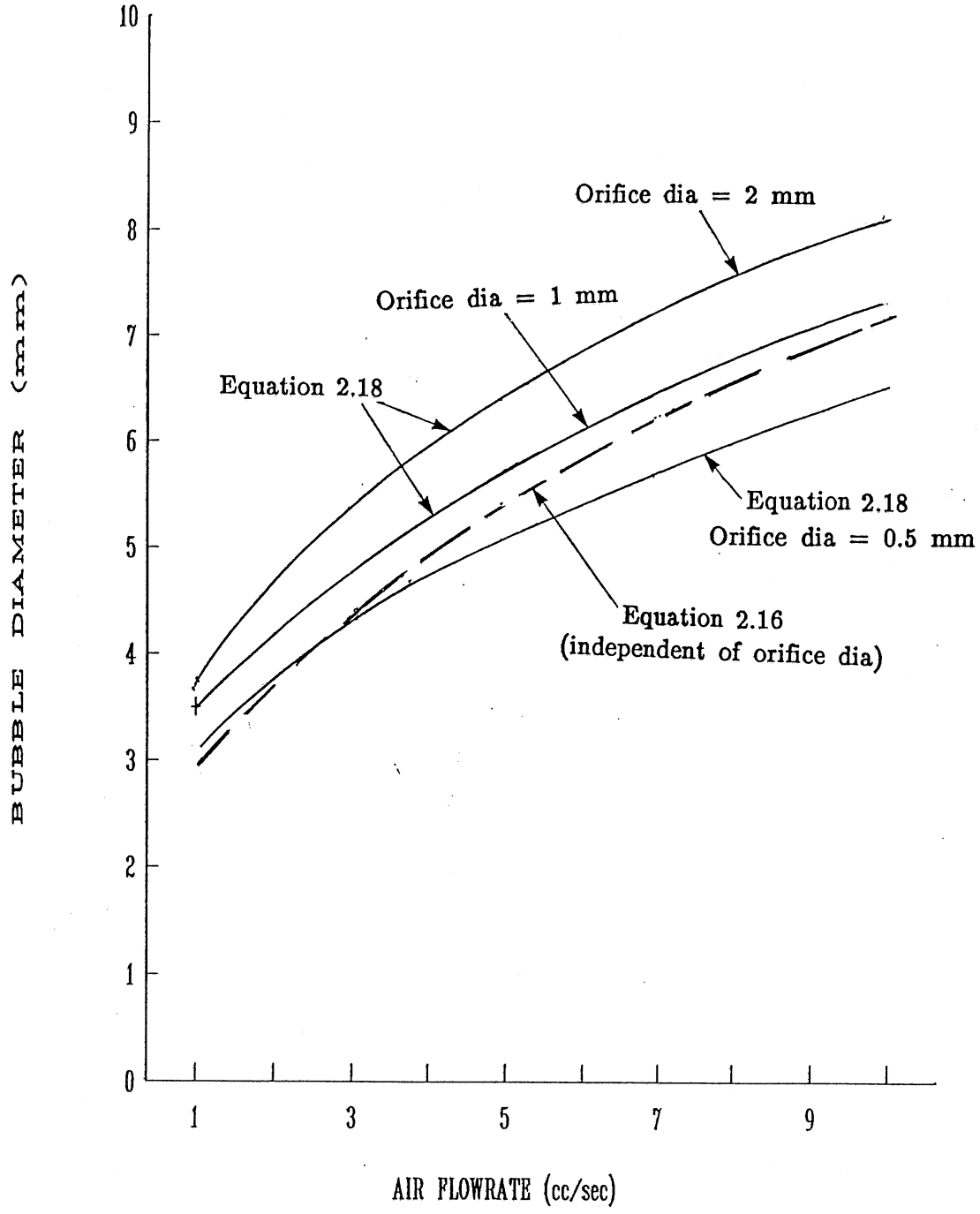

Fig. 2.2 Effect of orifice diameter on bubble size (computed using equations 2.16 and 2.18)

Figure 2.3 shows the effect of the induced water velocity on the bubble size predicted by equation (2.18) for a 0.5 mm diameter orifice. For a given air flowrate, as the water velocity is increased the bubble size decreases. Bubble diameter of 2.2 mm is achieved for an air flowrate of 1 cc/s with an induced water velocity of 50 cm/s. For an air flowrate of 3 cc/s, bubble sizes less than of 3 mm are achieved with induced water velocities of about 80 cm/s or more.

Figure 2.3 also shows comparison of the bubble sizes for orifices of diameters 0.5 mm and 1 mm. The results indicate that the bubble sizes for 1 mm diameter orifice are close to those of 0.5 mm diameter orifice though the associated induced velocities are higher.

The above analysis brings out the following conclusions:

- In the range of the orifice sizes and the air flowrates proposed in the study, the bubble size at formation depends on the orifice diameter, the air flowrate per orifice and the induced water velocity. For a given orifice diameter, the bubble size can be decreased by decreasing the air flowrate per orifice as well as by increasing the induced water velocity.

- The bubble size produced by 1 mm diameter orifice is slightly larger than the bubble size produced by 0.5 mm diameter orifice.

- The induced water velocity required for producing 2.2 mm diameter bubbles over a 0.5 mm diameter orifice, for an air flowrate of 1 cc/s through the orifice, would be about 50 cm/s.

Having obtained an estimate of the required induced water velocity in the tube, the details of the flow in the tube are analysed next.

2.2 FLOW CHARACTERISTICS IN THE TUBE

2.2.1 Flow Velocity

When the device is submerged in a homogeneous body of water without any air being injected into it, the weight of the water inside the tube is exactly balanced by the pressure exerted on it by the neighboring fluid outside the tube. Introduction of air modifies the hydrostatic pressure distribution inside the tube because of the reduction in the density of the air–water mixture in the tube as compared to the water outside. As a consequence, the fluid inside the tube gains kinetic energy.

Considering the fluid as ideal, through an energy balance across the tube, the following *chimney* equation is obtained (see Appendix A):

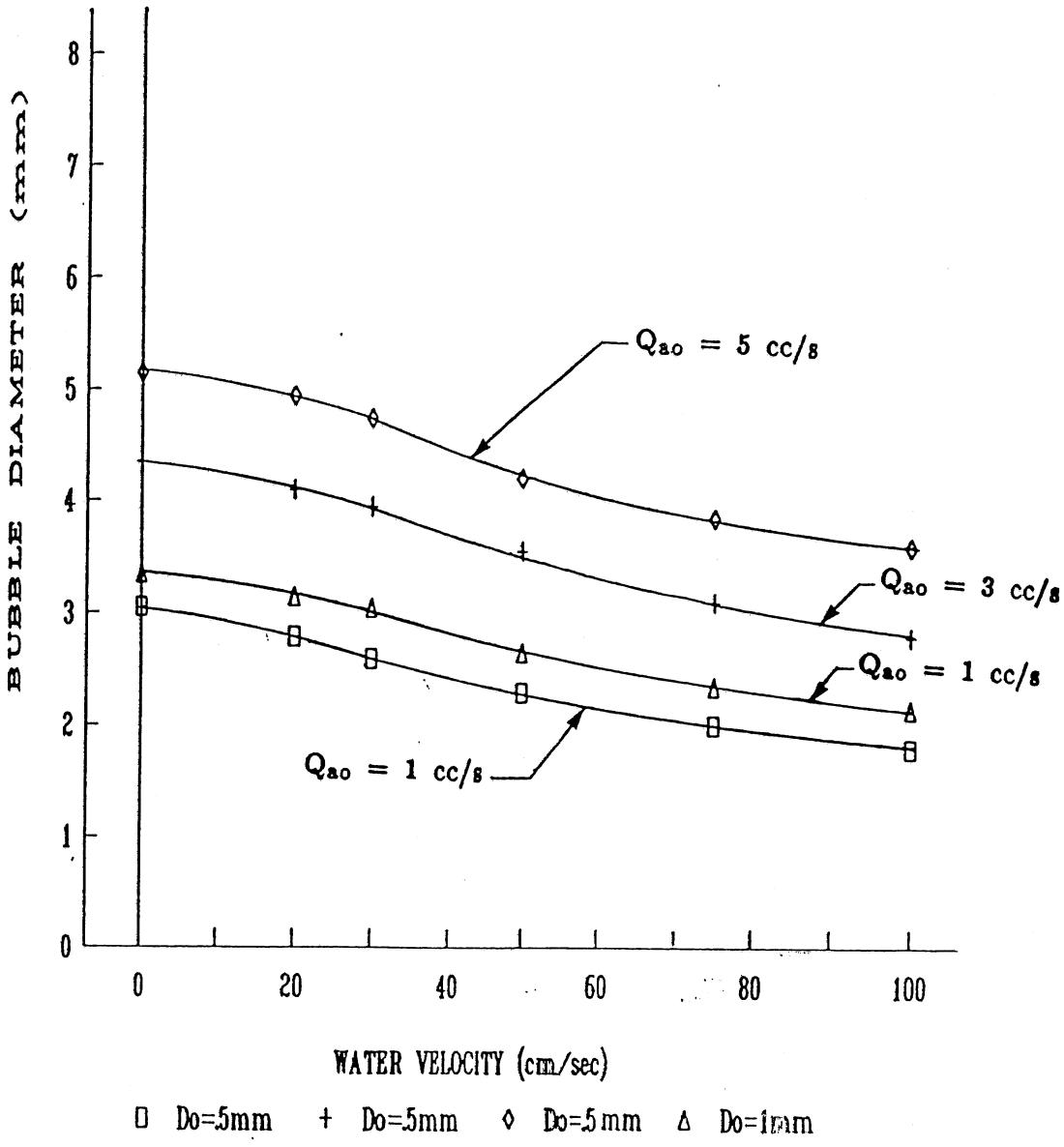

Fig. 2.3 Effect of induced velocity on bubble size (computed using equation 2.18)

$$F_{rw} = \frac{V_w}{\sqrt{L_e g}} = \left[\frac{2\alpha}{(1-\alpha)}\right]^{0.5} \tag{2.19}$$

where

F_{rw} = the tube Froude number based on water velocity

V_w = mean water velocity in the tube

L_e = effective tube length

$$= L_2 + [L_1 (A_{op}/A_p)] \tag{2.20}$$

A_{op} = cross sectional area of the tube inlet

A_p = cross sectional area of the tube

α = mean void fraction of air in the tube

The above analysis neglects the surface tension energy of the bubbles inside the tube and also all other energy exchanges within the tube.

Taking into account the energy losses, equation (2.19) is modified as below:

$$F_{rw} = \frac{V_w}{\sqrt{L_e g}} = \left[\frac{2\alpha}{(1-\alpha)K}\right]^{0.5} \tag{2.21}$$

where

K = overall loss coefficient

$$= 1 + K_e + K_{ex} + K_f + K_b + K_s \tag{2.22}$$

K_e = entrance loss term

$$= k_e D_r^4 (1-\alpha) \tag{2.23}$$

K_{ex} = expansion loss term

$$= (D_r^2 - 1)^2 \tag{2.24}$$

K_f = friction loss term

$$= f (L_e/D_p) (1-\alpha)$$

$$= f L_r (1-\alpha) \tag{2.25}$$

K_b = term representing the losses due to the lateral entry of air bubbles into the tube at the air inlet

$$= k_c \, D_r^4 / \, (1-\alpha) \tag{2.26}$$

f = friction factor for air–water bubbly flow

k_c = appropriate contraction loss coefficient at the bubble entrance region

K_s = coefficient of the secondary losses not considered by the above loss coefficients

D_p = diameter of the tube

D_{op} = diameter of the tube inlet

L_r = length ratio of the tube

$$= L_e/D_p \tag{2.27}$$

$$D_r = \text{diameter ratio} = D_p/D_{op} \tag{2.28}$$

There are terms in equations (2.21) – (2.26) that are not well known. First, the frictional pressure drop (represented by K_f) in bubbly flow through vertical pipes shows considerable departure from commonly used models of Lockhart and Martinelli (19) and Armand (20). For small liquid velocities and air volumetric quality, the bubbly flow frictional pressure drops have been reported to be of the order of 10 – 20 times the corresponding single phase flow values (21, 22, 23). Experimental studies of Nakoryakov et al (22) indicate that in the bubbly flow regime, the wall shear stress is significantly affected by the void fraction distribution within the tube and that the high values of friction factors result from the high void fraction peaks near the wall.

Second, one of the effects of the lateral entry of the bubbles from the peripheral orifices into the tube is to cause a contraction of the water flow and an associated energy loss. The loss coefficient k_c given in equation (2.26) would then depend on the void fraction and the void fraction distribution downstream of the peripheral orifices.

In addition, there are other energy terms to be considered such as the surface tension energy of the bubbles, the energy associated with the expansion and oscillation of the bubbles during the bubble formation and bubble rise. These terms are grouped into a single term K_s.

In an effort to develop a simplified expression for the three aforementioned losses, these losses are combined into a single loss and a combined loss term K_{fb} is defined as below.

$$K_{fb} = K_f + K_b + K_s \tag{2.29}$$

K_f and K_b are given by equations (2.25) and (2.26) respectively. Both f (eq. 2.25) and k_c (eq. 2.26) depend on the void fraction and the lateral void fraction distribution ie the void fraction distribution across the cross section of the pipe. Though it is recognized that the Reynold's stresses and the lift forces experienced by the bubbles are the significant mechanisms governing the lateral void fraction distribution, this phenomenon is as yet poorly understood (23, 24). In view of this, the limited available published results were studied with a view to identify the parameters to be considered for developing an empirical relationship for K_{fb} taking into account the lateral void fraction distribution. Experimental results of Nakoryakov et al (22) show that the lateral void fraction distribution depends on the mean void fraction and the water velocity. Equation (2.19) already suggests a dependence of the water velocity on the mean void fraction. Taking into account this dependence and the parameters affecting K_f and K_b as shown in equations (2.25) and (2.26) and also assuming that the secondary losses would depend on the void fraction and the tube geometry, it is postulated that K_{fb} could be approximated by a functional relationship of the following form

$$K_{fb} = K_{fb}\ (\alpha,\ D_r,\ L_r) \tag{2.30}$$

Above functional relationship would be established experimentally.

2.2.2 Void Fraction

In order to determine the water velocity using equation (2.21), an additional expression for the mean void fraction in the tube is required. The void fraction can be expressed as

$$\alpha = \frac{J_a}{V_a}$$

$$= \frac{J_a}{V_w + V_r} \tag{2.31}$$

where

J_a = mean superficial air velocity in the tube
$= (Q_a/A_p)$
Q_a = air flowrate
A_p = cross sectional area of the tube
V_a = mean velocity of air in the tube
V_r = mean velocity of air relative to that of water (mean slip velocity)

In the above expression for the void fraction, J_a depends on the air flowrate and the tube diameter. Considering an air water system, the independent parameters that conceivably affect the term (V_w+V_r) are the superficial air velocity J_a, the tube dimensions, densities of air and water, and the gravitational acceleration. These parameters can be grouped on dimensional considerations to give a functional relationship of the following form:

$$\alpha = \alpha \left(\left(\frac{J_a}{\sqrt{L_{eg}}} \right), D_r, L_r, \frac{\rho_w - \rho_a}{\rho_w} \right) \tag{2.32}$$

Since $\rho_a << \rho_w$, term $\frac{\rho_w - \rho_a}{\rho_w}$ would be practically a constant. Hence equation (2.32) can be written as

$$\alpha = \alpha \left(\left(\frac{J_a}{\sqrt{L_{eg}}} \right), D_r, L_r \right) \tag{2.33}$$

$$= \alpha \left(\left(F_{ra}, D_r, L_r \right) \right.$$

where

$$F_{ra} = \frac{J_a}{\sqrt{L_{eg}}}$$

= tube Froude number based on the superficial air velocity

Consider such a relationship for the case of homogeneous equilibrium flow within the tube. It is recognized that the actual flow within the tube would not be homogeneous equilibrium. Here the homogeneous equilibrium flow is considered only to examine the existence of the relationship of the form given by equation (2.33) for such flow. This approximation would mean zero slip velocity between water and air. Then we have

$$V_r = 0$$

$$V_w = V_a$$

The void fraction in the tube then would be given by

$$\alpha = \frac{J_a}{V_w} \tag{2.34}$$

Substituting for α from equation (2.34) in equation (2.21), we get,

$$\frac{J_a}{\alpha \sqrt{L_{eg}}} = \left[\frac{2\alpha}{(1-\alpha)K} \right]^{0.5} \tag{2.35}$$

On rearranging,

$$\alpha = (1/2)^{1/3} \left[\frac{J_a}{\sqrt{L_e\, g}}\right]^{2/3} K^{1/3}\, (1-\alpha)^{1/3} \qquad (2.36)$$

The above expression was derived on the assumption of zero slip between the water and the air phases. Merchuk (25) has shown through experimental studies that the void fraction in a two dimensional air lift reactor can be expressed in terms of the superficial air velocity by the following expression:

$$\alpha = 0.047\ J_a^{0.59} \qquad (2.37)$$

Merchuk (26) has also observed that the correlation for void fraction is affected by the system geometry. Merchuk's experimental correlation was obtained under conditions with slip velocities between the water and the air phases. These finding show that the the functional relationship of the form given by equation (2.36) for the void fraction could exist even with slip velocities between the water and the air.

The void fraction within the tube is an important parameter affecting the bubble coalescence. According to Radovcich and Moissis (27) the bubble collision frequency increased extremely rapidly above void fractions of 25 per cent. Hence it was contemplated that the device would be designed with low void fractions ranging up to about 15 per cent. For such low void fractions, the term $(1-\alpha)^{1/3}$ is very nearly equal to unity. Hence, neglecting this term, equation (2.36) reduces to the following form:

$$\alpha = 0.794 \left[\frac{J_g}{\sqrt{L_e\, g}}\right]^{2/3} K^{1/3} \qquad (2.38)$$

As shown by equations (2.21) through (2.26), the term K, representing the losses in the tube, depends on the tube geometry and the void fraction. Introducing this dependence into equation (2.38), we get

$$\alpha = \alpha \left(\left(\frac{J_a}{\sqrt{L_e g}} \right), D_r, L_r \right) \qquad (2.39)$$

Such a correlation would enable the determination of the mean void fraction in the tube from known values of the air flowrate and the parameters describing the tube geometry i.e. the length ratio, L_r and the diameter ratio, D_r.

2.3 MASS TRANSFER

The following parameters are commonly used for the performance evaluation of diffusers in respect of mass transfer (28):

1) Mass Transfer Coefficient
2) Standard Oxygen Transfer Rate
3) Standard Aeration Efficiency

These parameters are briefly discussed below:

Mass Transfer Coefficient, K_1A:

The well known "Two Film" theory was proposed by Lewis and Whitman (29). According to this theory, there exists a thin film of the gas and another of the liquid at the interface between a gas and a turbulent liquid. The gas passes through these films by a slow rate of molecular diffusion. The resistance to gas transfer is controlled by the molecular diffusion process through these films. In the case of a gas of low solubility, like oxygen in water, the gas film offers very little resistance as compared to the liquid film and the controlling resistance occurs in the liquid film (30). The concentration of oxygen at the liquid film interface is in equilibrium with the gas phase and yields a saturation condition as defined by Henry's law (2). On the liquid side of the film, the gas concentration is assumed to be uniform (ie a well mixed liquid).

Lewis and Whitman (29) assumed a steady state transfer process across the film. Subsequently, several theories have been put forth to take into account the unsteady nature of the film (31, 32).

Taking into account the resistance of the liquid film and neglecting the resistance of the gas film, the mass flux of oxygen across the interface can be expressed as

$$F_m = K_l (C_s - C) \tag{2.40}$$

where

F_m = mass flux (per unit area of interface): (mass/(area.time))

C_s = saturation concentration of oxygen in water: (mass/volume)

C = concentration of oxygen in water: (mass/volume)

K_l = liquid film coefficient: (length/time)

The rate of mass transfer across the interface can be expressed by introducing the interfacial area A into equation (2.40).

$$m' = \frac{dm}{dt} = K_lA (C_s - C) \tag{2.41}$$

where

m' = rate of mass transfer across the interface: (mass/time).

The product K_lA is termed the **mass transfer coefficient**: (volume/time)

The above equation can be expressed in terms of concentration units as below

$$\frac{dC}{dt} = \frac{1}{\forall}\frac{dm}{dt} = \frac{K_lA}{\forall}(C_s - C)$$

$$= K_la\,(C_s - C) \qquad (2.42)$$

where

$\forall$ = volume of the liquid in which the concentration, C, is determined

K_la = volumetric mass transfer coefficient

$$= \frac{K_lA}{\forall} : (1/\text{time}) \qquad (2.43)$$

From equation (2.43), it is seen that for a given water volume, K_la depends on the liquid film coefficient K_l and the interfacial area A.

Standard Oxygen Transfer Rate (SOTR):

The SOTR is defined as the oxygen transfer rate (mass of oxygen per unit time dissolved in a volume of water) when the dissolved oxygen concentration is zero at all points in the water volume, water temperature is 20°C and barometric pressure is 1 atm (28). From equation (2.41), we get SOTR as

$$SOTR = K_lA\,C_{ss} \qquad (2.44)$$

C_{ss} = dissolved oxygen saturation concentration at standard atmospheric pressure

(K_lA and C_{ss} are the values of the parameters at 20°C).

Standard Aeration Efficiency (SAE):

SAE is the SOTR per unit power input.

$$SAE = SOTR \ / \ \text{power input.} \tag{2.45}$$

Developing a relationship for K_lA:

Neglecting the effects of changes in bubble volume due to bubble expansion, coalescence, breakup and mass transfer and the change in air flowrate due to the pressure variations, the interfacial area A can be approximated as below in terms of the air flowrate, the bubble diameter, and the bubble residence time.

Let N denote the number of bubbles in the water body at any instant.

$$N = Q_a \ t_r / \ ((\pi/6) \ d_b^3) \tag{2.46}$$

where

Q_a = air flowrate through the diffuser

t_r = bubble residence time

d_b = equivalent bubble diameter at formation

The interfacial area A would be given by

$$A = (\text{number of bubbles}) \times (\text{surface area of one bubble})$$

$$= 6 \ Q_a \ t_r \ / \ d_b \tag{2.47}$$

In the case of conventional diffusers, excluding the mass transfer at the water surface, all of the mass transfer takes place in the plume and no mass transfer takes place inside the diffuser. However, in case of the SAF diffuser, the buoyancy induced flow has two parts; one part lying within the tube and the other, outside the tube. In the analysis that follow, the term bubble column is used to denote the entire buoyancy induced flow field including the part within the tube and the free shear flow outside. The term plume is used to denote the buoyancy induced free shear flow outside the tube. The mass transfer takes place within the tube as well as in the plume outside. Thus the overall mass transfer coefficient K_lA can be expressed as the sum of two components as below.

$$K_lA = K_lA_t + K_lA_{pl}$$

$$= 6 \ K_{lt} \frac{Q_a}{d_{bt}} \ t_{rp} + 6 \ K_{lp} \frac{Q_a}{d_{bp}} \ t_{rp} \tag{2.48}$$

where

K_lA = overall mass transfer coefficient
= mass transfer coefficient applicable to the entire bubble column

K_lA_t = mean K_lA for the tube

K_lA_{pl} = mean K_lA for the plume

K_{lt} = mean liquid film coefficient for the tube

K_{lp} = mean liquid film coefficient for the plume

t_{rt} = mean bubble residence time in the tube

t_{rp} = mean bubble residence time in the plume

d_{bt} = mean bubble diameter in the tube

d_{bp} = mean bubble diameter in the plume

The means are weighted in terms of their influence upon K_lA.

The parameter planned to be investigated in detail in the proposed experimental study was the overall mass transfer coefficient K_lA. Since mass transfer occurred within the tube as well as in the plume, the effect of the length of the tube relative to that of the submergence needed to be considered in the study.

In order to identify the appropriate non dimensional parameters that would influence K_lA, the following analysis was undertaken. The analysis considers an air water system. The two parameters K_l and A are considered separately. In the analysis that follows, simple buoyant plume theory (single phase) is applied to the bubble column. The analysis neglects the effect of the tube on the plume flow characteristics. The limitations of such an analysis are recognized. It is assumed that the Boussinesq approximation is still appropriate since the difference in the densities of the air–water mixture in the plume and of the ambient water is very small.

Parameters affecting the interfacial area A:

Consider an elemental volume/strip of the bubble column at a distance of Z form the air inlet (see figure 2.4). Let the number of air bubbles in this elemental strip be equal to N. Assuming the bubbles to be spherical, the volume of air in the elemental strip would be given by

$$\forall_c = N\ (\pi/6)\ d_{bc}^3 \qquad (2.49)$$

where

d_{bc} = equivalent mean bubble diameter in the elemental strip

This volume can also be expressed in terms of the void fraction as below

$$\forall_c = \alpha_c\ (\pi/4)\ D_c^2\ dZ \qquad (2.50)$$

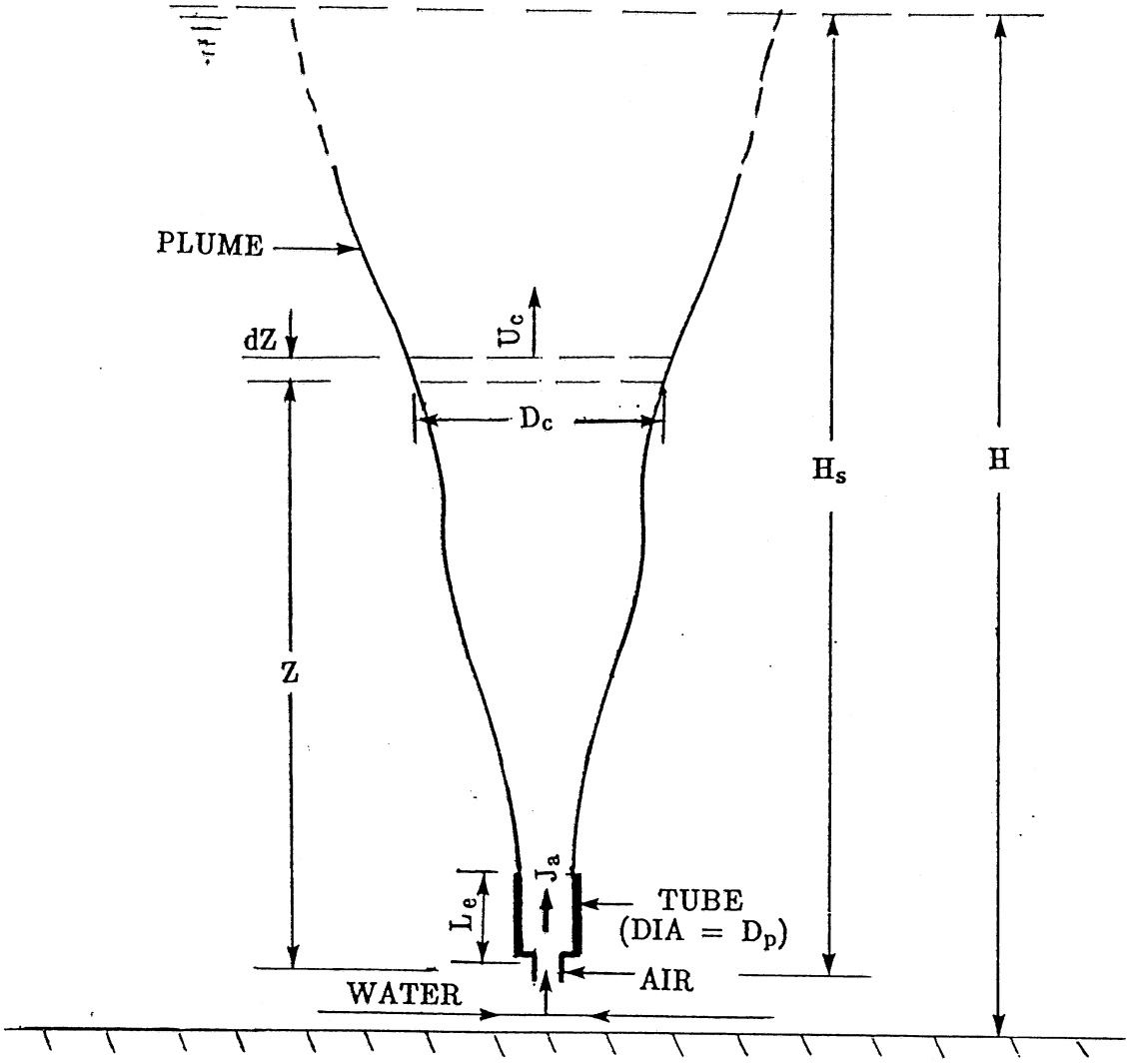

Fig. 2.4 Definition sketch of the bubble column

where

α_c = mean void fraction in the elemental strip

D_c = diameter of the elemental strip

The interfacial area A_c of all the bubbles in the elemental strip can be expressed as

$$A_c = N \pi d_{bc}^2 \tag{2.51}$$

From (2.48), (2.49) and (2.50), we get

$$A_c = (6\pi/4) \alpha_c \frac{D_c^2}{d_{bc}} dz \tag{2.52}$$

In order to estimate the interfacial area using (2.52), we need expressions for the terms α_c, D_c and d_{bc}. These terms are considered one by one below.

Consider the term α_c. This term represents the mean void fraction in the bubble column. Limited experimental results are available on the spatial variation of void fraction in bubble plumes. Some of the experimental results indicate that the void fraction profile follows Gaussian distribution (33, 34). Morton et al (35) have analysed the simple vertical round plume by making the simplifying assumption of uniform velocity profile within the plume. Results of their analysis are used here to make a qualitative assessment of the parameters that affect the interfacial area in the bubble column. Their analysis gave the following expression for the axial density variation:

$$g \frac{\rho_w - \rho_c}{\rho_w} = C \frac{B^{2/3}}{c_e^{4/3}} Z^{-5/3} \tag{2.53}$$

where

ρ_w = density of ambient water

ρ_c = density of the air–water mixture in the bubble column

B = initial specific buoyancy flux

Z = axial distance from the source or virtual origin

c_e = entrainment coefficient

C = constant

The initial specific buoyancy flux is given by

$$B = Q_a g (\rho_w - \rho_a)/\rho_w \tag{2.54}$$

ρ_a = density of air

The density of the air–water mixture in the bubble column is given by

$$\rho_c = (1-\alpha_c)\ \rho_w + \alpha_c\ \rho_a \tag{2.55}$$

Since $\rho_a << \rho_w$, the density of the air–water mixture can be written as

$$\rho_c = (1-\alpha_c)\ \rho_w \tag{2.56}$$

Assuming that the distance between the virtual plume origin and the air inlet is very small compared to Z and substituting for the buoyancy flux from equation (2.54) and the mixture density from equation (2.56) into equation (2.53), an expression for the void fraction in the strip is obtained as below:

$$g\alpha_c = C_3\ (Q_a\ g)^{2/3}\ Z^{-5/3} \tag{2.57}$$

or

$$\alpha_c = C_3\ \frac{Q_a^{2/3}}{g^{1/3}}\ Z^{-5/3} \tag{2.58}$$

where

C_3 = constant containing the entrainment coefficient

The above expression for α_c can be expressed in terms of the superficial air velocity in the tube as

$$\alpha_c \propto \left[\frac{J_a}{\sqrt{gD_p}}\right]^{2/3} \left[\frac{Z}{D_p}\right]^{-5/3} \tag{2.59}$$

$$\propto F_{dt}^{2/3} \left[\frac{Z}{D_p}\right]^{-5/3} \tag{2.60}$$

where

F_{dt} = tube Froude number based on the superficial air velocity and the tube diameter.

Now consider the term D_c. D_c is the diameter of the air filled portion of the bubble column at distance of Z from the origin. Morton et al (35) have shown that for simple plumes the width varies linearly with the distance from the virtual origin. Assuming a similar variation for the column diameter,

$$D_c = C_4\ Z \tag{2.61}$$

C_4 = constant

Next consider the mean bubble size d_{bc}. Neglecting the effects of the static pressure variations, the mean bubble size within the bubble column would be governed by the processes of bubble formation at the peripheral orifices and the bubble coalescence occurring as the bubbles rise through the tube and plume outside. For a given water quality and orifice configuration, these processes would depend on the air flowrate, void fraction, the distance of the strip from the origin, and the geometric configuration of the tube. Azbel (36) has shown that the mean bubble size in mass bubbling depends on the diffuser submergence and the void fraction. As seen from the equation (2.60), the void fraction depends on the tube Froude number F_{dt} and the distance Z. Thus the mean bubble size should depend on the Froude number F_{dt}, the distance Z and the geometric parameters of the tube namely the diameter ratio D_r and the length ratio L_r. The experimental results of Akita and Yoshida (37) also show the dependence of the mean bubble size in a bubble column on the Froude number based on the superficial gas velocity.

Considering the above, from dimensional considerations the following relationship is assumed for the bubble size:

$$d_{bc} \propto \left[\frac{Q_a}{U_c} \right]^{1/2} L_r^{\ a} \ D_r^{\ b} \tag{2.62}$$

where

U_c = mean velocity in the bubble column at distance of Z from the origin

As shown below, equation (2.62) is equivalent to assuming a functional relationship for the bubble size in terms of the Froude number, distance from the origin and the tube geometry.

The simple plume theory is again used here to express the mean velocity U_c in terms of the distance Z from the origin. The mean velocity in a plume can be expressed in terms of the initial buoyancy flux and the distance from the origin (35):

$$U_c = C_5 \ B^{1/3} \ Z^{-1/3} \tag{2.63}$$

where

C_5 = constant containing the entrainment coefficient

Substituting for the buoyancy flux in terms of the air flowrate from equation (2.54) into equation (2.63) and then substituting equation (2.63) into equation (2.62),

$$\frac{d_{bc}}{D_p} \propto \left[\frac{J_a}{\sqrt{gD_p}}\right]^{1/3} \left[\frac{Z}{D_p}\right]^{1/6} L_r^{\,a} D_r^{\,b} \qquad (2.64)$$

Thus it is seen that the equation (2.62) expresses the bubble size in terms of the Froude number, the distance Z and the tube geometric parameters.

Substituting for α_c, D_c and d_{bc} from equations (2.59), (2.61) and (2.62) into equation (2.52), we get the following expression for the interfacial area A_c:

$$A_c = C_6 \frac{Q_a^{1/3} Z^{1/6}}{g^{1/6}} L_r^{\,a} D_r^{\,b} \, dz \qquad (2.65)$$

where

C_6 = constant

Expressing the air flowrate Q_a in terms of the superficial air velocity J_a, the above expression becomes

$$A_c = C_7 \frac{J_a^{1/3} D_p^{2/3}}{g^{1/6}} L_r^{\,a} D_r^{\,b} Z^{1/6} \, dZ \qquad (2.66)$$

C_7 = constant

Parameters affecting K_l:

The liquid film coefficient K_l depends on the bubble size as indicated in the experimental results of Barnhart (2), Motarjemi et al (38) and Akita and Yoshida (37). In addition, K_l would also be influenced by the liquid phase diffusivity, liquid density, kinematic viscosity of the liquid and the rise velocity of the bubbles (37).

There exists considerable differences in the variation of K_l with bubble size reported in various studies. The results of Barnhart (2) and Motarjemi (38) show that K_l reaches a maximum value for the bubble size of about 2.2 mm whereas the results of Akita and Yoshida (37) show that in the bubble size range of 1 to 8 mm, K_l increases with the bubble diameter as $d_b^{1/2}$ (d_b = bubble diameter). The differences observed in these results appear to be mainly due to the differences in the flow field around the bubbles in these experiments. The experiments of Barnhart and Motarjemi were conducted with bubbles rising in nearly stagnant water with low void fractions whereas the experimental results of Akita and Yoshida pertained to mass bubbling in vertical bubble columns.

The surface renewal theory (39, 40) gives the following expression for K_l:

$$K_l \propto \sqrt{\frac{D_{ow}}{\tau}} \tag{2.67}$$

where

D_{ow} = molecular diffusivity of oxygen in water

τ = characteristic time constant

τ represents the average residence time for an element in the interfacial region (40). When the surface renewal is very quick, τ will be correspondingly small. τ would depend upon the characteristics of the flow around the bubble.

Considering a bubble in a turbulent flow field, let l be the size of the eddy causing the surface renewal. If we assume that the characteristic time constant can be approximated as the time scale of the boundary layer formed by the eddy, then τ can be expressed as

$$\frac{1}{\tau} \propto \frac{u_e}{\delta} \propto \frac{u_e}{l}\left[\frac{u_e l}{\nu}\right]^{1/2}$$

$$\propto \frac{u_e^{3/2}}{(l\nu)^{1/2}} \tag{2.68}$$

where

u_e = characteristic velocity of the eddy

ν = kinematic viscosity of the liquid

Azbel (36) has shown that K_l for mass transfer from bubbles in a bubble swarm can be expressed as

$$K_l = \frac{D_l^{1/2}}{4\pi}\frac{u^{3/4}}{(\ell\,\nu)^{1/4}}\frac{(1-\phi)^{1/2}}{(1-\phi^{5/3})^{1/4}} \tag{2.69}$$

where

ϕ = void fraction

D_l = molecular diffusivity of the gas in the liquid

u = velocity of large scale eddies

ℓ = size of largest eddies.

For low void fractions, the terms containing ϕ would be close to unity. Hence the above equation can be simplified as

$$K_l = \frac{D_l^{1/2}}{4\pi}\frac{u^{3/4}}{(\ell\,\nu)^{1/4}} \tag{2.70}$$

It can be seen that the time constant associated with expression (2.70) is identical to that given by expression (2.68).

The size of the largest eddies in the bubble column would be of the order of the column width and the eddy velocity would scale with the mean flow velocity.

$$u \propto U_c \tag{2.71}$$

The mean velocity in a plume can be expressed by equation (2.63) in terms of the initial buoyancy flux and the distance from the origin (35).

$$U_c = C_5 \, B^{1/3} \, Z^{-1/3} \tag{2.72}$$

Since the plume width varies linearly as the distance from the origin the eddy size can be expressed as

$$\ell = C_4 \, Z \tag{2.73}$$

Substituting for u and ℓ from equations (2.71), (2.72) and (2.73) into equation (2.70) and considering an air water system, we get

$$K_{lc} = C_8 \left[\frac{D_{ow}}{Z} \right]^{1/2} \left[\frac{B}{\nu_w} \right]^{1/4} \tag{2.74}$$

where

K_{lc} = mean liquid film coefficient for the strip

D_{ow} = molecular diffusivity of oxygen in water

ν_w = kinematic viscosity of water

Substituting for the buoyancy flux in terms of the superficial air velocity in the tube, the above expression becomes

$$K_{lc} = C_9 \frac{D_{ow}^{1/2} \, g^{1/4}}{\nu_w^{1/4}} \, D_p^{7/6} \, J_a^{1/4} \, Z^{-1/2} \tag{2.75}$$

C_9 = constant

Functional relation for K_lA:

Combining expressions (2.66) and (2.75) we get the following form of relationship for $K_{lc}A_c$.

$$K_{lc}A_c \propto \frac{D_{ow}^{1/2} \, g^{1/12}}{\nu_w^{1/4}} \, D_p^{7/6} \, J_a^{7/12} \, L_r^{a} \, D_r^{b} \, Z^{-1/3} \, dZ \tag{2.76}$$

To get the value of the K_1A for the entire plume, integrate the above expression from the inlet to the water surface.

$$K_1A \propto \frac{D_{ow}^{1/2}\, g^{1/12}}{\nu_w^{1/4}} D_p^{7/6}\, J_a^{7/12}\, L_r^{a}\, D_r^{b} \int_0^{H_s} Z^{-1/3}\, dz \tag{2.77}$$

$$\propto \frac{D_{ow}^{1/2}\, g^{1/12}}{\nu_w^{1/4}} D_p^{7/6}\, J_a^{7/12}\, L_r^{a}\, D_r^{b}\, H_s^{2/3} \tag{2.78}$$

The above expression can be grouped into dimensionless variables as below

$$\frac{K_1\ A}{J_a D_p^{\,2}} \propto \left[\frac{H_s}{D_p}\right]^{5/6} \left[\frac{D_{ow}}{\nu_w}\right]^{1/2} \left[\frac{\nu_w^{\,2}}{H_s^{\,3} g}\right]^{1/8} \left[\frac{H_s^{\,1/2} g^{1/2}}{J_a}\right]^{5/12} L_r^{\,a}\, D_r^{\,b} \tag{2.79}$$

or

$$S_{tm} \propto H_r^{5/6}\ S_c^{-1/2}\ G_a^{-1/8}\ F_s^{-5/12}\ L_r^{\,a}\ D_r^{\,b} \tag{2.80}$$

where

S_{tm} = modified Stanton number

$$= \frac{K_1\ A}{J_a D_p^{\,2}} \tag{2.81}$$

H_r = submergence ratio

$$= H_s/D_p \tag{2.82}$$

S_c = Schmidt number

$$= (\nu_w/D_{ow}) \tag{2.83}$$

G_a = Galileo number

$$= \frac{H_s^{\,3} g}{\nu_w^2} \tag{2.84}$$

F_s = submergence Froude number

$$= \frac{J_a}{\sqrt{gH_s}} \tag{2.85}$$

L_r = length ratio

$$= (L_e/D_p) \tag{2.86}$$

D_r = diameter ratio

$$= (D_p/D_{op}) \tag{2.87}$$

The proposed studies are planned for an air–water system only. Hence in this case, the Schmidt number will be a constant ($S_c \simeq 500$). Eliminating the Schmidt number, equation (2.80) can be written as

$$S_{tm} \propto H_r^{5/6} G_a^{-1/8} F_r^{-5/12} L_r^{a} D_r^{b} \tag{2.88}$$

Considering the assumptions made in the theoretical considerations, a functional relationship exactly the same as the above cannot be expected from the experimental results. The experimental results can be expected to have the following functional form:

$$\frac{K_l A}{J_a D_p^{2}} = f_1 (F_s, G_a, H_r, L_r, D_r) \tag{2.89}$$

The above analysis thus indicates that the experimental results can be expressed non–dimensionally in terms of the Stanton number, the Froude number, the Galileo number, the submergence ratio and the parameters defining the tube geometry.

The dependence of the mass transfer coefficient on the superficial gas velocity has been reported by several researchers. Yoshida and Akita (41) found the oxygen transfer coefficient in an aeration tower to be described in the form

$$K_lA = C_1 J_g^{0.7} \tag{2.90}$$

where

J_g = the superficial gas velocity.

Similar results have also been reported by Murphy et al (42), Blanco et al (43) and Hatch (44) with the exponents varying from 0.5 to 1.

Developing a correlation for the Stanton number in the form given by equation (2.89) was one of the objectives of the experimental study.

Such a correlation can be used to estimate K_lA for different diffuser submergences as well as tube dimensions. Also an estimate of K_lA_t can be obtained by substituting the value of the appropriate air flowrate and the submergence ratio corresponding to the top of the tube in the correlation.

2.4 EXPERIMENTAL OBJECTIVES

Based on the theoretical considerations dealt with above, experimental studies in an air–water system were planned with the following objectives:

a) To determine an expression for the unknown loss term K_{fb} in the form given by equation (2.30)
b) To evolve the empirical relationship for the void fraction in the tube given by equation (2.39)
c) To study the effect of the following parameters on the mass transfer coefficient K_lA of the SAF diffuser.
   - Number of orifices
   - Tube geometry
   - Air flowrate
   - Diffuser submergence
d) To evolve the correlation given by equation (2.89) for the mass transfer coefficient K_lA
e) To select an optimum configuration of the SAF diffuser and assess its performance characteristics in terms of the Standard Oxygen Transfer Rate and the Standard Aeration Efficiency.

Chapter 3

Experimental Studies - I
Air-Water Flow in the Tube

3.1 OBJECTIVE

The objective of these studies was to develop empirical correlations of the form given by equations (2.30) and (2.39) which could be used to predict the mean phase velocities and the mean void fractions for a family of tubes over a wide range of air flowrates in the bubbling regime.

3.2 THE EXPERIMENTAL FACILITY

Figure (3.1) shows the details of the experimental facility (45). The facility essentially comprised a large tank filled with water at the center of which the tube under study was mounted. Air was injected into the tube through peripheral orifices located near the inlet end. The air was drawn from the laboratory air supply through a piping system comprising an air filter, pressure regulator, surge chamber, rotameter, pressure and temperature indicators and needle valve.

The studies were proposed on tubes of different diameters and lengths as shown in table 3.1. The tubes of diameters up to 1.6 cm were studied in a tank of size 0.45 m x 0.45 m x 0.65 m (height). The larger tubes were studied in a tank of size 1.2 m x 1.2 m x 1.4 m (height).

The experimental procedure essentially comprised adjusting the air flowrate through the device using the rotameter and the needle valve and then measuring the mean water flowrate and the mean void fraction of the induced flow through the device. The water depth up to the air inlet into the tube was kept at 0.5 m for all the tubes. Each tube was tested up to a maximum air flowrate which corresponded to about 1.4 to 3.6 cc/s per orifice depending upon the design. The diameter of the peripheral orifices was 1 mm. The water temperature was maintained at 20° C (± 2° C). The temperature of air in the supply tube varied between 18° C and 22° C.

Special arrangements were made for the measurements of the mean water flowrate through the tube and the mean void fraction in the tube. These arrangements are described below.

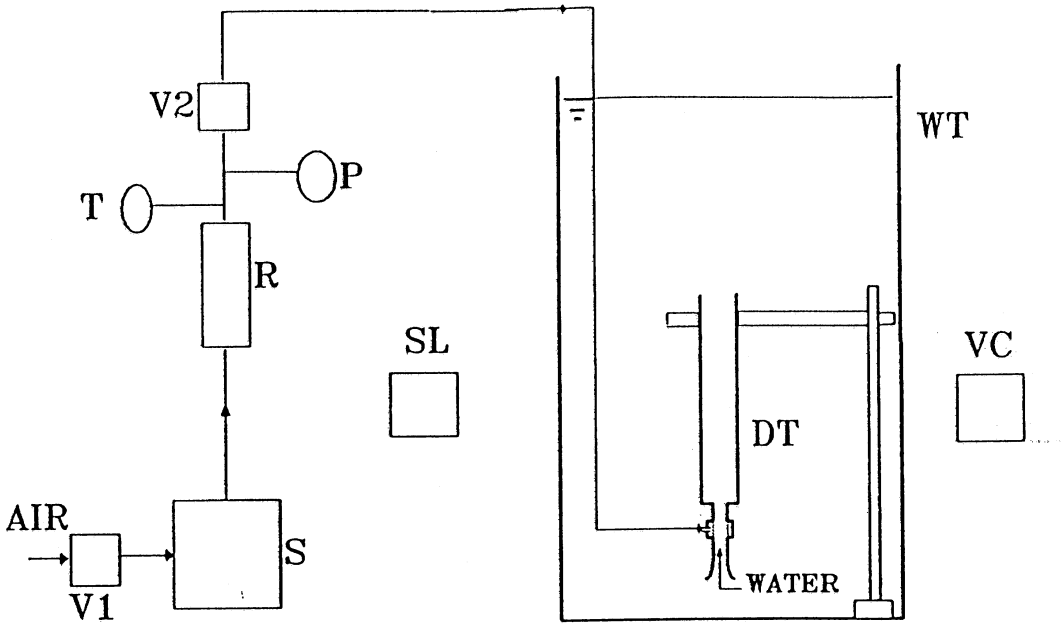

V1–PRESSURE REGULATOR
V2–NEEDLE VALVE
S–SURGE CHAMBER
DT–DRAFT TUBE
T–TEMPERATURE INDICATOR
WT–WATER TANK
R–ROTAMETER
VC–VIDEO CAMERA
P–PRESSURE INDICATOR
SL–STROBOSCOPE

Fig. 3.1 Details of experimental facility

Table 3.1

Details of Tubes Studied

Note:
Qam = Maximum air flowrate
Nop = Number of peripheral orifices
Orifice dia. = 1 mm

Design	Dop cm	Dp cm	Le cm	Dr	Lr	Nop	Qam/Nop
A	1.1	1.1	18.92	1.0	17.2	32	1.44
B	1.1	1.1	26.54	1.0	24.13	32	1.63
C	1.1	1.265	19.05	1.15	15.06	32	1.65
D	1.1	1.265	26.58	1.15	21.01	32	1.65
E	1.1	1.605	18.49	1.46	11.50	32	1.65
F	1.1	1.605	26.1	1.46	16.26	32	1.65
G	5.17	5.17	29.82	1.0	5.76	108	3.62
H	5.79	5.79	25.0	1.12	4.31	108	3.62
I	5.79	5.79	36.2	1.12	6.25	108	3.06

Mean water flowrate through the tube

Figure (3.2) shows the arrangement for the measurement of the mean water flowrate. The arrangement consisted of an inner tank and an outer tank. The tube under study was mounted at the bottom of the inner tank. Air water mixture from the tube would discharge into the inner tank. Water from the inner tank would be pumped back into the main (outer) tank through a circulating pipe housing a flowmeter for measurement of the water flowrate. For each experimental condition, the valve in the circulating pipe would be throttled so as to maintain the same water level in the inner and the outer tanks and the corresponding water flowrate would be equal to the mean water flowrate through the tube. In order to ensure that the introduction of the inner tank did not alter the flow through the tube, pressures at two locations were measured in two of the tubes by operating the tubes in the outer tank without the inner tank and it was verified that the same pressures were obtained while measuring the flow through the tubes by mounting them in the inner tank.

Mean void fraction

The volumetric mean void fraction in the tube was measured using a quick shut–off valve. Figure (3.3) shows the details of the shut off valve. The valve consisted of a spring actuated rotating arm mounted over a fixed base. The rotating arm was supported by a trigger. The outlet end of the tube under study was connected air tight to a matching opening provided in the body of the fixed base. The air supply tube also passed through a hole provided in the body of the fixed base. With the rotating arm supported by the trigger, a portion of the air supply tube (in the immediate upstream vicinity of the location where it passed through the fixed base) is juxtaposed in the clearance between the rotating arm and a fixed solid block. The rotating arm was mounted in such a way that on releasing the trigger the arm would swing over the outlet end of the tube and close the tube, and at the same time press the air inlet tube against the solid block thereby simultaneously shutting off the air supply. The void fraction would be equal to the ratio of the volume of air entrapped inside the tube upon closure of the valve to the volume of the tube above the air inlet.

Two such valves were used in the study, one for the smaller tubes up to 1.6 cm dia and the other for the larger tubes detailed in the table 3.1. The shut off time of the valve measured in air was in the range of 13 to 15 milliseconds.

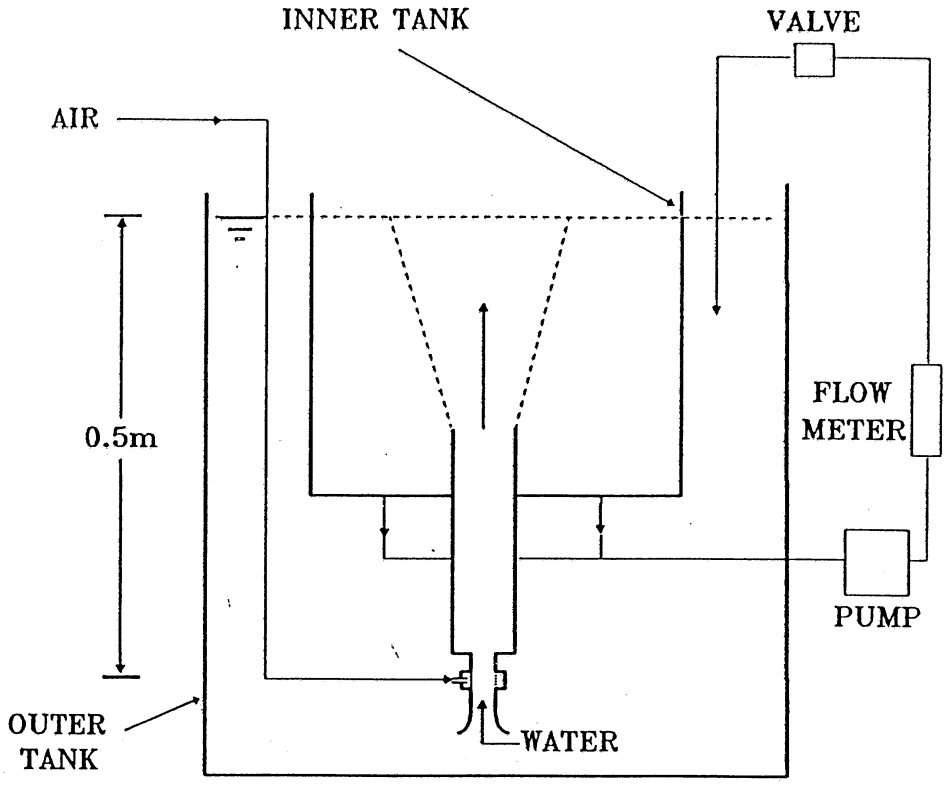

Fig. 3.2 Arrangement for measurement of water flowrate

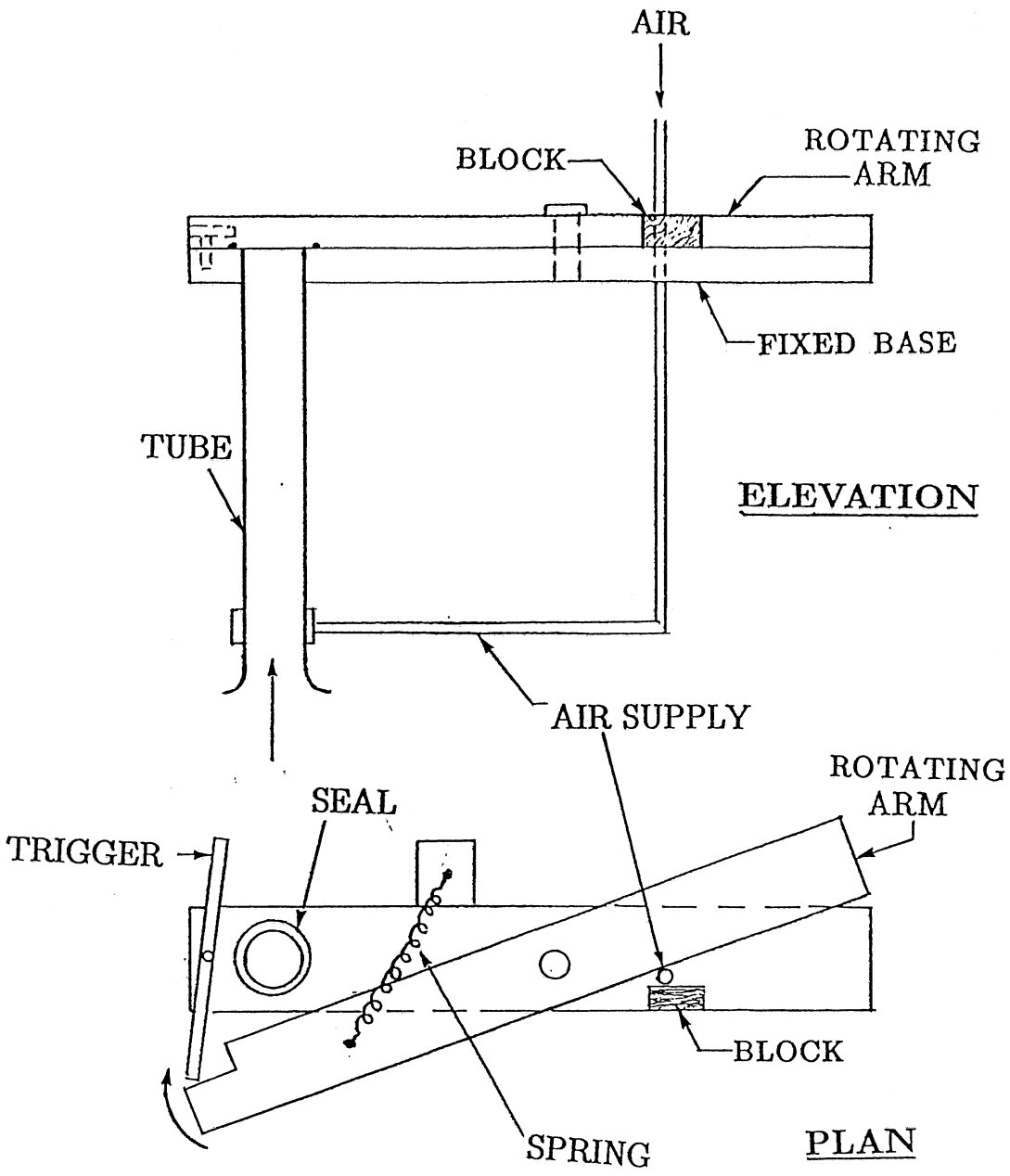

Fig. 3.3 Valve for measurement of void fraction

Mean velocities in the tube

From the measured values of the the mean water flowrate Q_w and the mean void fraction α, the mean water and air velocities were calculated using the relationships given below:

A_p = cross sectional area of the tube
$= (\pi/4)\ D_p^2$

A_{op} = cross sectional area of the tube inlet
$= (\pi/4)\ D_{op}^2$

J_w = superficial water velocity
$= Q_w/A_p$ (3.1)

V_w = mean water velocity in the tube
$= J_w/(1-\alpha)$ (3.2)

V_o = mean water velocity in the tube inlet u/s of the orifices (termed as orifice water velocity in the text)
$= Q_w/A_{op}$ (3.3)

J_a = superficial air velocity in the tube
$= Q_a/A_p$ (3.4)

V_a = mean air velocity in the tube
$= J_a/\alpha$ (3.5)

3.3 EXPERIMENTAL RESULTS AND DISCUSSIONS

The experimental results are shown in Appendix B and figures 3.4 through 3.18.

Figures 3.4 through 3.8 show the water flowrates through the tubes. As the air flowrate was increased, the water flowrate increased, the rate of increase of the water flowrate decreasing with the increase in the air flowrate until the water flowrate reached an asymptotic maximum. The experiments were stopped at this upper limit of the water flowrate. For all the cases, the tubes with larger diameter ratios were found to have larger water flowrate for a given air flowrate. Also the water flowrate was higher for the longer tubes.

The results of the void fraction measurements are shown in the figures 3.9 through 3.13. The void fraction increased with the increase of the air flowrate and decreased with the increase of the diameter ratio. The void fraction decreased as the length of the tube was increased.

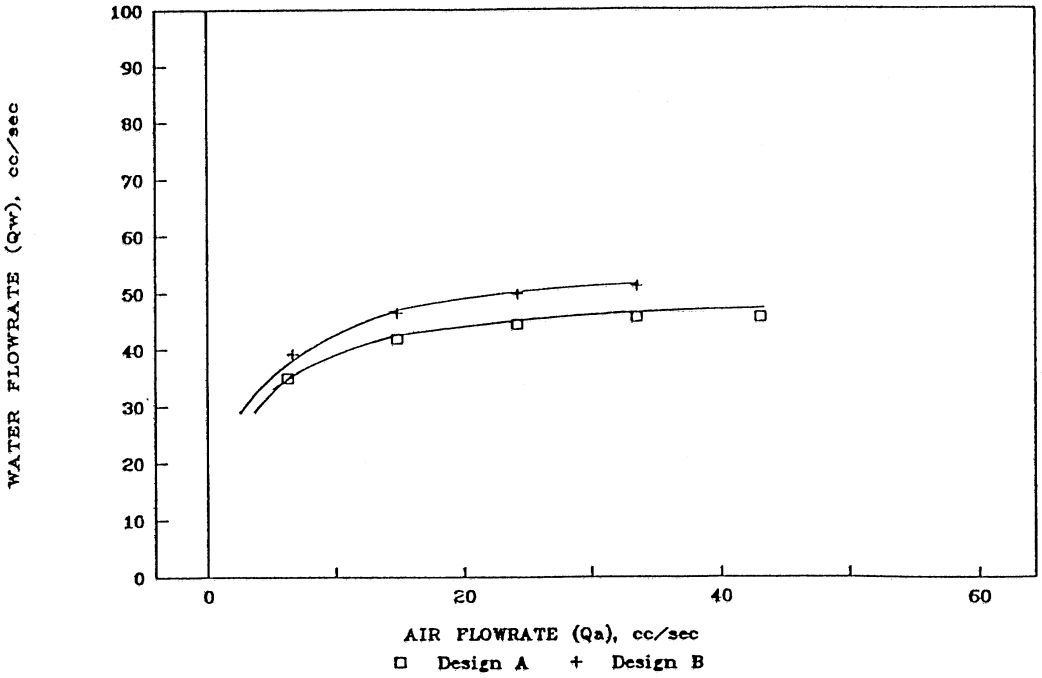

Fig. 3.4 Water flowrate versus air flowrate (Designs A & B)

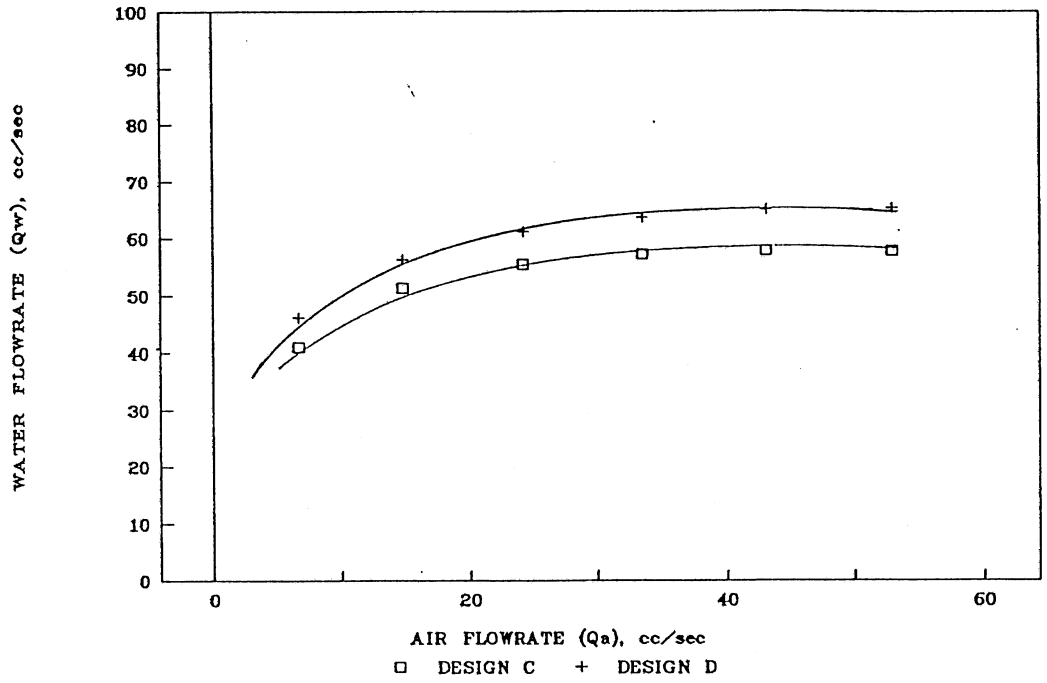

Fig. 3.5 Water flowrate versus air flowrate (Designs C & D)

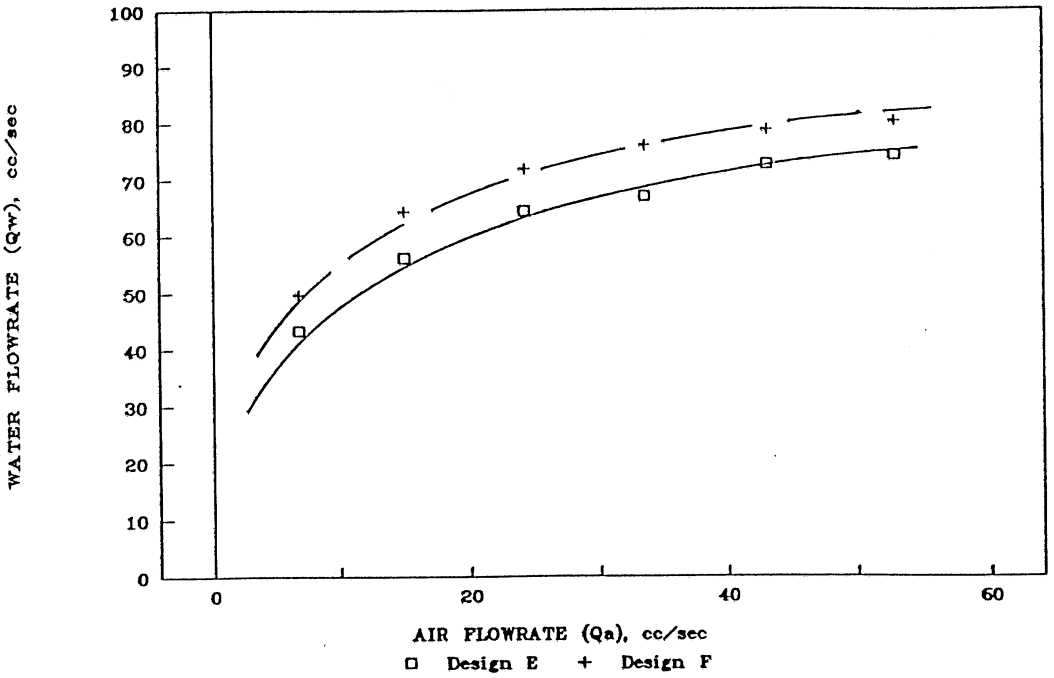

Fig. 3.6 Water flowrate versus air flowrate (Designs E & F)

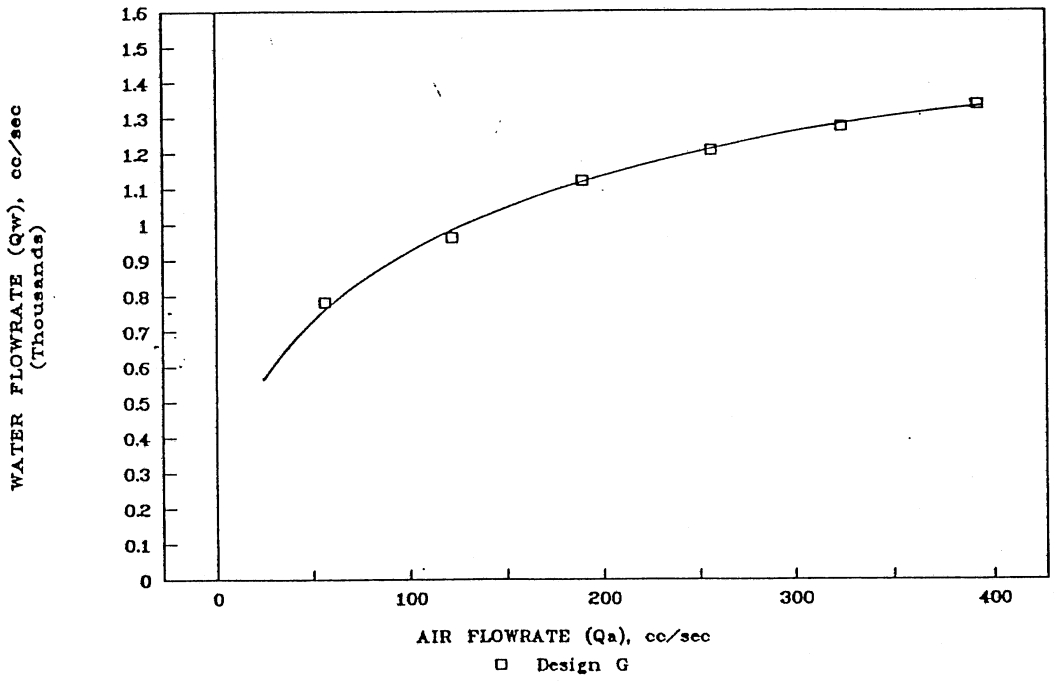

Fig. 3.7 Water flowrate versus air flowrate (Design G)

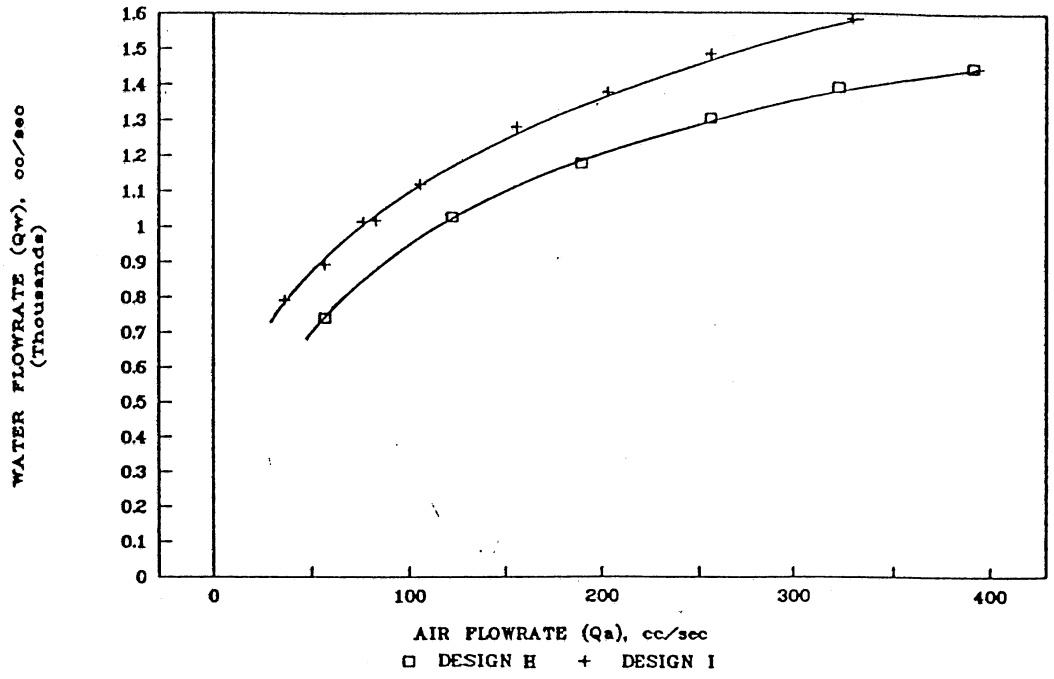

Fig. 3.8 Water flowrate versus air flowrate (Designs H & I)

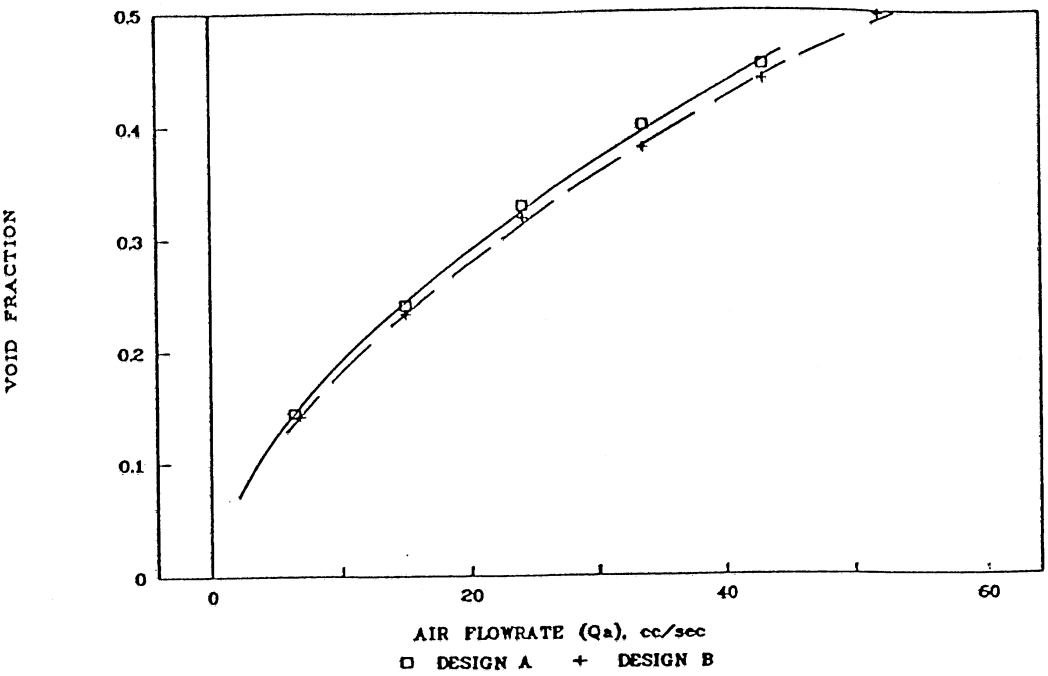

Fig. 3.9 Void fraction versus air flowrate (Designs A & B)

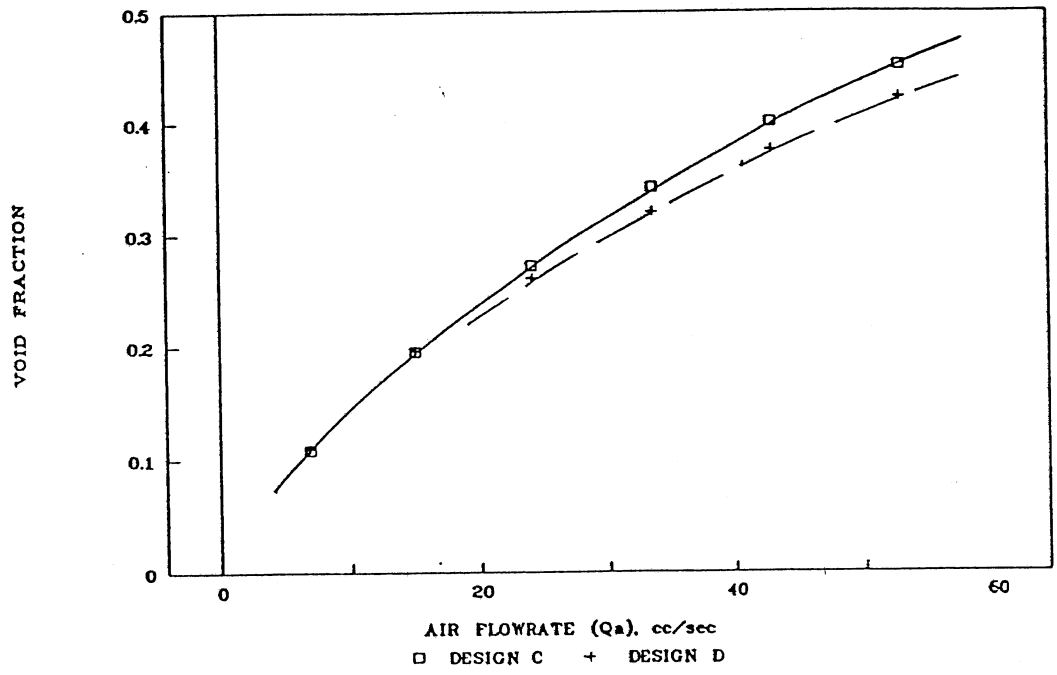

Fig. 3.10 Void fraction versus air flowrate (Designs C & D)

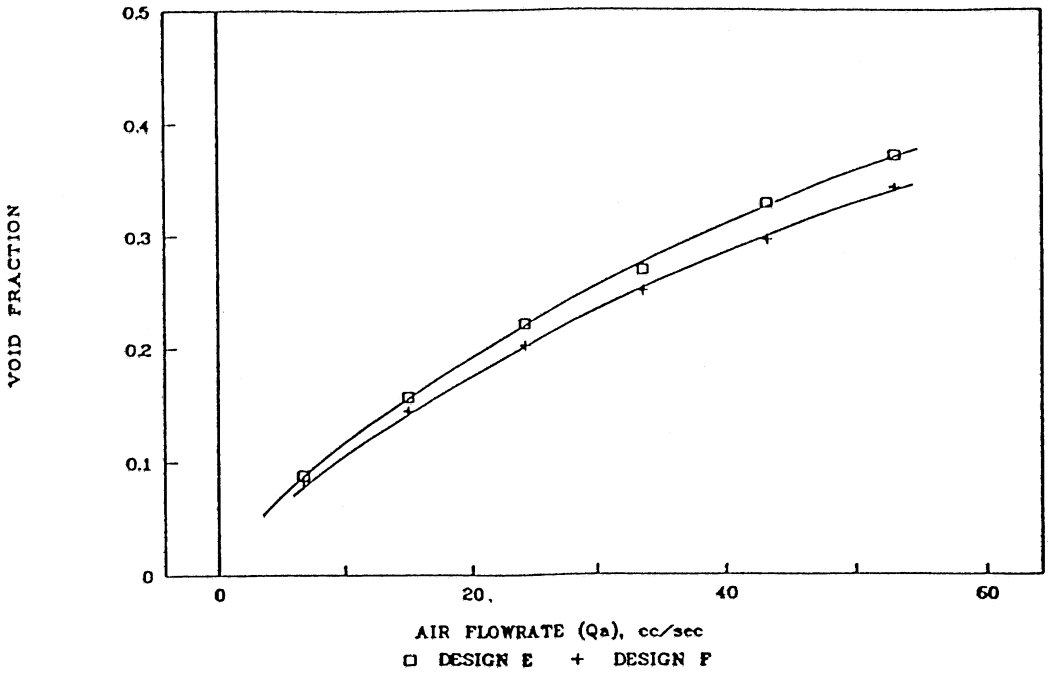

Fig. 3.11 Void fraction versus air flowrate (Designs E & F)

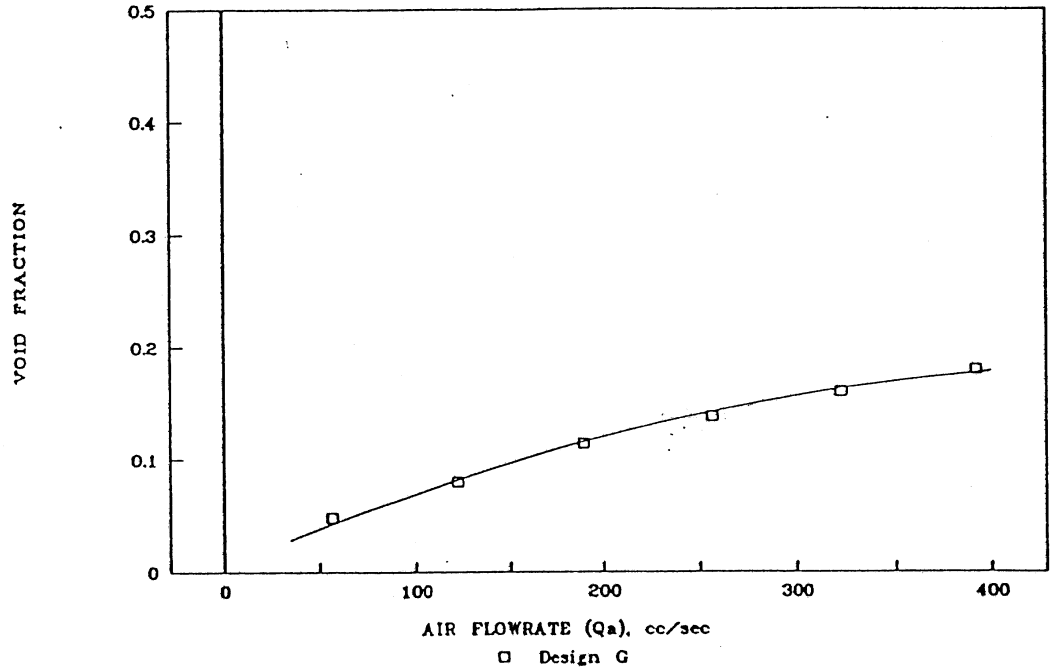

Fig. 3.12 Void fraction versus air flowrate (Design G)

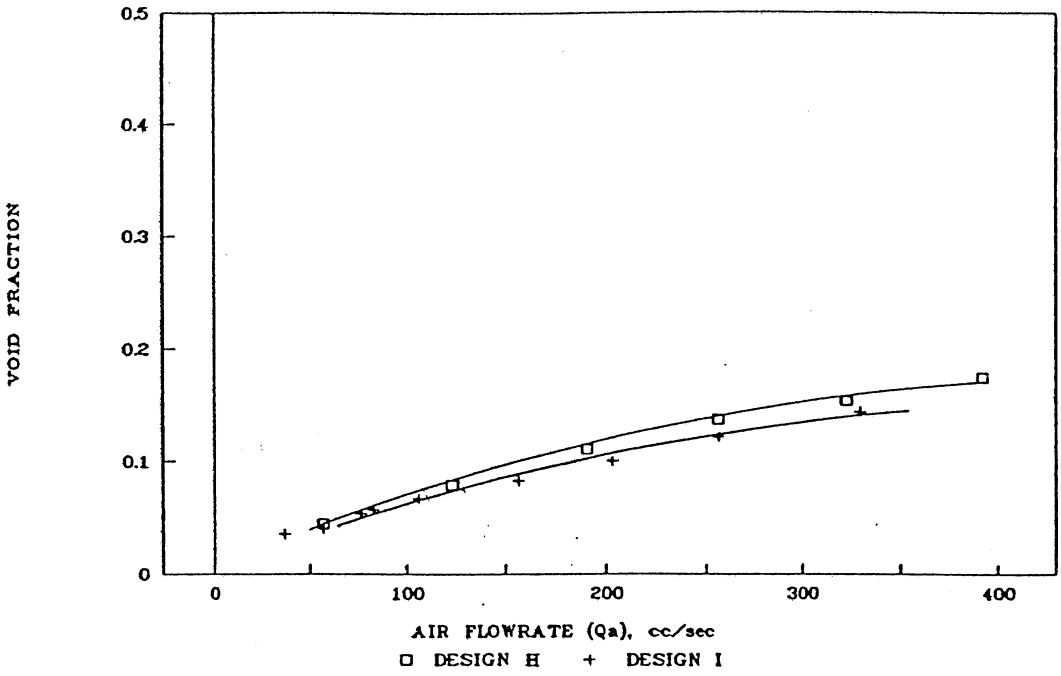

Fig. 3.13 Void fraction versus air flowrate (Designs H & I)

Figures 3.14 through 3.18 show the water velocities in the tube V_w, calculated from the measured water flowrates and void fractions using equations (3.1) and (3.2). The water velocity increased with the increase of the air flowrate and the tube length. For a given air flowrate, the water velocity decreased as the diameter ratio was increased.

Using the values of the water velocities in the tube, the Froude number defined by equation (2.21) was calculated for each experimental point. The ideal flow Froude number for each experimental point was also calculated from the experimental values of the void fraction using the ideal chimney equation (equation 2.19). Figure 3.19 shows the comparison of the ideal flow Froude number with the real flow values. The difference between the ideal chimney equation and the experimental values arises out of the energy losses in the tube.

As outlined in Chapter 2, in order to incorporate the losses in the equation (2.21), an expression for the loss term K_{fb} was required. The experimental data was used to calculate the loss term K_{fb} using the equations (2.21) through (2.24) and equation (2.29) and an empirical functional relationship of the form (2.30) was established through multiple regression. This yielded the following expression with a coefficient of determination $r^2 = 0.964$ and a standard error of 0.22 (number of observations = 56; degrees of freedom = 51) (see figure 3.20):

$$K_{fb} = 0.354\ \alpha^{-0.026}\ (1-\alpha)^{-0.724}\ D_r^{1.969}\ L_r^{0.561} \tag{3.6}$$

Substituting for K_{fb} from equation (3.6) into equation (2.21), we get the following relation for the tube Froude number F_{rw}:

$$F_{rw} = \frac{V_w}{\sqrt{L_e g}} = \left[\frac{2\alpha}{(1-\alpha)(1+K_e+K_{ex}+K_{fb})}\right]^{0.5} \tag{3.7}$$

where

$$K_{fb} = 0.354\ \alpha^{-0.026}\ (1-\alpha)^{-0.724}\ D_r^{1.969}\ L_r^{0.561}$$

Equation (3.7) expresses the water velocity in the tube in terms of the void fraction and the tube geometry. Figure 3.21 shows the plot of equation (3.7) alongwith the experimental data.

The experimental data on void fraction was analyzed to evolve a functional relationship of the form given by equation (2.39) for the mean void fraction in the tube. The analysis yielded the following empirical relation with a coefficient of determination $r^2=0.997$ and a standard error of 0.008 (number of observations = 56; degree of freedom = 52):

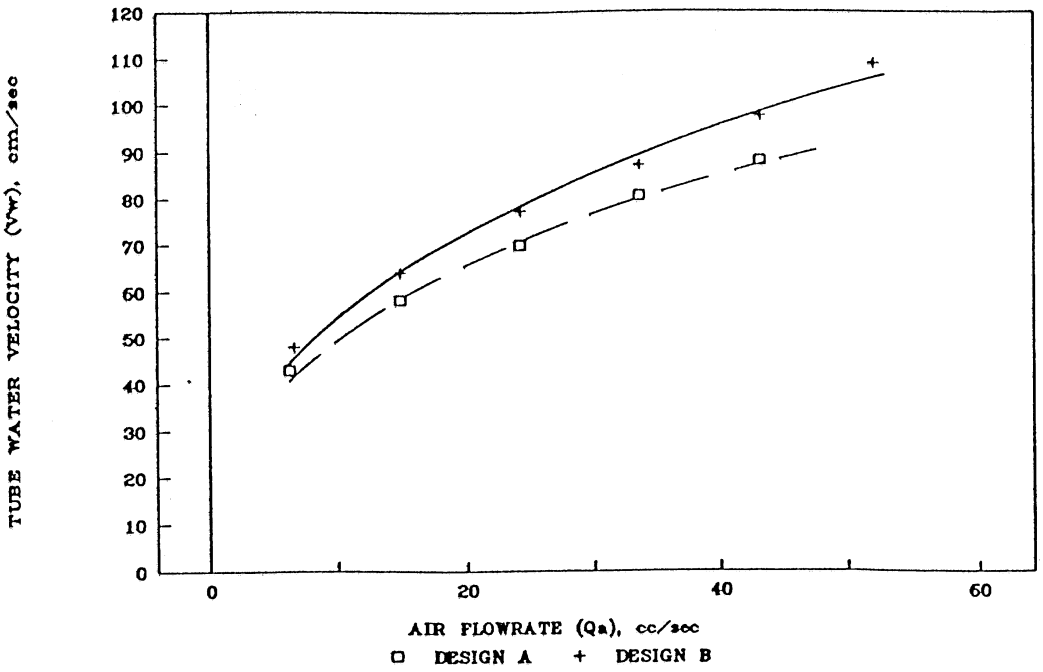

Fig. 3.14 Tube water velocity versus air flowrate (Designs A & B)

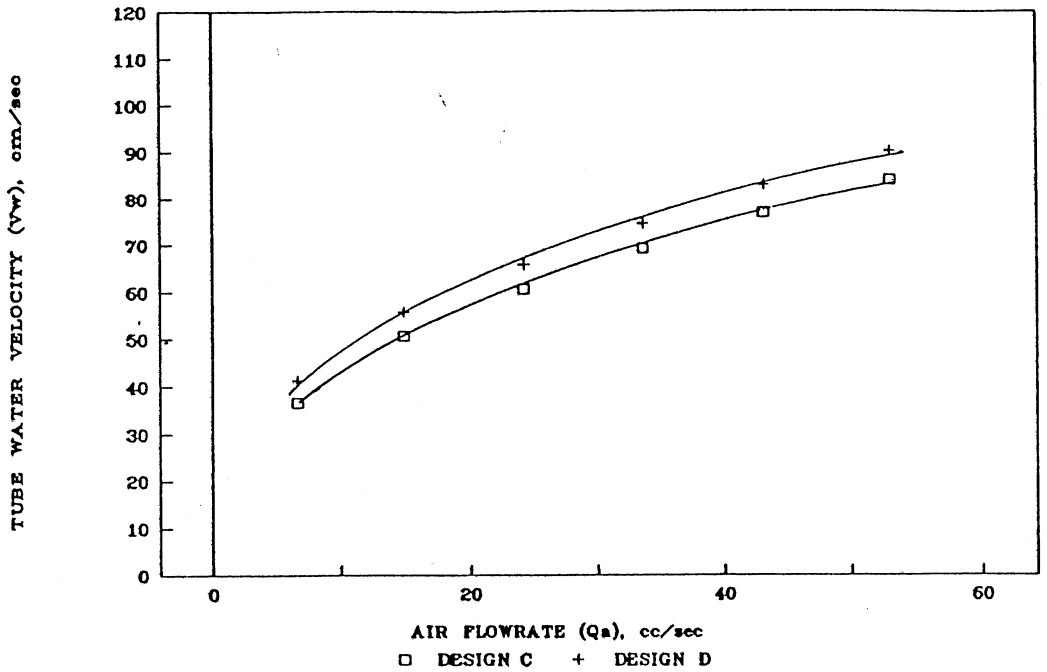

Fig. 3.15 Tube water velocity versus air flowrate (Designs C & D)

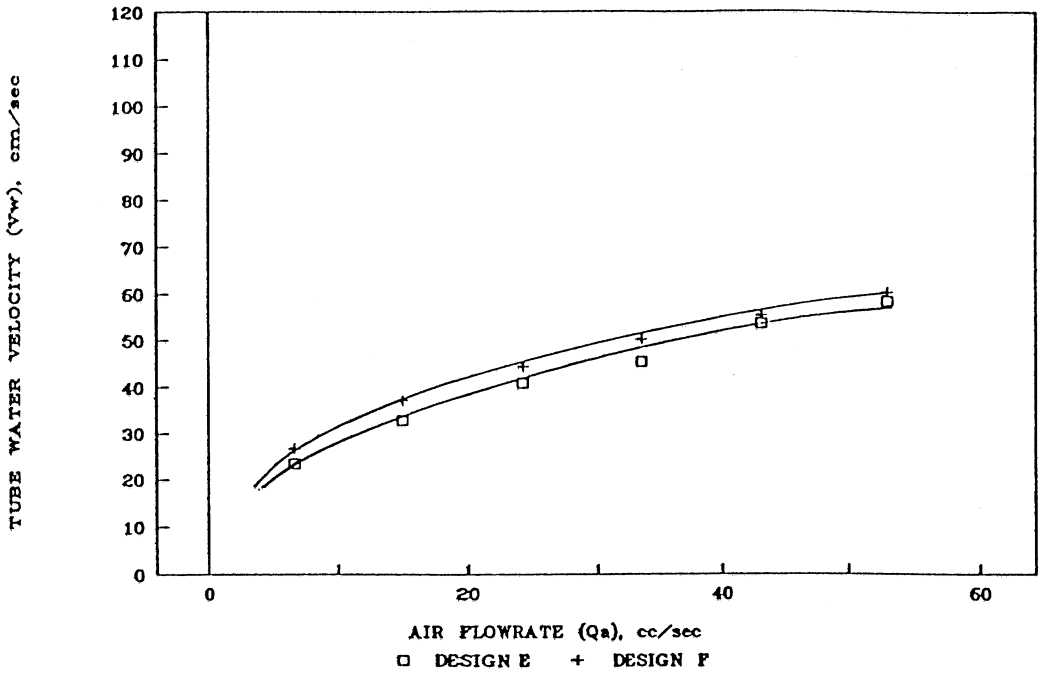

Fig. 3.16 Tube water velocity versus air flowrate (Designs E & F)

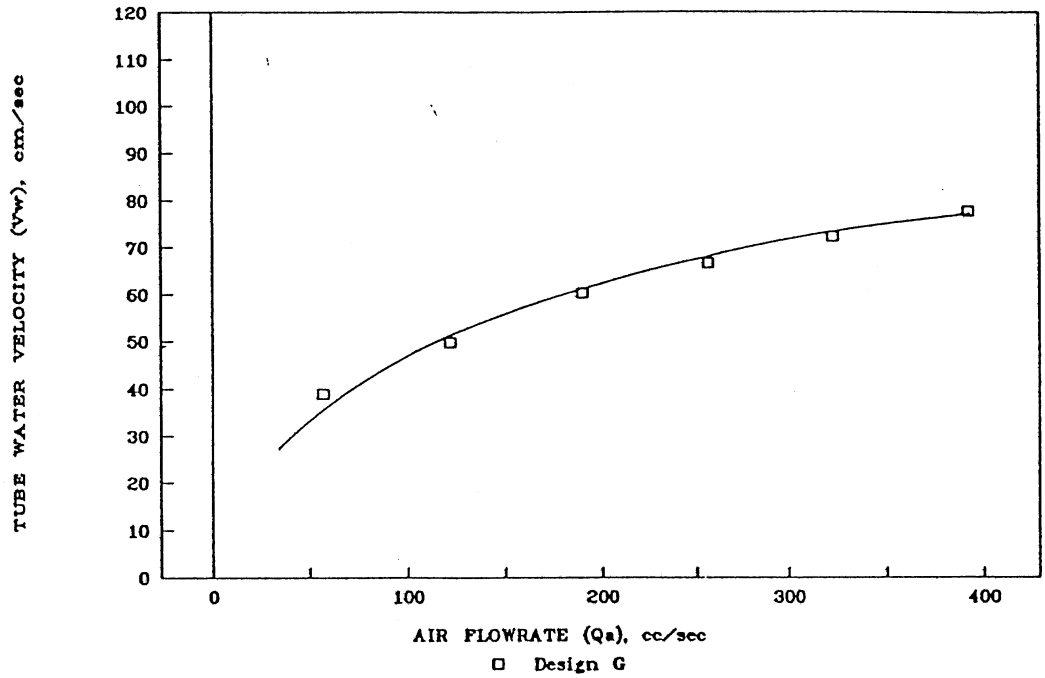

Fig. 3.17 Tube water velocity versus air flowrate (Design G)

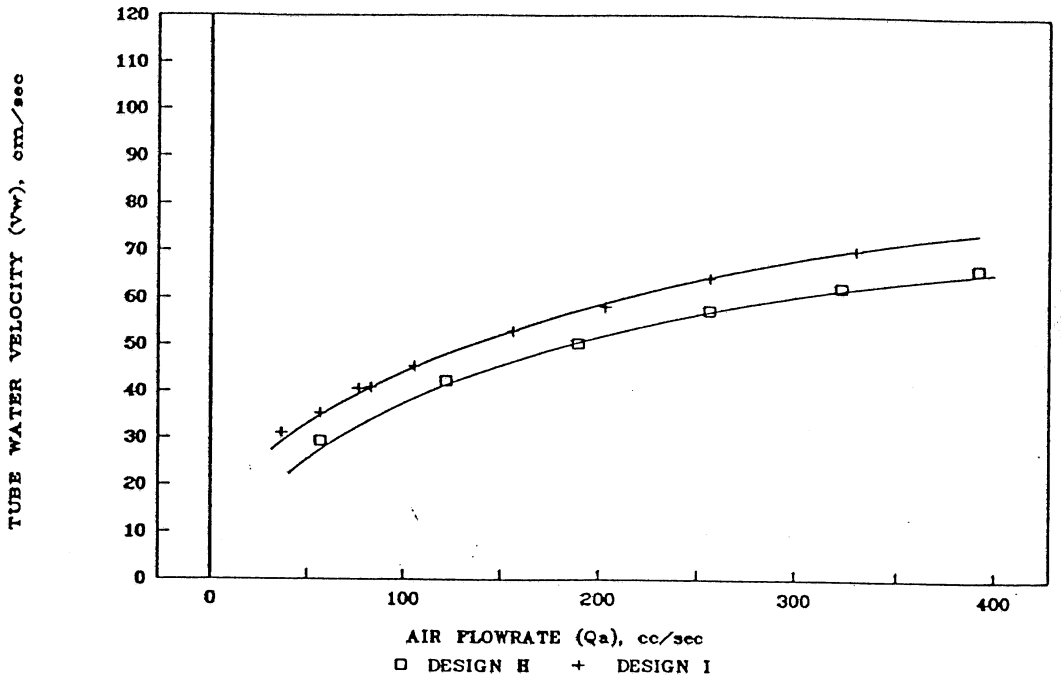

Fig. 3.18 Tube water velocity versus air flowrate (Designs H & I)

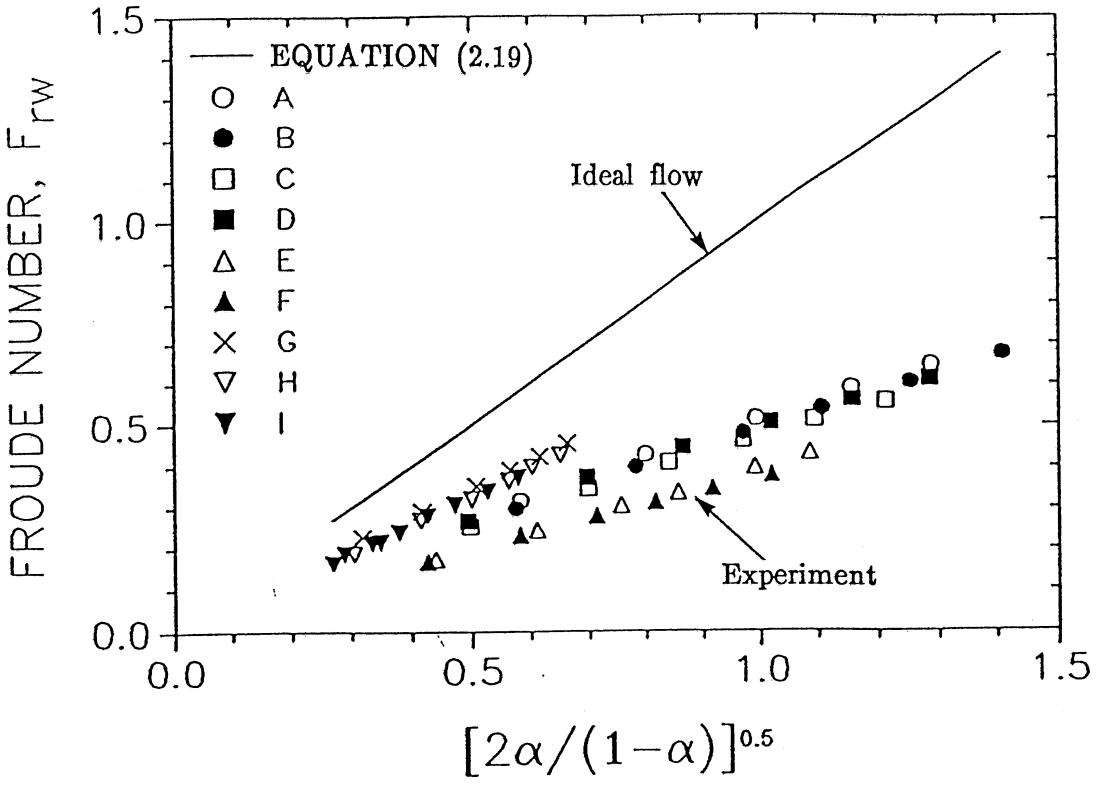

Fig. 3.19 Comparison of ideal flow Froude number and experimental values

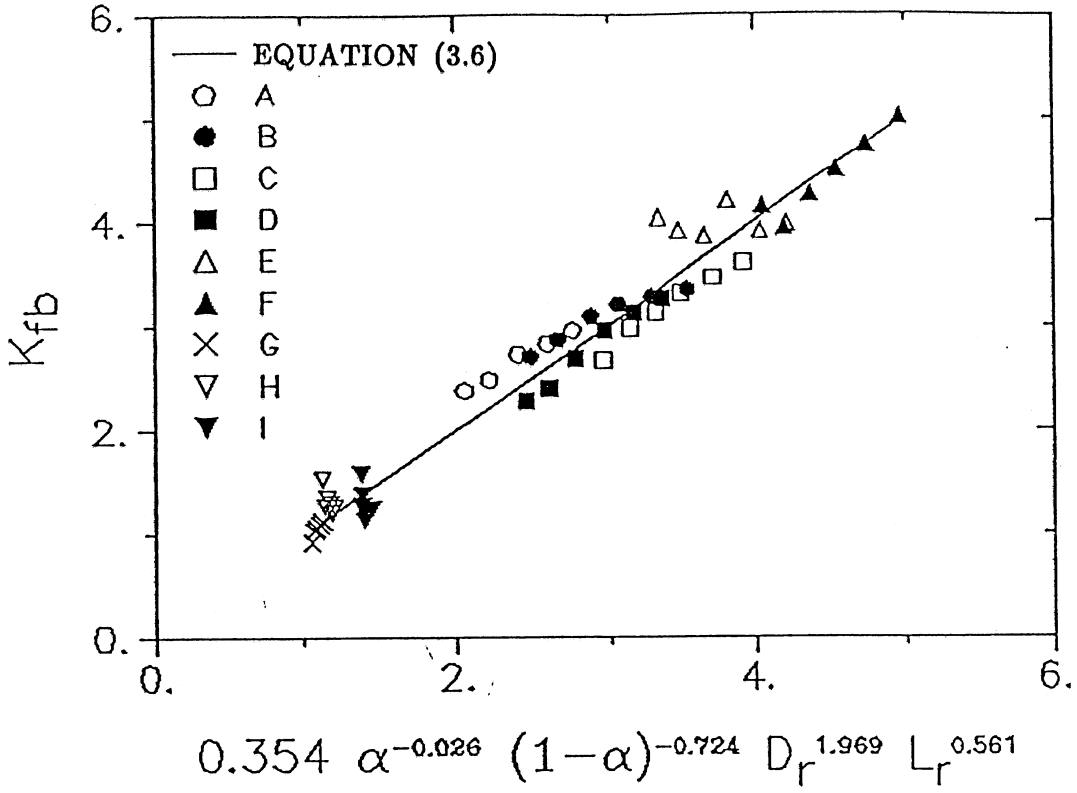

Fig. 3.20 Experimental correlation for K_{fb}

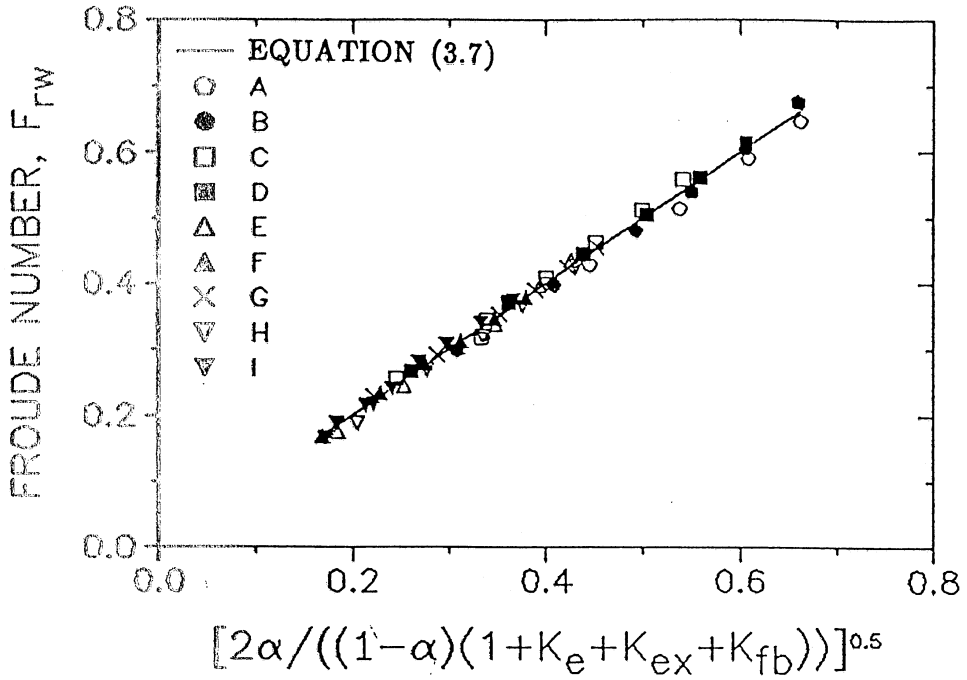

Fig. 3.21 Experimental correlation for Froude number

$$\alpha = 0.603 \left[\frac{J_a}{\sqrt{L_{eg}}}\right]^{0.67} D_r^{0.419} L_r^{0.176} \qquad (3.8)$$

Equation (3.8) and the experimental data are plotted in figure 3.22. Using the equations (3.7) and (3.8), the mean water velocities and void fractions in the tube for given air flowrate and tube dimensions can be determined.

A detailed study of the bubble size in the tube and in the plume was not envisaged as part of this study. Based on a few video shots and visual observations, the bubbles in the tube were estimated to be in the size range of about 1.5 mm to 5 mm with the mean bubble size in the range of 2 to 3 mm.

From the figures 3.9 through 3.11, it is seen that the void fractions in the small tubes (designs A, B, C, D, E and F) reached values as high as 40 to 50 per cent, the smaller tubes being associated with larger void fractions. The flow in these tubes was in the bubbly flow regime for all these void fractions. For low void fractions the bubbles rose along the wall of the tube and as the void fraction increased, the bubbles gradually filled the central portions of the tube. In the larger tubes (designs G, H and I) the void fractions were relatively low, reaching a maximum of about 18 per cent. The flow in these tubes was also in the bubbly flow regime. The bubbles in these tubes rose close to the tube walls for all the void fractions, giving rise to large void fraction peaks near the wall.

The studies covered a Reynolds number range of 4000 to 36000 as shown in the figures 3.23 and 3.24. The Reynolds number is based on the superficial water velocity through the tube and is defined as below:

$$R_{ew} = (J_w D_p)/\nu_w \qquad (3.9)$$

where

ν_w = kinematic viscosity of water

The correlations given by equations (3.6), (3.7) and (3.8) were used to analyze the variations of the flow velocities and void fractions in a composite draft tube which was proposed to be used later for detailed experimental studies of oxygen transfer in water. The tube had an inlet diameter of 5.8 cm. The main reasons for selection of this tube size were that first, it was a reasonable size for many practical applications and second, its ready availability. The results of the analysis are presented in figures 3.25 through 3.30.

Figure 3.25 shows the variation of the tube water velocity with the tube length for a given air flowrate. The tube water velocities increased with increase in the tube length and decreased with increase in the diameter ratio.

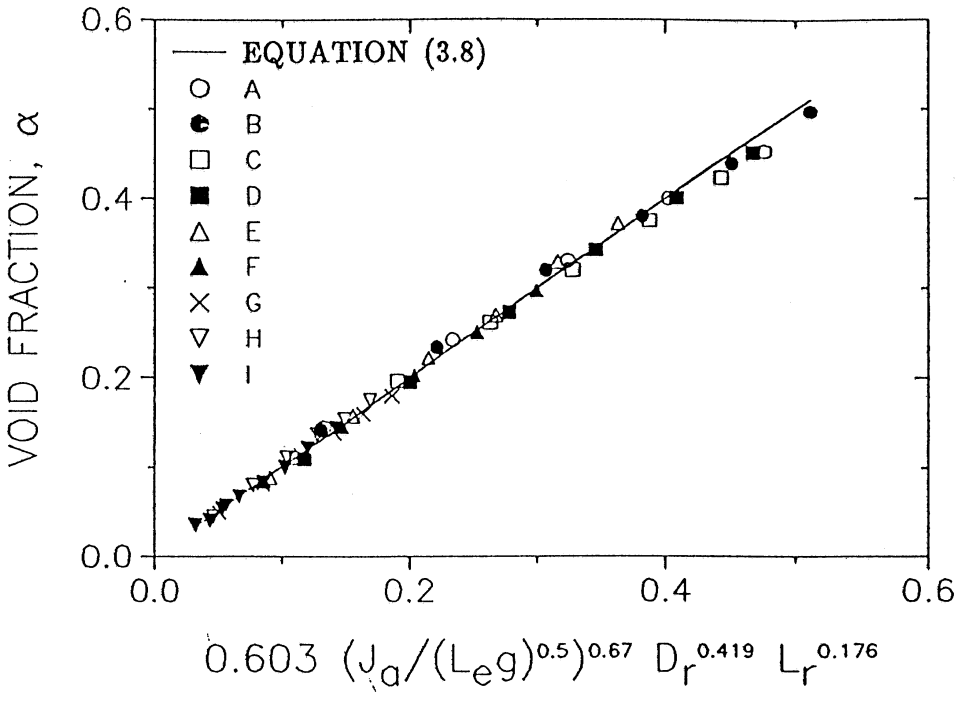

Fig. 3.22 Experimental correlation for void fraction

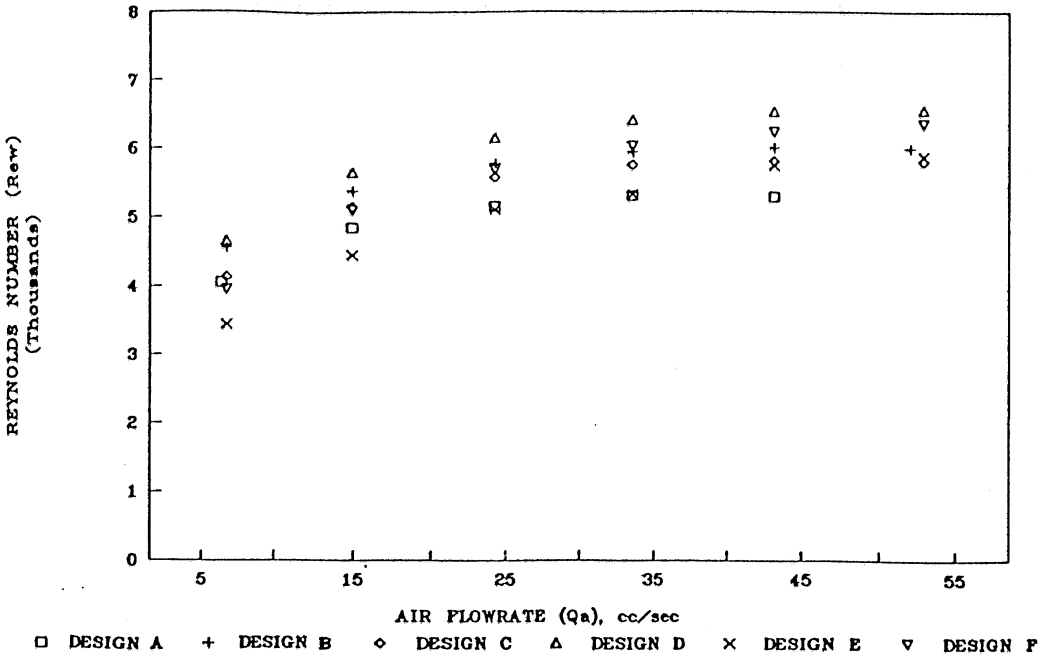

Fig. 3.23 Reynolds number versus air flowrate

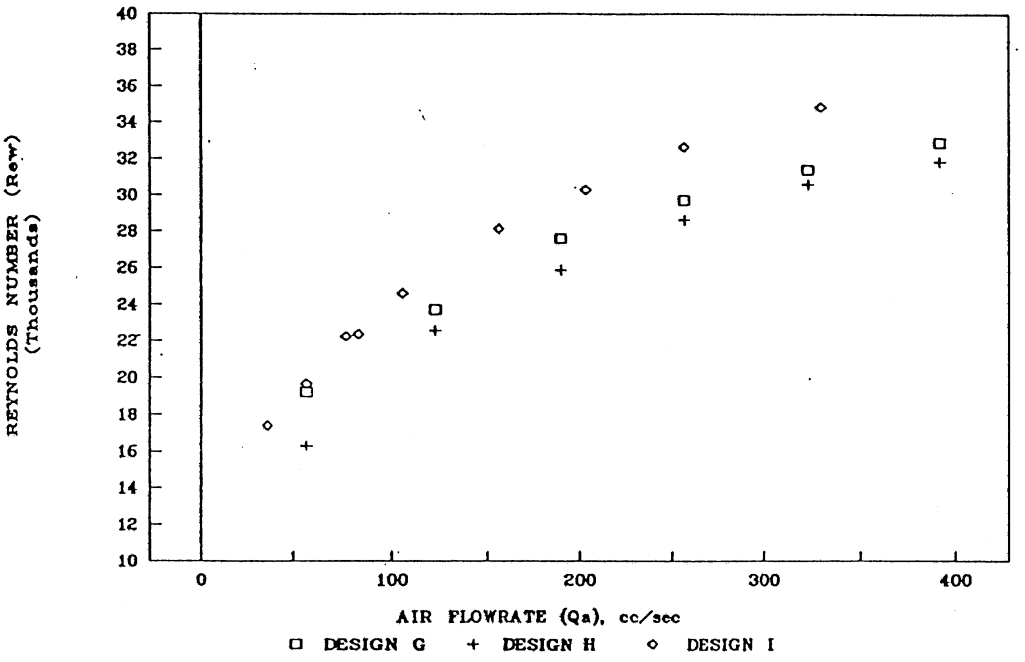

Fig. 3.24 Reynolds number versus air flowrate

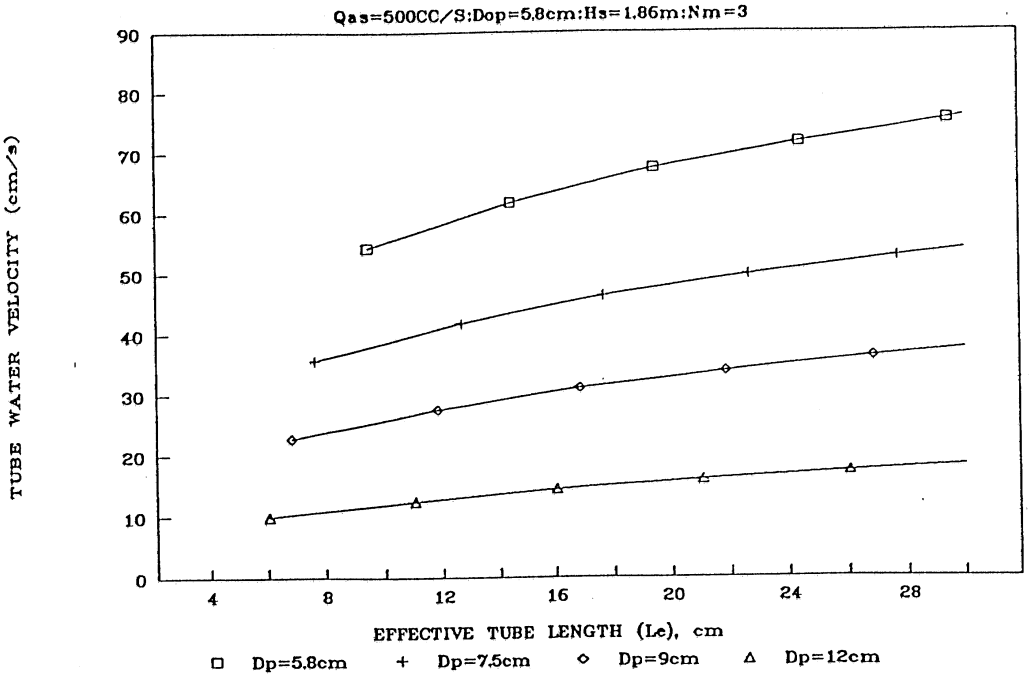

Fig. 3.25 Computed tube water velocity versus tube length (Eq.3.6,3.7,3.8)

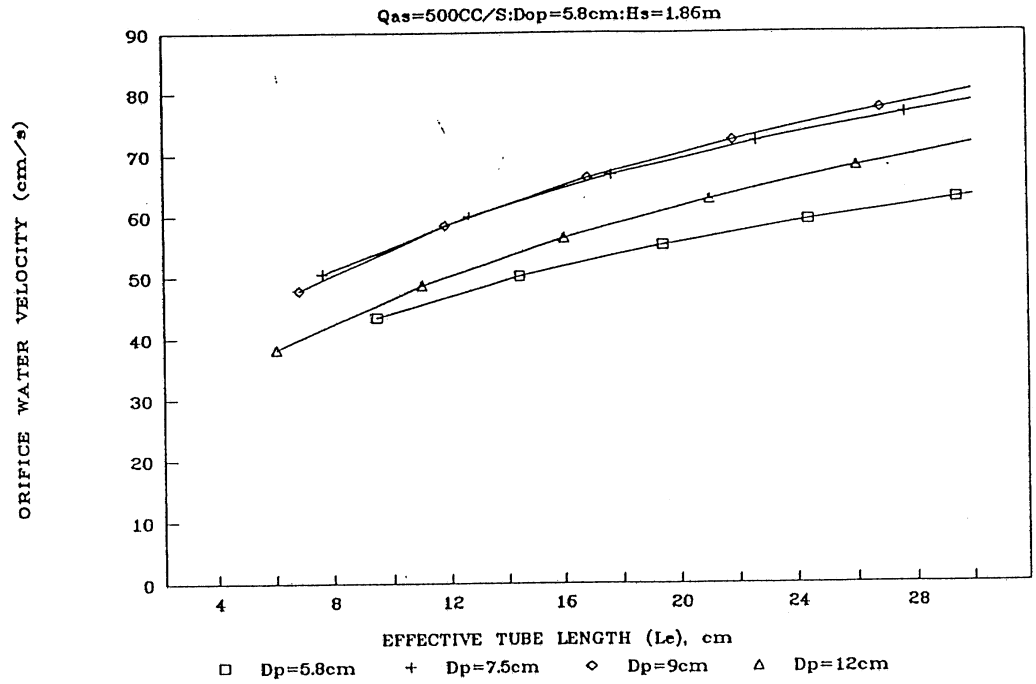

Fig. 3.26 Computed orifice water velocity versus tube length (Eq.3.6,3.7,3.8)

r the straight tube ($D_r = 1$), the induced water velocity in the tube was in the range of 55 to 75 cm/s. As the diameter ratio was increased, this velocity gradually decreased to reach values of 10 to 15 cm/s for the diameter ratio of 2.07. Thus we see that for a given air flowrate, increasing the diameter ratio resulted in the decrease of the water velocity in the tube.

Figure 3.26 shows the variation of the orifice water velocity with the tube length and the tube diameter. The orifice water velocities increased as the tube length was increased. However, as the tube diameter was increased, the orifice water velocity increased to reach a maximum and then decreased. This trend was the same for all the tube lengths.

Figure 3.27 shows the variation of the void fraction in the tube with the tube length and the tube diameter. The void fraction decreased as the tube length or the tube diameter was increased.

Figure 3.28 shows the variation of the tube water velocity, the orifice water velocity and the void fraction in the tube with the diameter ratio for a given tube length. From these results, it can be seen that increasing the diameter ratio has the advantage of increasing the orifice water velocity within a range of diameter ratios and at the same time decreasing the water velocity in the tube. Increase of the orifice water velocity reduces the bubble size for a given air flowrate. The bubble rise velocity being the sum of the water velocity and the velocity of the bubble relative to that of water, the decrease of the water velocity in the tube should have the beneficial effect of the decrease of the bubble rise velocity and hence higher bubble residence time and larger mass transfer. In addition, increasing the diameter ratio also decreases the void fraction. The decrease of the void fraction would decrease the bubble coalescence. Thus the composite draft tube provides the advantage of controlling the bubble size as well as the bubble rise velocities by controlling the tube geometry.

The variation of the air velocities in the tube are shown in figure 3.29. The air velocity in the tube decreased as the tube diameter was increased. One of the reasons for this decrease would be the reduction in the water velocity in the tube with the increase of tube diameter as shown in figure 3.25.

Figure 3.30 shows the mean relative velocity of air (the mean slip velocity) computed as the difference between the rise velocity of air shown in figure 3.29 and the water velocity shown in figure 3.25. Considerable differences in the variation of the slip velocity with the tube length for the different tubes are noticed. For the tube with diameter ratio $D_r = 1$, the slip velocity progressively decreased as the tube length was increased. As the diameter ratio increased, this variation became less steeper as shown in the figure. For the diameter ratio of 1.55, the slip velocity remained nearly constant for all the tube lengths. For the diameter ratio of 2.08, the slip velocity increased as the tube length was increased. The curves for all the diameter ratios, extrapolated to zero effective tube length, converged to a value close to 30 cm/s.

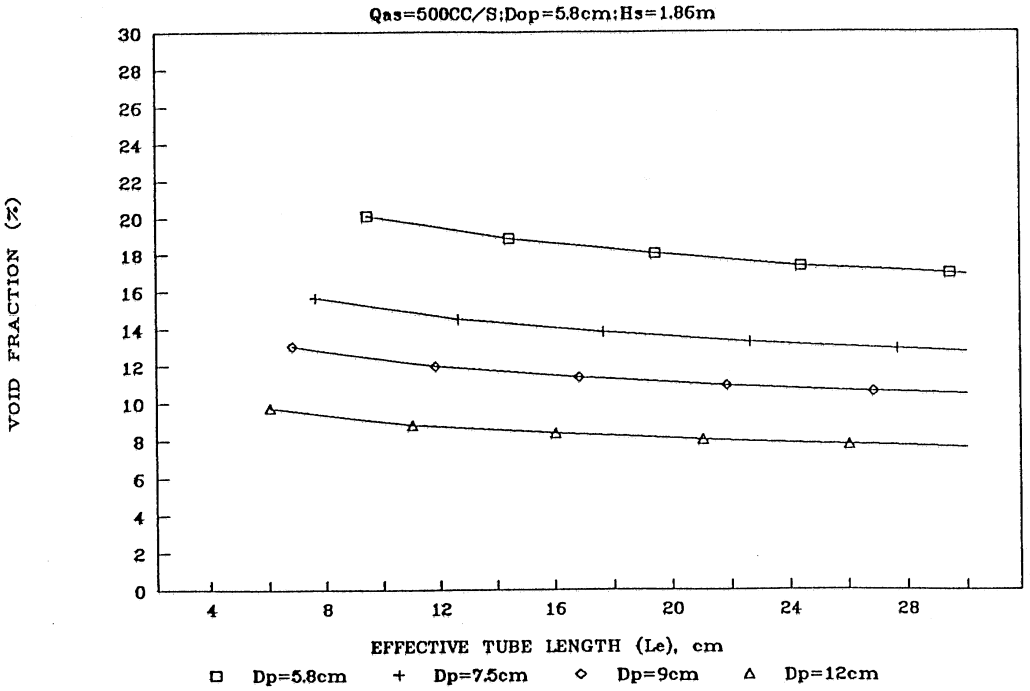

Fig. 3.27 Computed void fraction versus tube length (Eq.3.6,3.7,3.8)

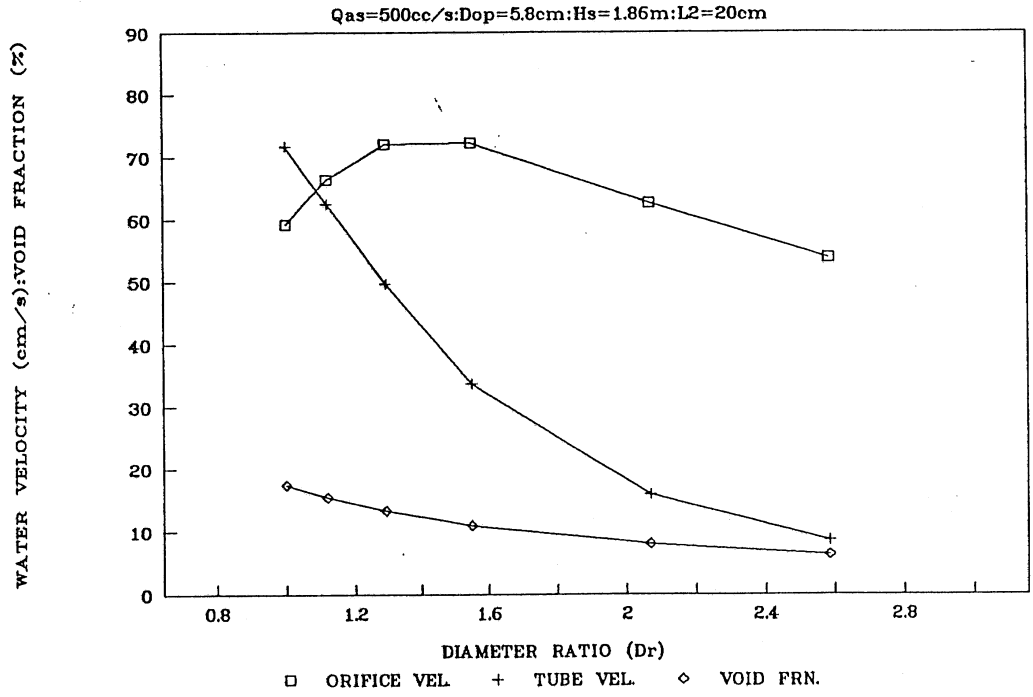

Fig. 3.28 Computed water velocities and void fraction (Eq.3.6,3.7,3.8)

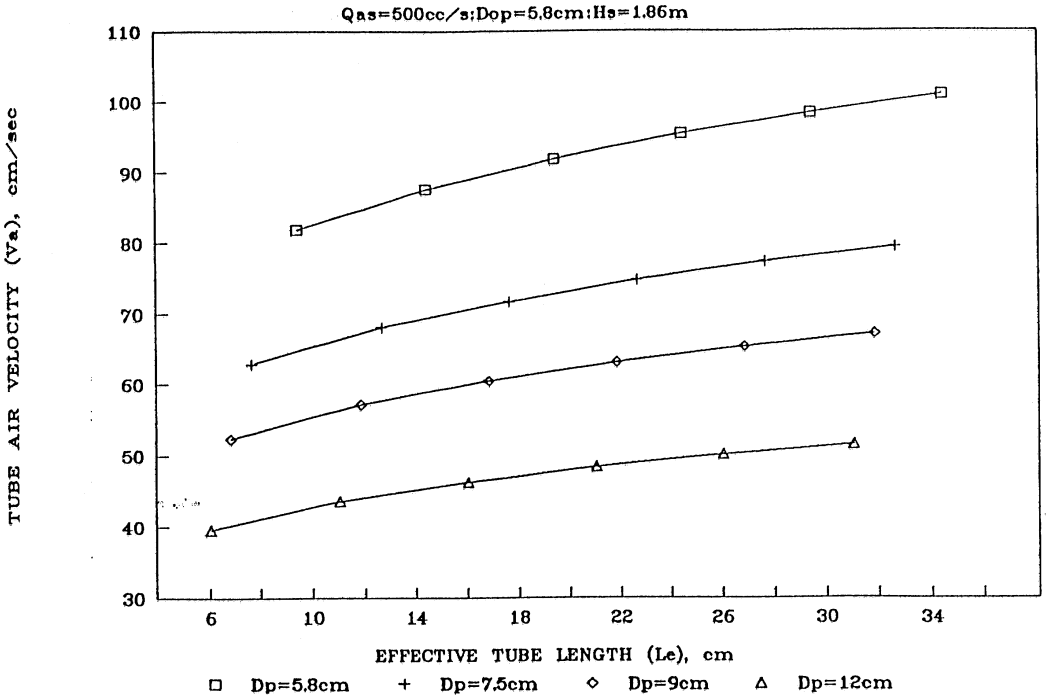

Fig. 3.29 Computed tube air velocity vs tube length (Eq.3.6,3.7,3.8)

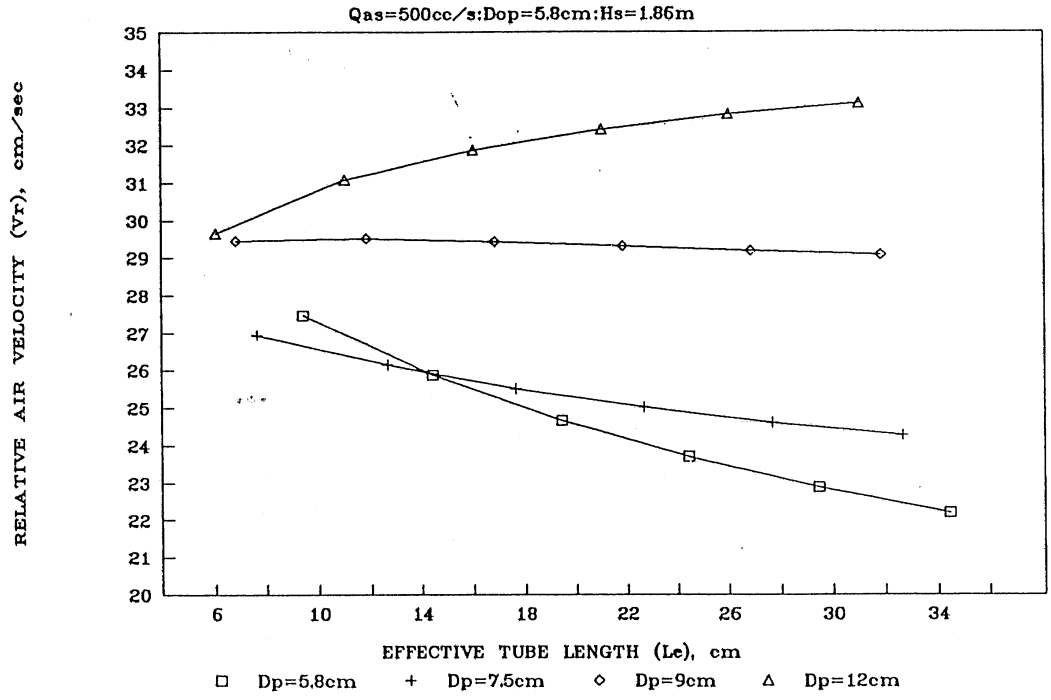

Fig. 3.30 Computed relative air velocity vs tube length (Eq.3.6,3.7,3.8)

Since the maximum orifice water velocities were observed for the diameter ratios between 1.3 and 1.6, the effect of the air flowrate on the orifice water velocity for a diameter ratio of 1.55 was examined using equations (3.6), (3.7) and (3.8). Figure 3.31 shows the effect of the air flowrate on the orifice water velocity. As can be seen from the figure, the induced velocity at the orifice increased with the increase of the air flowrate. Referring to the figure 2.3 (Chapter 2), for an air flowrate of 1cc/s per orifice, the induced water velocity required to produce a bubble of 2.2 mm diameter over a 0.5 mm diameter orifice would be about 50 cm/s. From figure 3.31 it is seen that for the air flowrate of 500 cc/s this velocity is achieved with an effective tube length of 8 cm. If we provide 500 peripheral orifices, the air flowrate per orifice would be 1 cc/s and with an effective tube length of 8 cm, bubbles of 2.2 mm diameter could be produced. Let us assume that this size corresponds to the optimum for mass transfer. If we now decrease the number of the orifices to 250, the air flowrate per orifice would increase to 2 cc/s. This would in turn increase the bubble size, say to 3.2 mm. To decrease the bubble size, the induced velocity has to be increased by increasing the tube length. Increase of the tube length would increase the tube water velocity and the rise velocity of the bubbles as shown in figures 3.25 and 3.29. Thus the effects of increasing the tube length are the following:

- reduction in the bubble size resulting in variation of the mass transfer coefficient
- reduction in the bubble residence time resulting in a decrease of the mass transfer coefficient

The balance between the above two effects would result in a new optimum tube length and an associated mass transfer coefficient. Thus, for a given air flowrate, as we change the number of the peripheral orifices, the optimum tube length and the corresponding mass transfer coefficient would vary. Adjusting the tube length and the number of the peripheral orifices for optimum performance is the basic principle of design of the SAF diffuser.

3.4 MEASUREMENT ERRORS

An estimate of the errors associated with the measurement of each parameter is given below.

3.4.1 Water Flowrate

The water flowrate through the larger tubes were measured with an orifice plate conforming to the ASME standards and the water flowrates through the smaller tubes were measured with a rotameter. The errors associated with these measurements are estimated below separately.

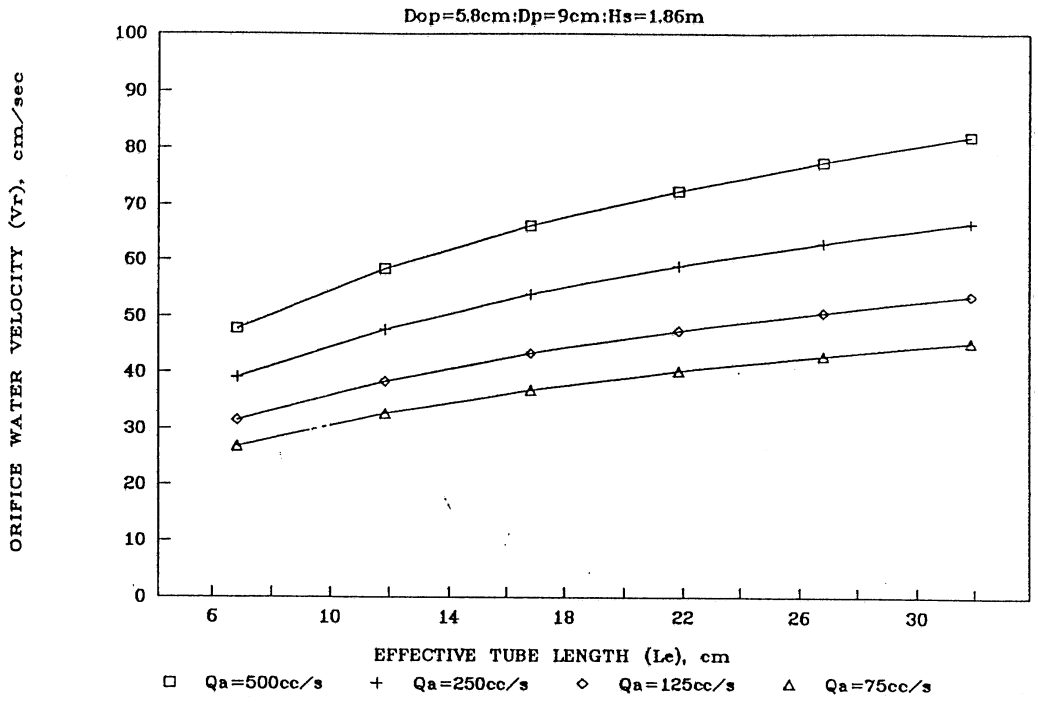

Fig. 3.31 Computed orifice water velocity vs tube length (Eq.3.6,3.7,3.8)

Orifice Plate:

The water flowrate through the orifice plate is given by the following equation (46):

$$Q_w = (D^2 \; I \; h_w^{1/2}) \; / \; \gamma_w^{1/2} \qquad (3.10)$$

where

Q_w = water flowrate

D = diameter of the pipe

I = meter constant

h_w = differential head across the orifice

γ_w = specific weight of water

The diameter of the pipe was measured with a vernier having a least count of 1/1000 th of an inch and rounded off to the nearest 1/100th of an inch. The error arising out of this rounding would be 0.25 per cent. The value of the specific weight of the water was taken from the standard tables and the associated error is not considered here.

The error (95 per cent confidence limit) associated with the value of the Meter Constant I is 0.5 per cent (46).

In order to estimate the error of the differential pressure measurements, these measurements were repeated six times for one of the experimental conditions. The standard deviation observed was 0.62 per cent of the mean. To get the 95 per cent confidence interval value, the standard deviation was multiplied by the corresponding student t value of 2.571 (degree of freedom = 5). This gave an error value of 1.59 per cent.

From the above error estimates, the error associated with the flowrate was estimated as below assuming that all the errors estimated above pertain to the 95 degree confidence level.

$$\frac{dQ_w}{Q_w} = \left[\left[\frac{2\,dD}{D}\right]^2 + \left[\frac{1}{2}\frac{dh_w}{h_w}\right]^2 + \left[\frac{dI}{I}\right]^2 \right]^{1/2} \qquad (3.11)$$

$$= 0.014 \quad (1.4 \text{ per cent})$$

Rotameter:

$$\frac{dQ_w}{Q_w} = 0.02 \text{ (from information supplied by the manufacturer)}$$

3.4.2 Air flowrate

$$\frac{dQ_a}{Q_a} = 0.02 \text{ (from information supplied by the manufacturer)}$$

3.4.3 Void Fraction

The void fraction was calculated from the measured values of the length of the entrapped air column inside the tube upon the closure of the valve using the following equation

$$\alpha = L_a / L_e \tag{3.12}$$

where

L_a = length of the air column entrapped inside the tube

L_e = effective length of the tube

The length of the air column was measured using a cathetometer having a least count of 0.1 mm. Assuming 0.05 mm as the error associated with this measurement, for the shortest length of the air column, the error works out to 0.55 per cent. On similar lines, the error in the determination of the effective tube length works out to 0.26 per cent.

In addition to the errors associated with the measurement of the lengths of the air column and the tube, there would be errors arising from the non–uniformity in the closing time of the quick shut–off valve. To assess this error, the void fraction measurement was repeated seven times under the same experimental condition and the standard deviation was calculated. The value of the standard deviation obtained was 1.37 per cent of the mean. The value of the standard deviation observed was multiplied by the value of Student t corresponding to a degree of freedom of 6 to obtain the error corresponding to the 95 per cent confidence level. This gave an error estimate of 3.3 per cent.

It is also possible that there might be a difference between the actual closing times of the air inlet and the water outlet of the tube by the rotating arm of the valve. This time delay would cause an error in the determination of the accumulated air volume. To estimate this error, it was assumed that the time delay would be 25 percent of the valve closure time. With this assumption, for the smallest tube, with the largest air flowrate for which it was tested, the error was calculated as 1.86 per cent.

Combining all the above errors and assuming that each of the errors has a confidence limit of 95 per cent, the error in the void fraction is calculated as

$$\frac{d\alpha}{\alpha} = \left[0.55^2 + 0.26^2 + 3.3^2 + 1.86^2 \right]^{1/2}$$

$$= 3.8 \text{ per cent.}$$

3.5 CONCLUSIONS

i) Despite the complex nature of the flow, the mean phase velocities and void fractions of the flow of air–water mixture in the tube, in the bubbly flow regime, can be determined fairly accurately using the experimental correlations (3.6), (3.7) and (3.8) that have been developed in this study.

ii) Analysis of flow using the above correlations in a tube, with an inlet diameter of 5.8 cm, proposed for the mass transfer studies indicated that for an air flowrate of 500cc/s, induced orifice water velocities of 50 to 80 cm/s could be achieved with tube lengths in the range of 8 to 35 cm. The orifice water velocities would be maximum at diameter ratios in the range of 1.3 to 1.6. With 0.5 mm diameter peripheral orifices and air flowrate of 1 cc/s per orifice, the effective tube length required to produce bubbles of 2.2 mm diameter would be about 8 cm.

iii) The analysis also indicated the necessity of taking into account the effects of the number and the size of the peripheral orifices as well as the tube geometry while optimizing the device for an application.

Chapter 4

Experimental Studies - II
Mass Transfer Performance of the SAF Diffuser

4.1 OBJECTIVE

As outlined in Chapter 2, the objectives of these studies were the following:

i) To study the effect of the following parameters on the mass transfer coefficient K_1A of the SAF diffuser

- Number of orifices
- Tube geometry
- Air flowrate
- Diffuser submergence

ii) To evolve the correlation given by equation (2.89) for the mass transfer coefficient K_1A

iii) To select an optimum configuration of the SAF diffuser and assess its performance characteristics in terms of Standard Oxygen Transfer Rate and Standard Aeration Efficiency.

4.2 DIFFUSER DETAILS

As mentioned in Chapter 3, the effect of the number of peripheral orifices is an important parameter to be considered while optimizing the device. In order to study this effect, the peripheral orifices were arranged in modules. Each module contained 144 orifices, 0.5 mm in diameter, arranged in four rows. The modules were constructed in such a way that they could be easily stacked one above the other concentrically. Three such modules were made for the study. The tube inlet diameter was 5.8 cm. Figure 4.1 shows details of the modules and the diffuser studied.

The plenum chamber of each module had a volume of 225 cc. With 144 holes per module, the chamber volume per orifice was 1.56 cc. This value was much less than the value of 6.8 cc per hole observed in the experiments of Miyahara et al (see Chapter 2) for the chamber volume to have any effect on the bubble size. Each module was provided with a separate air inlet, 7.1 mm in diameter. The air flow to each module was measured separately and adjusted to equal values.

Inlet details:

Diameter of Orifices	= 0.5 mm	D_{op} = 5.8 cm
Number of Orifices per module	= 144 (4 rows x 36 orifices per row)	
Orifice spacing	= 5 mm (horizontal) 3 mm (vertical)	

W = 4.6 cm ; B = 1.5 cm ; L_1 = 4.45 cm ; L_3 = 8.25 cm

R = 12.5 mm

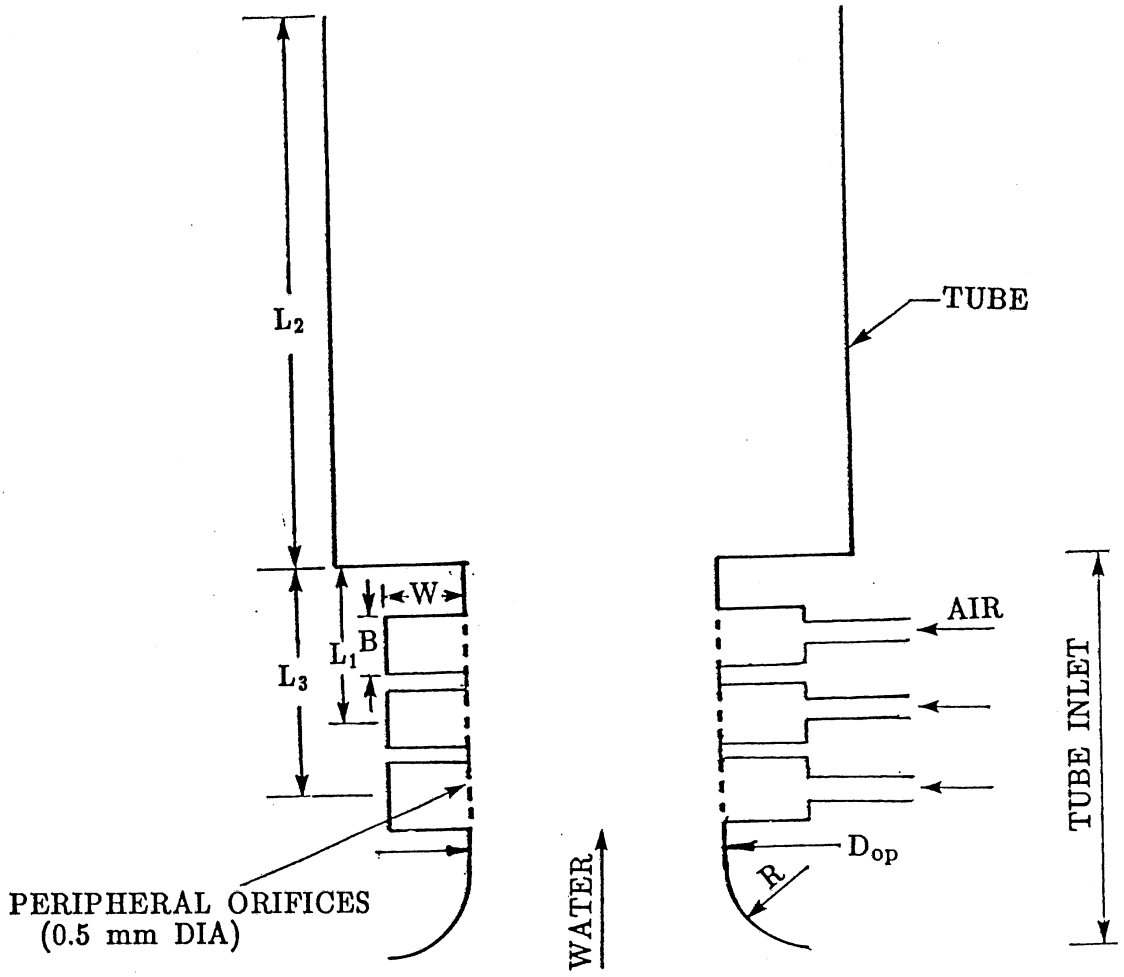

Fig. 4.1 Inlet details of Diffuser studied

With the three modules stacked one above the other, the distance L_1 from the centre of the orifices to the outlet end of the tube inlet was 4.45 cm. Thus the effective tube length for any value of tube length L_2 would be

$$L_e = L_2 + 4.45\ (D_{op}^2/D_p^2)$$

(all dimensions are in centimeters)

4.3 THE EXPERIMENTAL FACILITY

The studies were carried out in a cylindrical tank 1.02 m in diameter and 2.4 m in height. Local tap water was used for the studies. A mixing pump was mounted on top of the tank for mixing the water with chemicals prior to the tests. The air supply system was the same as shown in figure 3.1 (Chapter 3). The diffuser under study was mounted at the centre of the tank with the air inlet at a height of 0.27 m from the tank floor. A floating cover (having an air escape opening) was placed over the water surface in order to minimize the mass transfer from the atmosphere to the test water.

The studies were conducted as per the test procedure given by the ASCE Standard for the Measurement of Oxygen Transfer in Clean Water, July 1984. The oxygen transfer measurements were done using a Dissolved Oxygen probe (YSI 5700) and a digital recorder (YSI 58). The measurements were carried out for different tube diameters varying from 5.8 cm to 12 cm and tube lengths up to 30 cm under submergences up to 1.86 m. The water temperature during the measurements was maintained at 20° C (±0.3° C). The air temperature in the air supply line varied between 17° C and 22° C.

The experimental determination of the mass transfer coefficient involved the removal of the oxygen from the test water volume by adding sodium sulfite followed by reoxygenation to near the saturation level by aerating the water using the device under study. The experimental procedure is outlined below step wise:

- Mount the diffuser at the centre of the tank and fill the tank with tap water up to the desired level.
- Add the catalyst Cobalt Chloride (0.5 mg/l) and mix well with the water by operating the aeration system for about 30 minutes.
- Stop the air supply, add the deoxygenation chemical Sodium Sulfite (reagent quality), 90 mg/l, in a slurry form into the water and mix well by operating the mixing pump until the concentration uniformly falls to about 0.1 mg/l.
- Set the diffuser air supply to the desired value and record the oxygen concentration at regular intervals till about 98 per cent saturation was achieved

The DO probe was calibrated before and after each experiment using the air–calibration technique (47).

In order to determine the number of locations at which the oxygen concentration was to be measured, few trial runs were made initially by measuring the DO concentration at two depths (one fourth and three fourth the depth). The mass transfer coefficient values obtained at these locations were practically the same, agreeing within 2 per cent. Hence for all the experiments the DO concentration was measured only at the centre of the tank at a distance of half the tank radius from the wall.

4.4 DATA ANALYSIS

The basic model used for the analysis of the test data is the one given by the equation (2.42) which is again reproduced below:

$$\frac{dc}{dt} = K_1a\ (C_s - C) \tag{4.1}$$

On integration the above equation gives

$$\ln \left[\frac{C_s - C}{C_s - C_o}\right] = - K_1a\ t \tag{4.2}$$

or

$$C = C_s - (C_s - C_o)\ \exp(- K_1a\ t) \tag{4.3}$$

where

C_s = average dissolved oxygen (DO) concentration attained at infinite time

K_1a = volumetric mass transfer coefficient (1/time)

C_o = DO concentration at t=0, estimated from the model

C = effective average DO concentration in the liquid phase at any time t

The model basically assumes completely mixed liquid with uniform DO through–out the tank.

The DO concentration versus time data obtained from the experiments was analysed using a non–linear regression routine of the ASCE (ASCE 87) to fit equation (4.3) to the data. The program provides least square estimate of the parameters K_1a, C_s and C_o. The value of K_1a was multiplied by the volume of water in the tank to obtain the value of K_1A. The designs studied and the results are summarised in Appendix C. The experimental results are discussed below.

4.5 EXPERIMENTAL RESULTS AND DISCUSSIONS

Effect of the number of peripheral orifices

It was concluded in Chapter 3 that the number of peripheral orifices would affect the mass transfer coefficient as well as the dimensions of the diffuser for optimum performance. Hence this aspect was studied first.

Figures 4.2, 4.3 and 4.4 show the effect of the number of peripheral orifices on the mass transfer coefficient. As explained under 4.2, the peripheral orifices were arranged in modules, each module containing 144 holes, 0.5 mm in diameter, in four rows. The experiments were conducted by varying the number of the modules and thereby the number of peripheral orifices. One to three modules were studied. The results show that for all the tube diameters studied, as the number of peripheral orifices was increased, the value of the maximum mass transfer coefficient (K_1A_{max}) increased and the effective tube length corresponding to the maximum value of the mass transfer coefficient decreased resulting in smaller tube length and larger mass transfer. The results shown in figure 4.2 correspond to an air flowrate Q_{as} of 500 cc/s through the tube having a diameter ratio of 1.55 (D_p= 9 cm, D_{op}= 5.8 cm). From these results it is seen that the effective tube length corresponding to the maximum value of K_1A decreased from about 40 cms with single module to 7 cms with three modules. With three modules, the number of the peripheral orifices would be 432 and the air flowrate per orifice would be about 1 cm/s. For this flowrate, the tube length worked out in Chapter 3 was 8 cm. The trend of variation of the optimum tube length and the mass transfer coefficient was as anticipated from the theoretical considerations.

Figures 4.5 and 4.6 show the effect of the number of peripheral orifices on K_1A for different air flowrates through the diffuser for a constant tube length. For each air flowrate, the value of K_1A increased with increase in the number of the peripheral orifices/modules to reach a maximum which remained fairly constant over a range of number of modules/peripheral orifices. The number of peripheral orifices corresponding to the maximum K_1A value was greater at larger air flowrates. For example, from the figure 4.6 it can be seen that for the air flowrate of 83 cc/s, the maximum K_1A was nearly reached with two modules whereas from figure 4.5 it is seen that for the air flowrate (Q_{as}) of 500 cc/s, even with three modules the value of K_1A was still increasing and the maximum K_1A would be reached with about five modules though the corresponding increase in K_1a was only marginal. The results indicate that the air flowrate per orifice should be kept at about 1 cc/s or less for optimum performance in clean water applications.

The above trend of variation of K_1A with the number of peripheral orifices is a significant advantage of the SAF design. As seen from the experimental results shown in figures 4.5 and 4.6, the K_1A is nearly constant when it reaches the maximum. Providing more orifices than that corresponding to the maximum K_1A would ensure that the performance of the

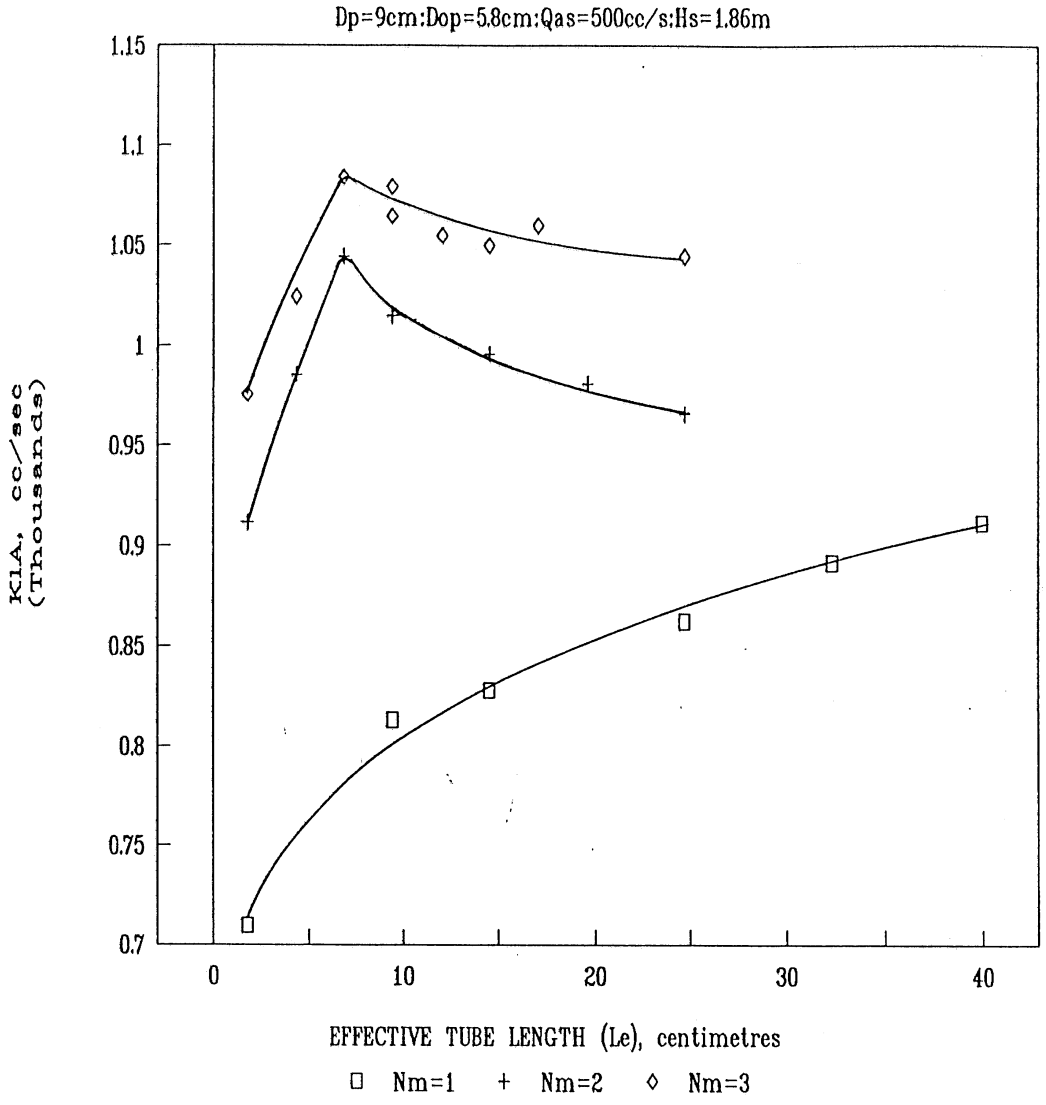

Fig. 4.2 Effect of number of modules on K_1A (D_p=9 cm)

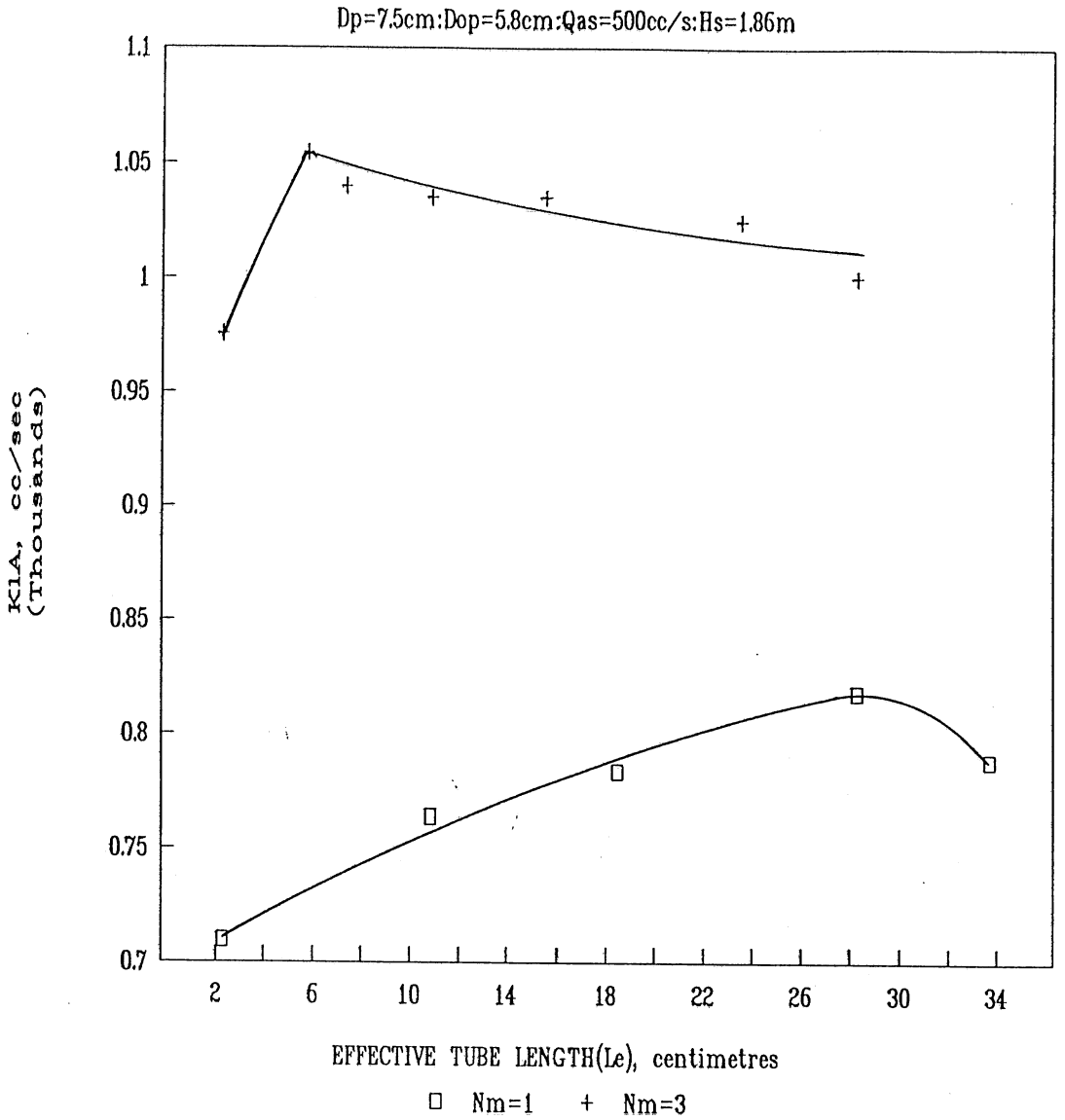

Fig. 4.3 Effect of number of modules on K_1A (D_p=7.5 cm)

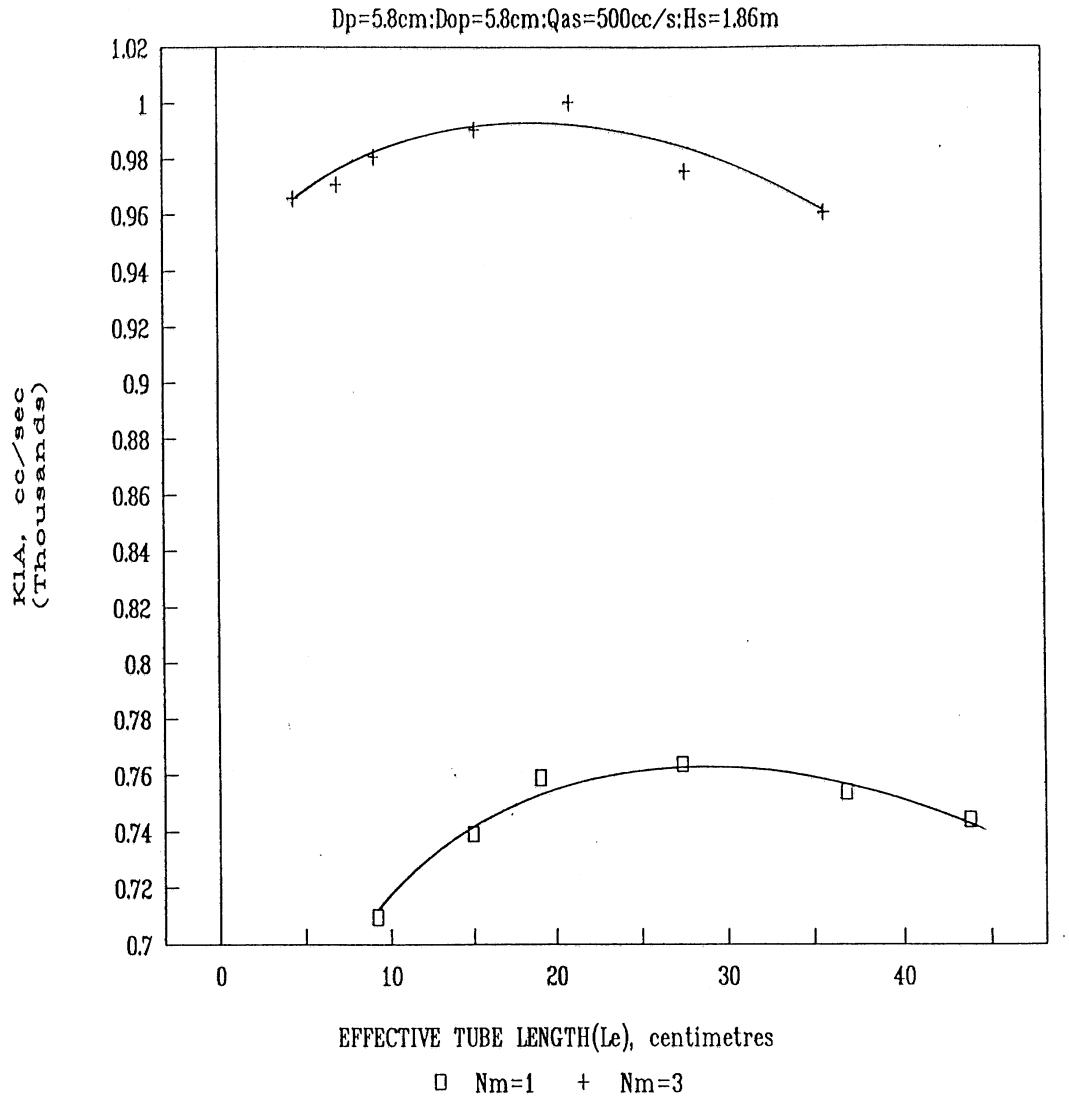

Fig. 4.4 Effect of number of modules on K_1A (D_p=5.8 cm)

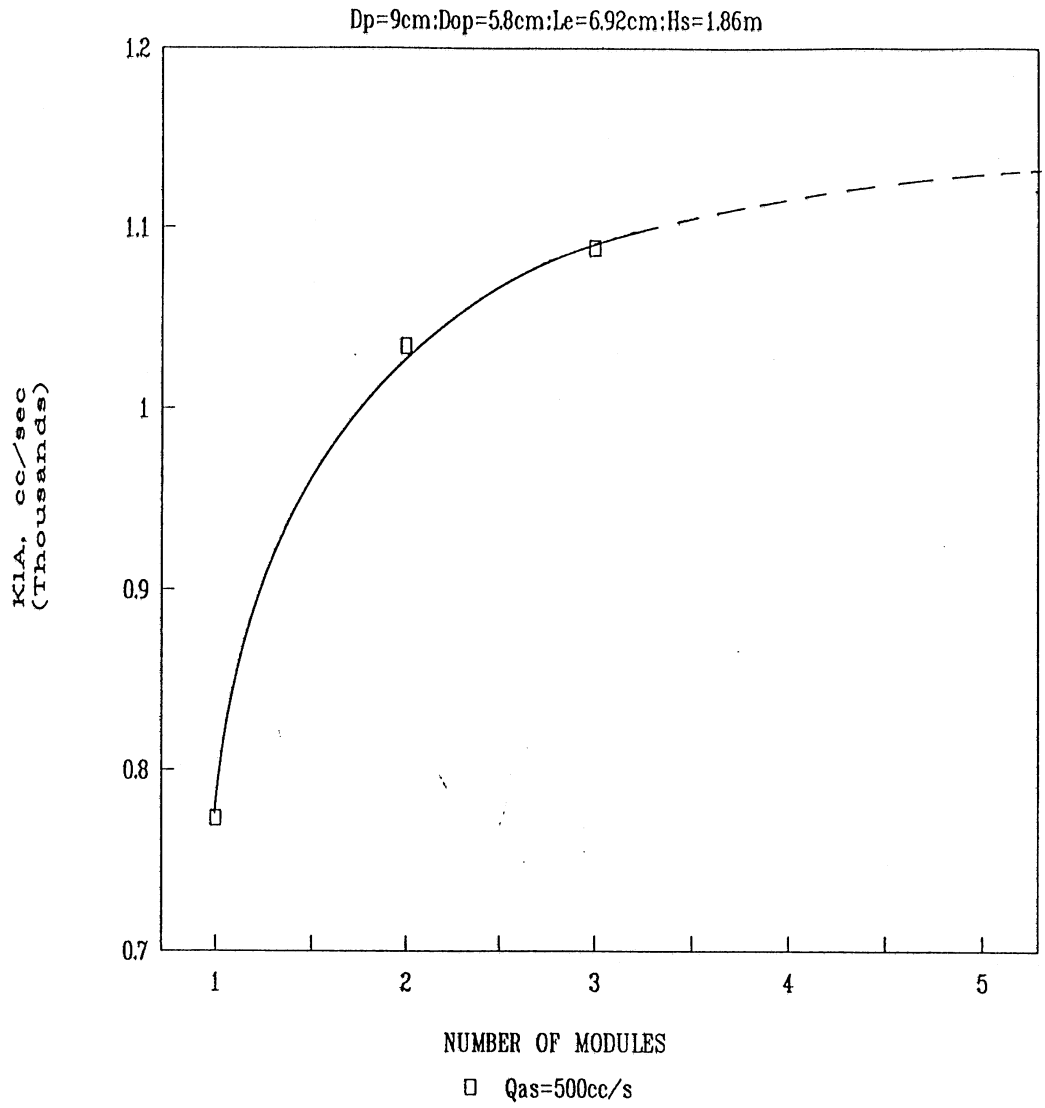

Fig. 4.5 Effect of number of modules on K_1A (D_p=9 cm, L_e=6.92 cm)

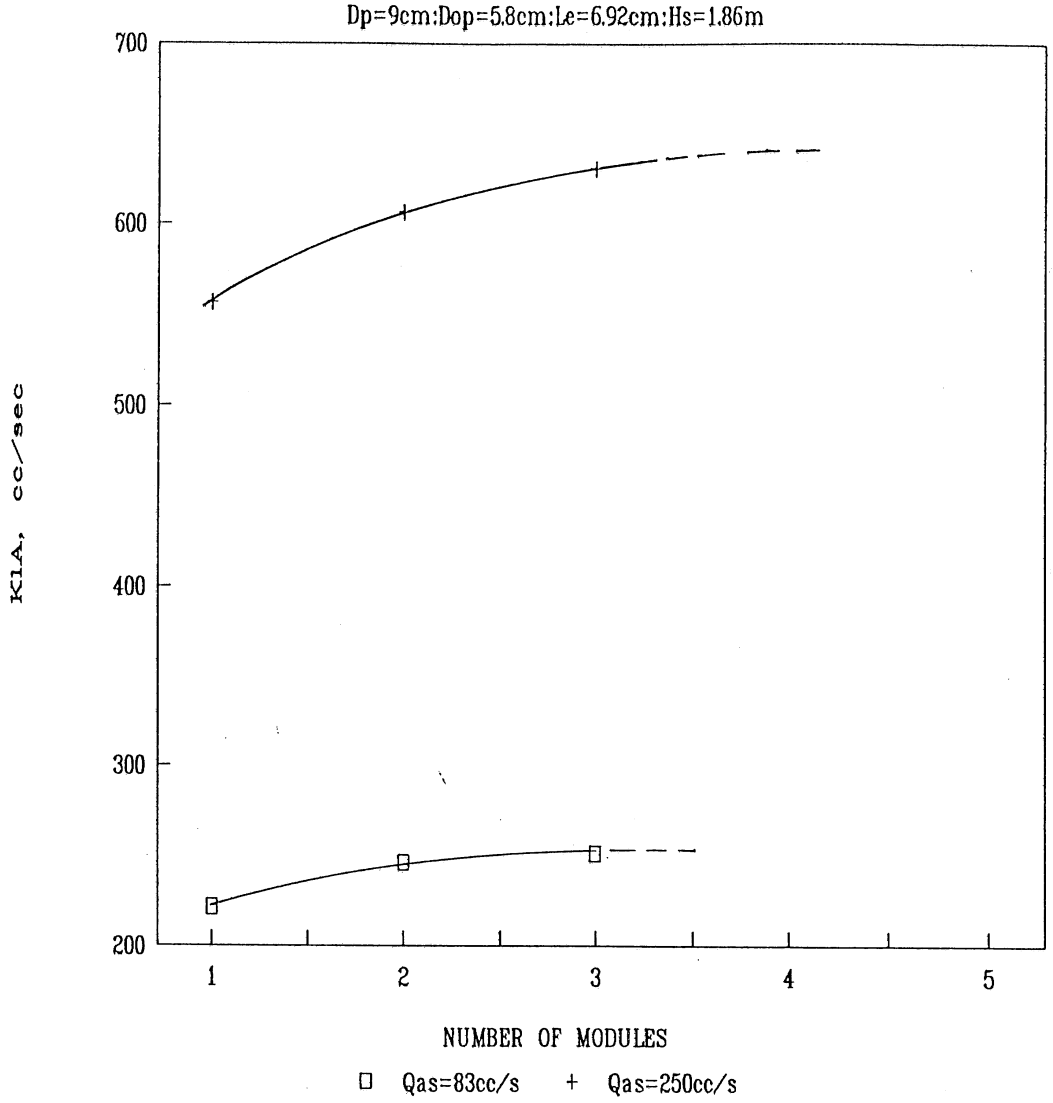

Fig. 4.6 Effect of number of modules on K_1A (D_p=9 cm, L_e=6.92 cm)

device would not be affected even if some of the orifices were clogged. This enables us to account for the diffuser clogging in the diffuser design itself. Based on actual field experience on the extent of clogging for various applications, the diffuser clogging could be accounted for in the diffuser design stage by providing adequate number of additional orifices. Since the peripheral orifices are arranged in the vertical plane, it would be possible to accommodate more orifices for a given plan area of the diffuser than would be possible with conventional designs having holes arranged in a horizontal plane. This would result in much reduced energy losses and increased rangeability in addition to better performance in terms of diffuser clogging.

Effect of tube geometry

Figures 4.7 and 4.8 show the effect of tube geometry on mass transfer coefficient. For a given tube diameter D_p, the mass transfer coefficient varied with the tube length and peaked at a particular tube length. The tube length at which the mass transfer coefficient reached the maximum was not the same for all the tube diameters. As seen from figure 4.7, for the tube diameter of 5.8 centimetres, the maximum mass transfer was attained at an effective tube length of about 20 centimetres. As the tube diameter was increased, the effective tube length corresponding to the maximum mass transfer coefficient decreased. For the tube diameter of 7.5 centimetres, this length was about 6 centimetres. With further increase of the tube diameter, the tube length corresponding to the maximum mass transfer coefficient increased. From figures 4.7 and 4.8 it is seen that for a given diameter of the tube inlet, as the diameter of the tube was increased, the maximum mass transfer coefficient increased.

Figure 4.9 shows the variation of the maximum mass transfer coefficient with air flowrate for several outlet tube diameters. Figure 4.10 shows the performance comparison on the basis of the areal specific mass transfer coefficient K_{lf} defined as the mass transfer coefficient per unit area of the diffuser. The figure shows the variation of the maximum areal specific mass transfer coefficient with area ratio for two values of air flux through the diffuser. It is seen that the maximum K_{lf} is associated with a particular area ratio. Over the range of the air flowrates considered, the optimum area ratio was between about 1.5 and 3.

Figure 4.11 shows the optimum effective tube length corresponding to the maximum K_lA for different tube diameters. The optimum tube length is minimum in the area ratio range of 1.5 to 2.4.

The variation of the mass transfer coefficient with a peak at an intermediate tube length can be explained by considering the effects of the tube length on the bubble size and the bubble residence time. Increase in the tube length increases the water velocity in the tube. An increase in the water velocity in the tube has the following effects:

i) A decrease in the bubble size resulting in a change of the mass transfer coefficient.
ii) A decrease in the bubble residence time.

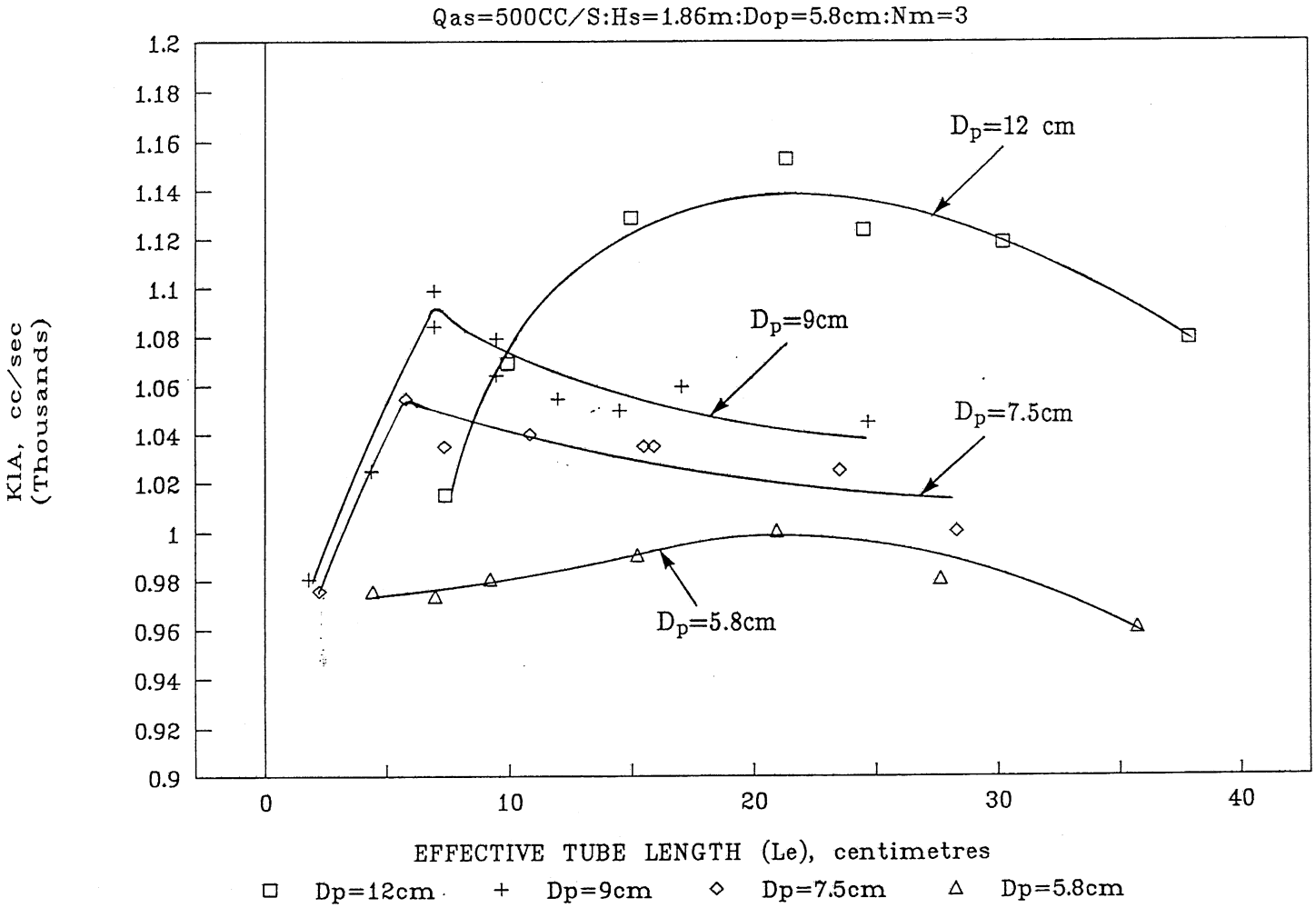

Fig. 4.7 Effect of tube geometry on K_1A

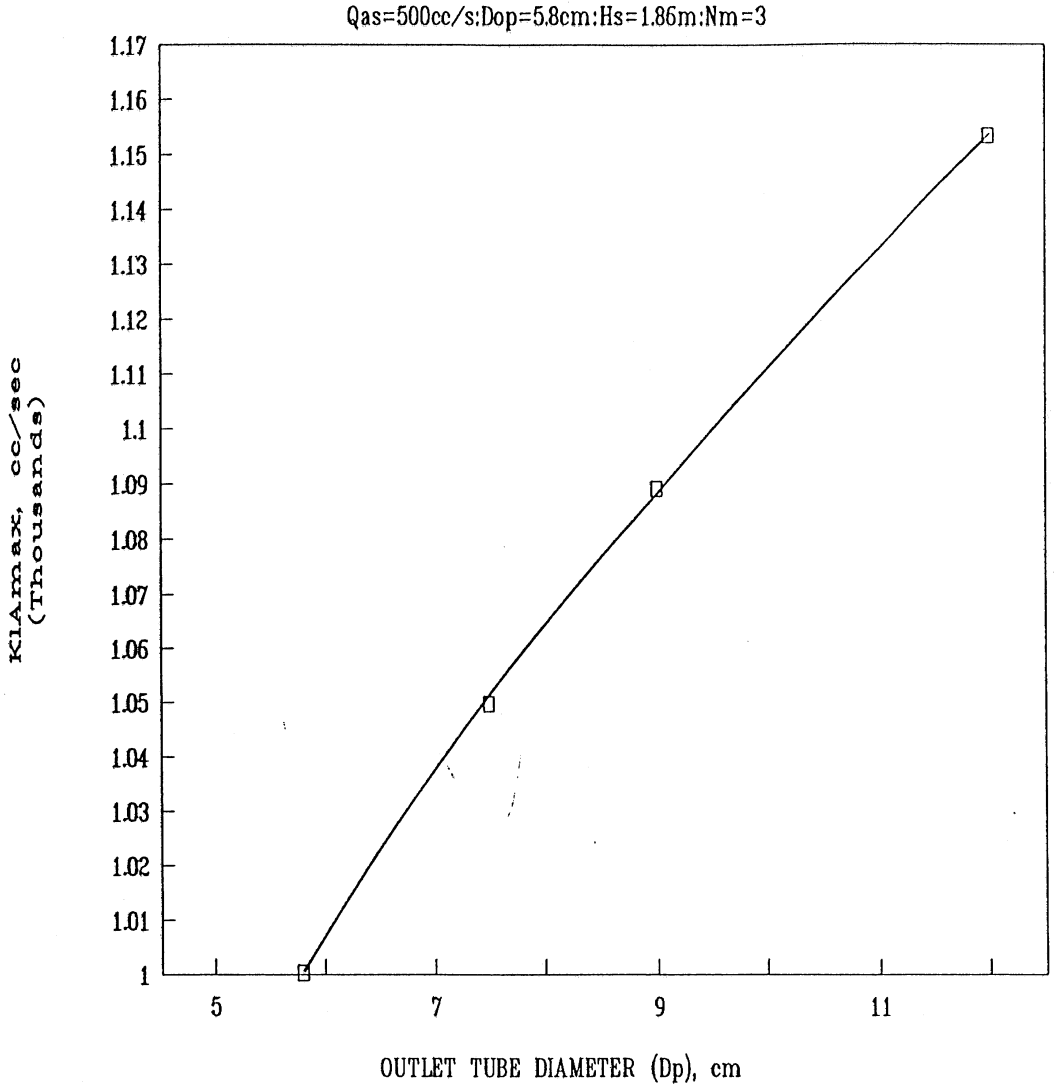

Fig. 4.8 Effect of tube geometry on K_1A_{max}

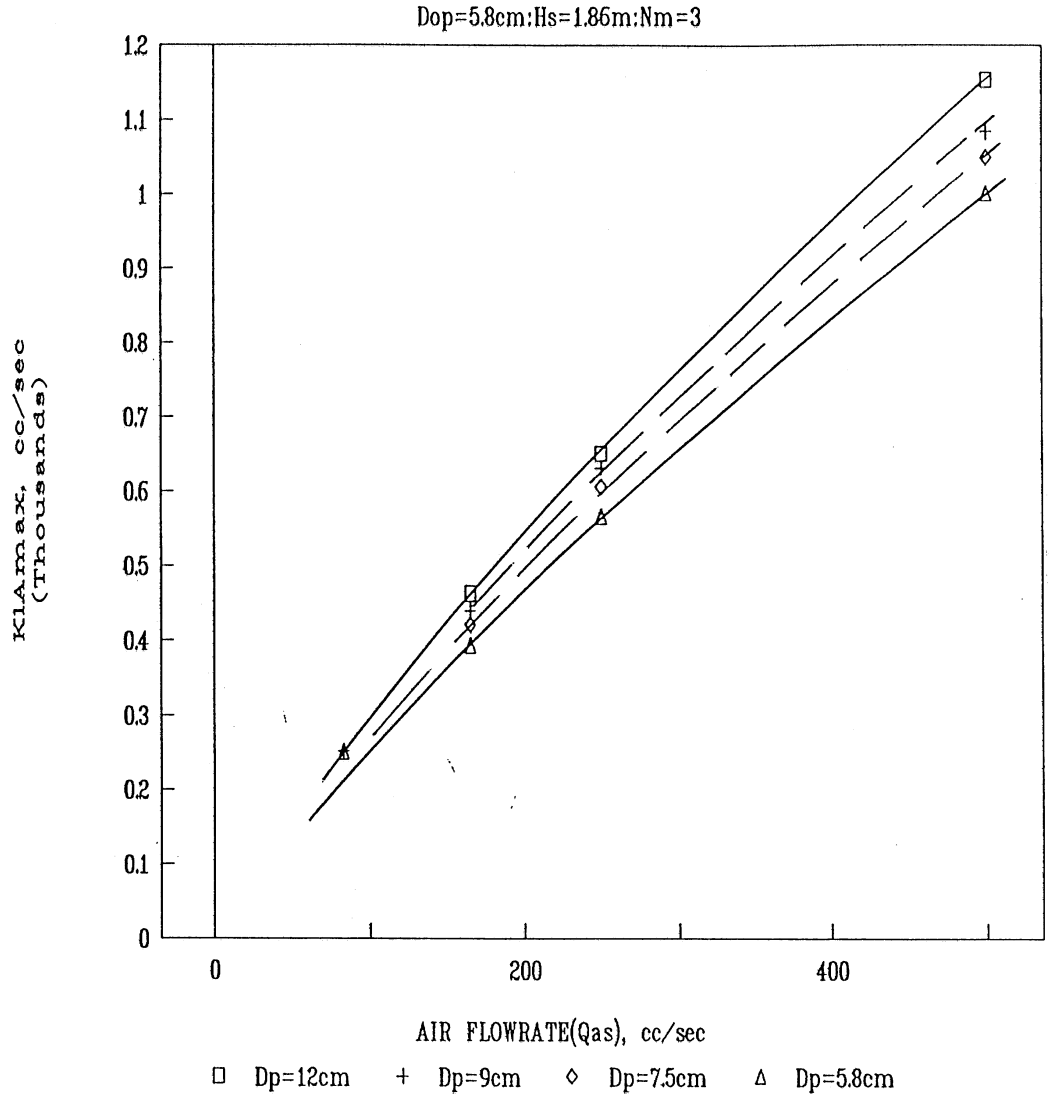

Fig. 4.9 Effect of air flowrate on K_1A_{max}

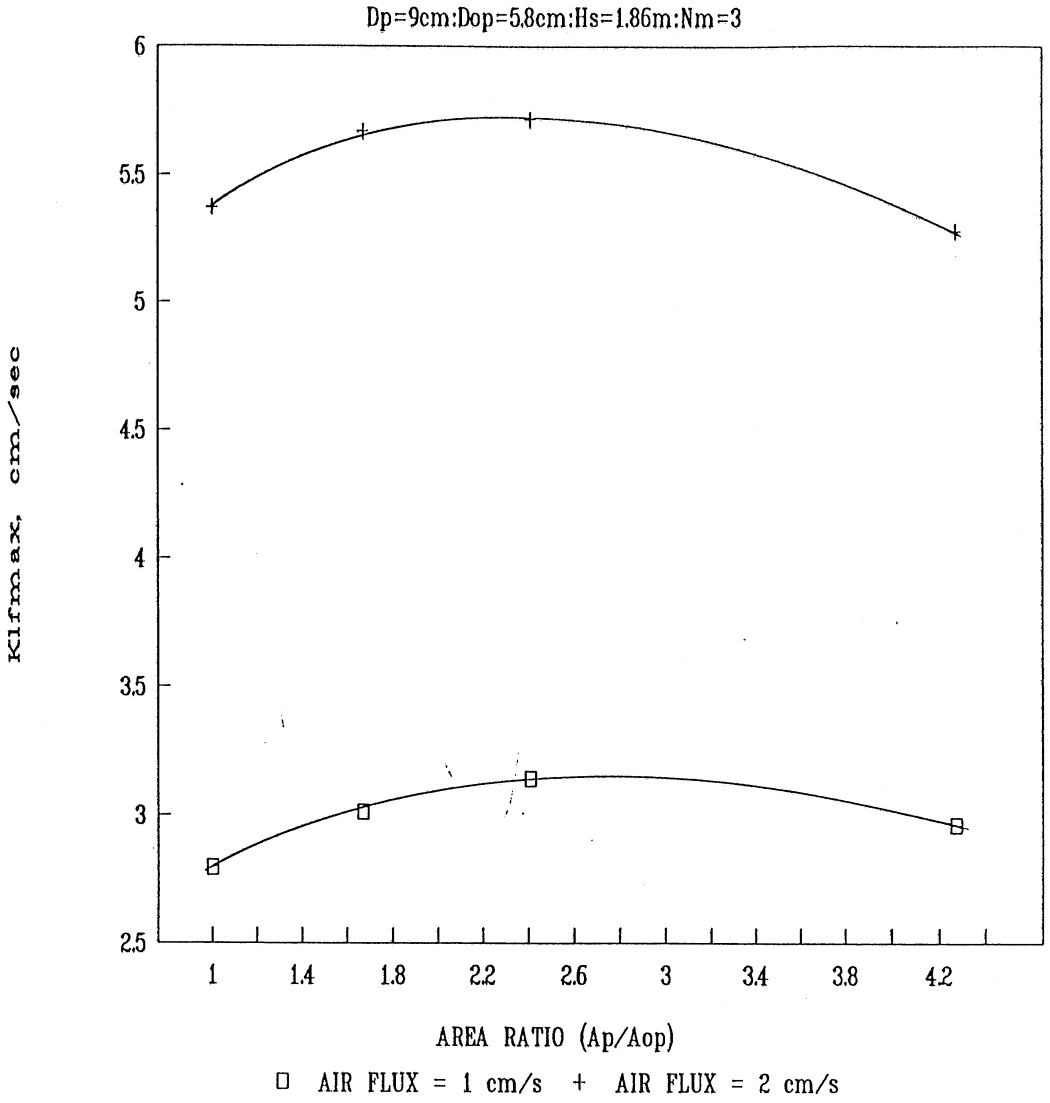

Fig. 4.10 Effect of area ratio on K_{lfmax}

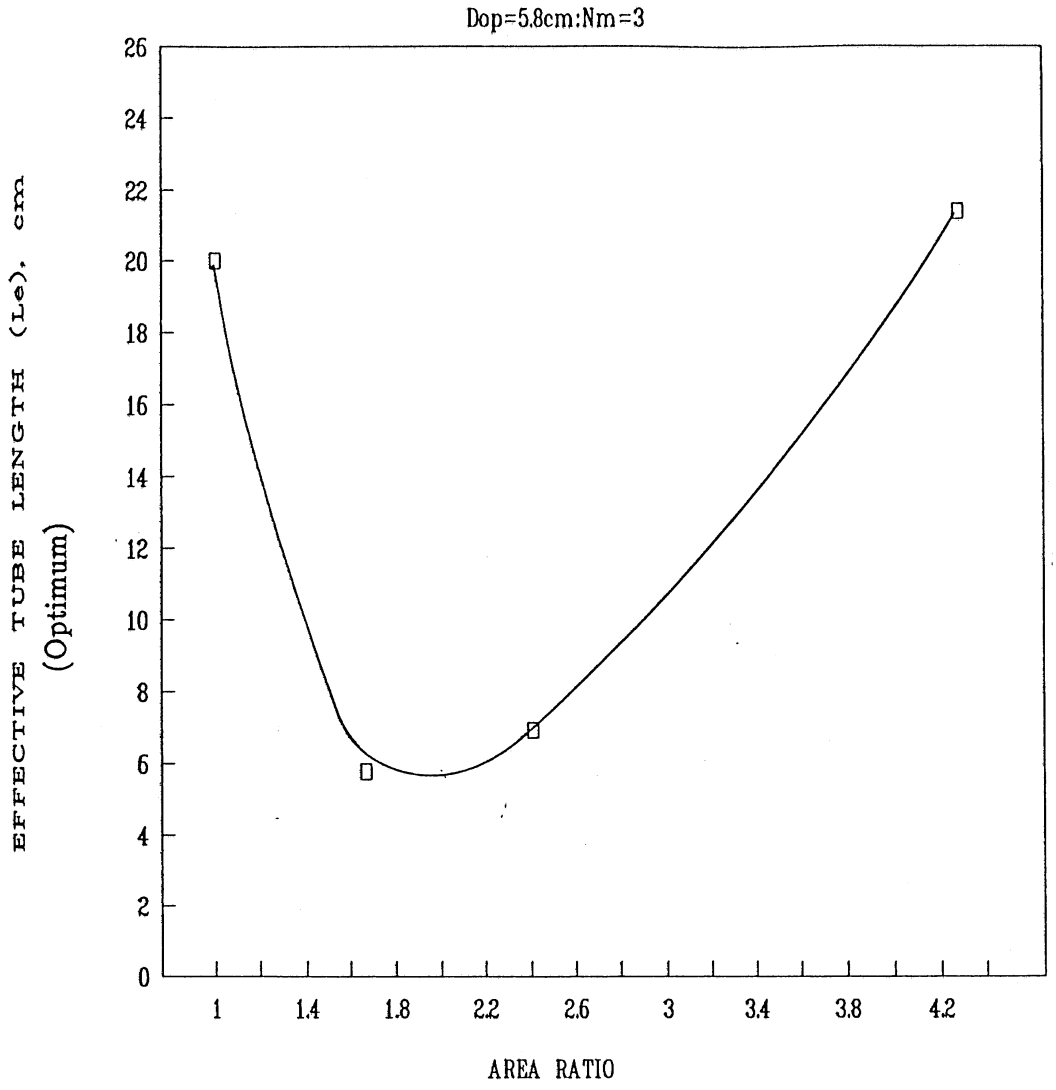

Fig. 4.11 Effect of area ratio on optimum tube length

The above two effects are additive resulting in the particular trend of variation of K_lA with change in tube length observed in the experimental results.

Effect of air flowrate

Figure 4.12 shows the effect of air flowrate on the mass transfer coefficient. The mass transfer coefficient increased with increase in the air flowrate. The variation of the mass transfer coefficient with tube length was the same for both the air flowrates. These results show that the optimum geometry of the diffuser does not vary with the air flowrate.

Effect of diffuser submergence

Figures 4.13, 4.14 and 4.15 show the effect of diffuser submergence on the mass transfer coefficient for different air flowrates and tube lengths. As the diffuser submergence was increased, the mass transfer coefficient increased.

Figure 4.16 shows the variation of the mass transfer coefficient with the tube length for three values of diffuser submergences. The results show that the optimum tube length as well as the trend of variation of the mass transfer coefficient with tube length does not vary with the diffuser submergence.

Effect of air temperature

As mentioned under 4.3, though the water temperature during the experiments was maintained at 20° C, the air temperature varied between 17° C and 22° C. In order to study the effect of this temperature variation on K_lA, one set of experiments were repeated under different air temperatures keeping the water temperature at 20° C. These results are shown in the table 4.1. It is seen from these results that the variation in the air temperature did not significantly affect the values of the mass transfer coefficient.

Table 4.1 Effect of air temperature on K_lA

Experimental condition: D_p=9 cm, H_s=1.86 m, Q_{as}=500 cc/s

L_e=6.92 cm, N_m=3

Air temperature (° C)	K_lA (cm^3/s)
17.1	1084
18.0	1079
20.3	1084
21.2	1089

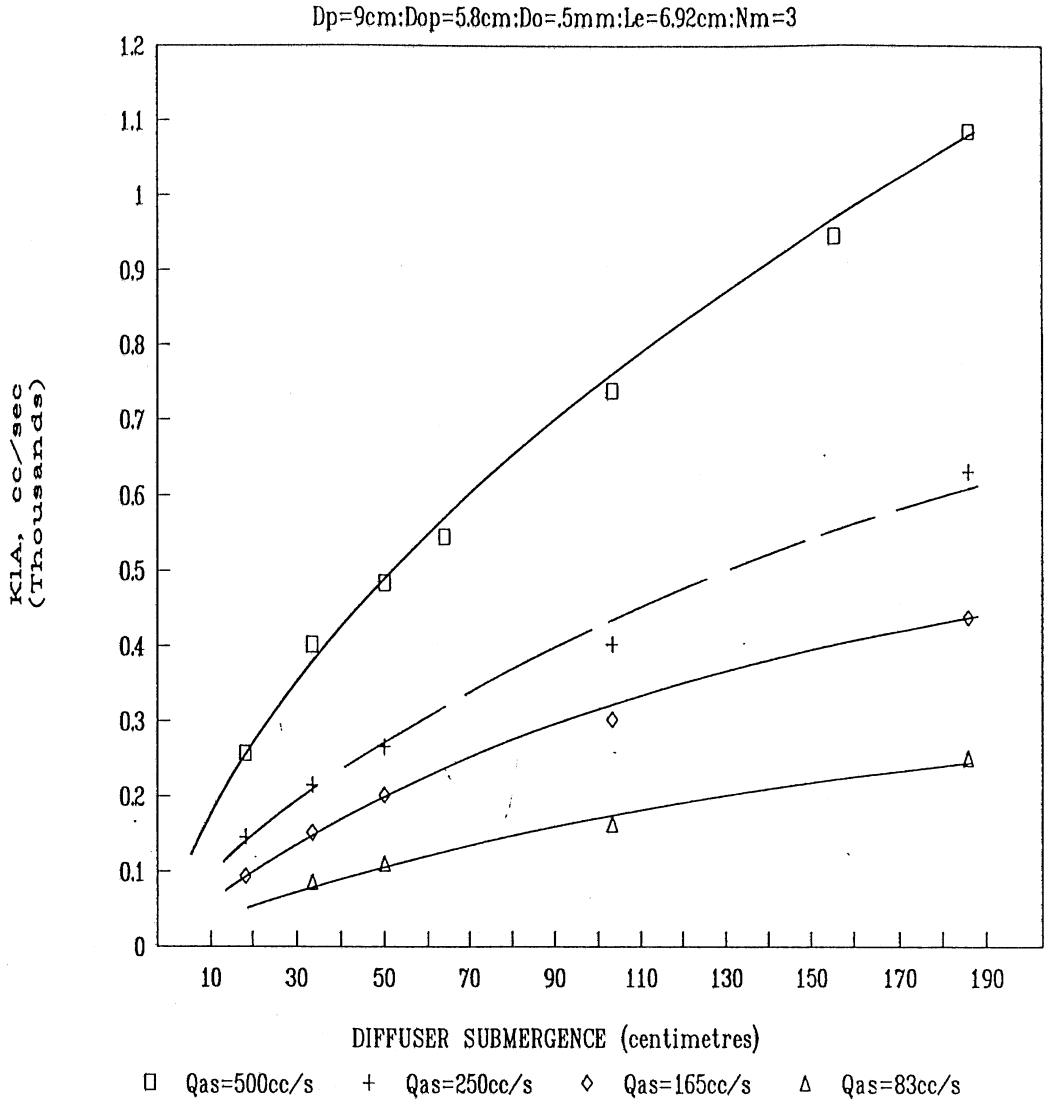

Fig. 4.13 Effect of diffuser submergence on K_1A

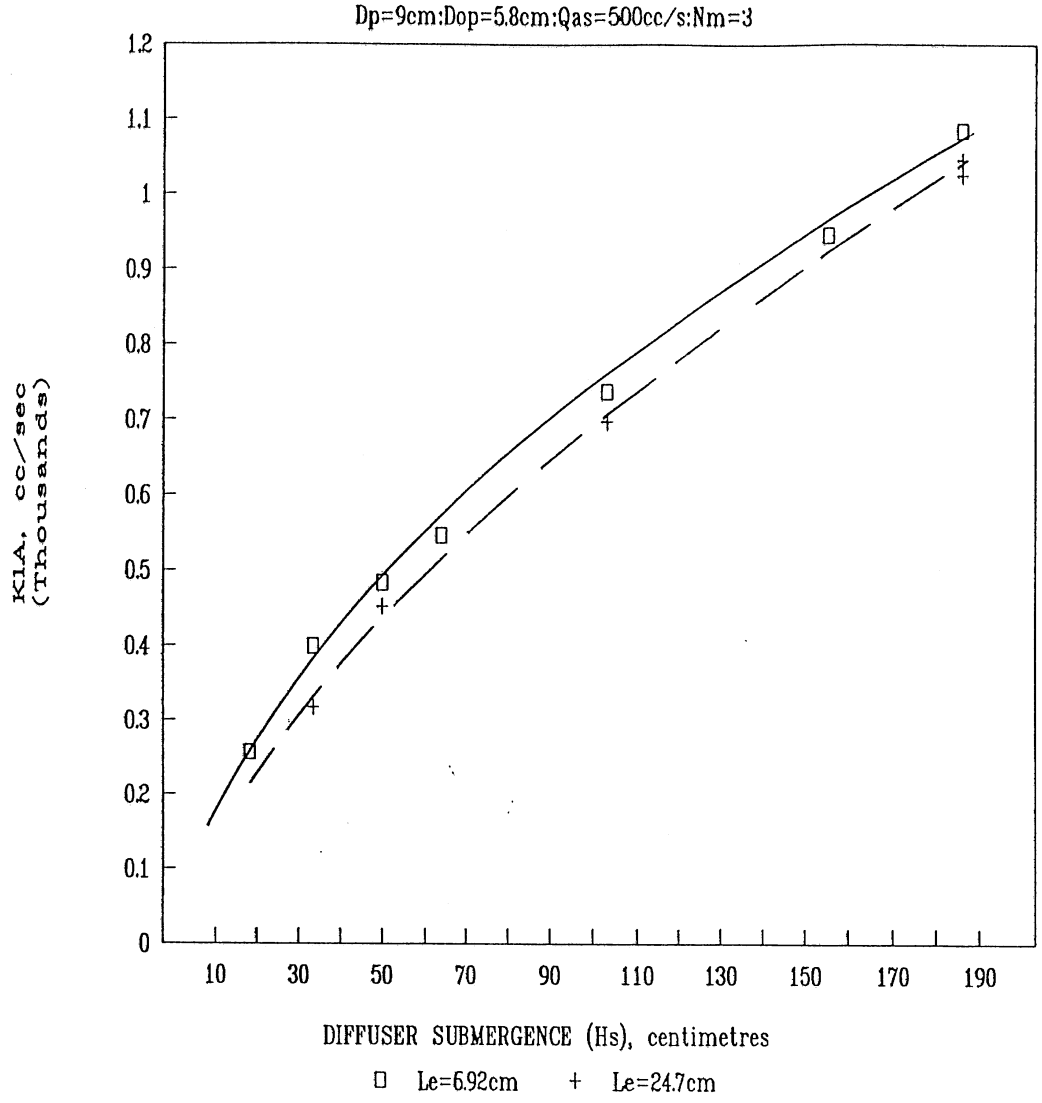

Fig. 4.14 Effect of diffuser submergence on K_1A

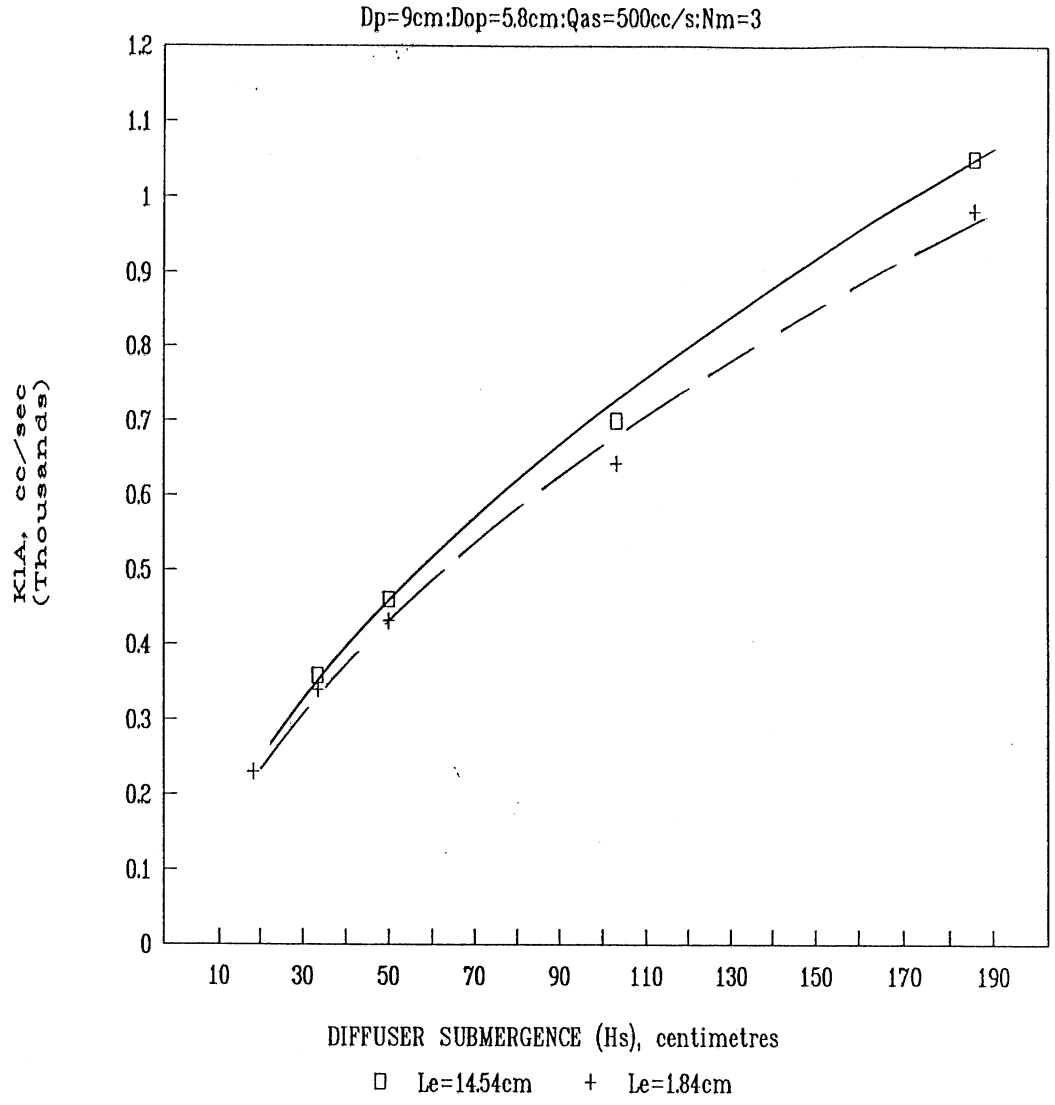

Fig. 4.15 Effect of diffuser submergence on K_1A

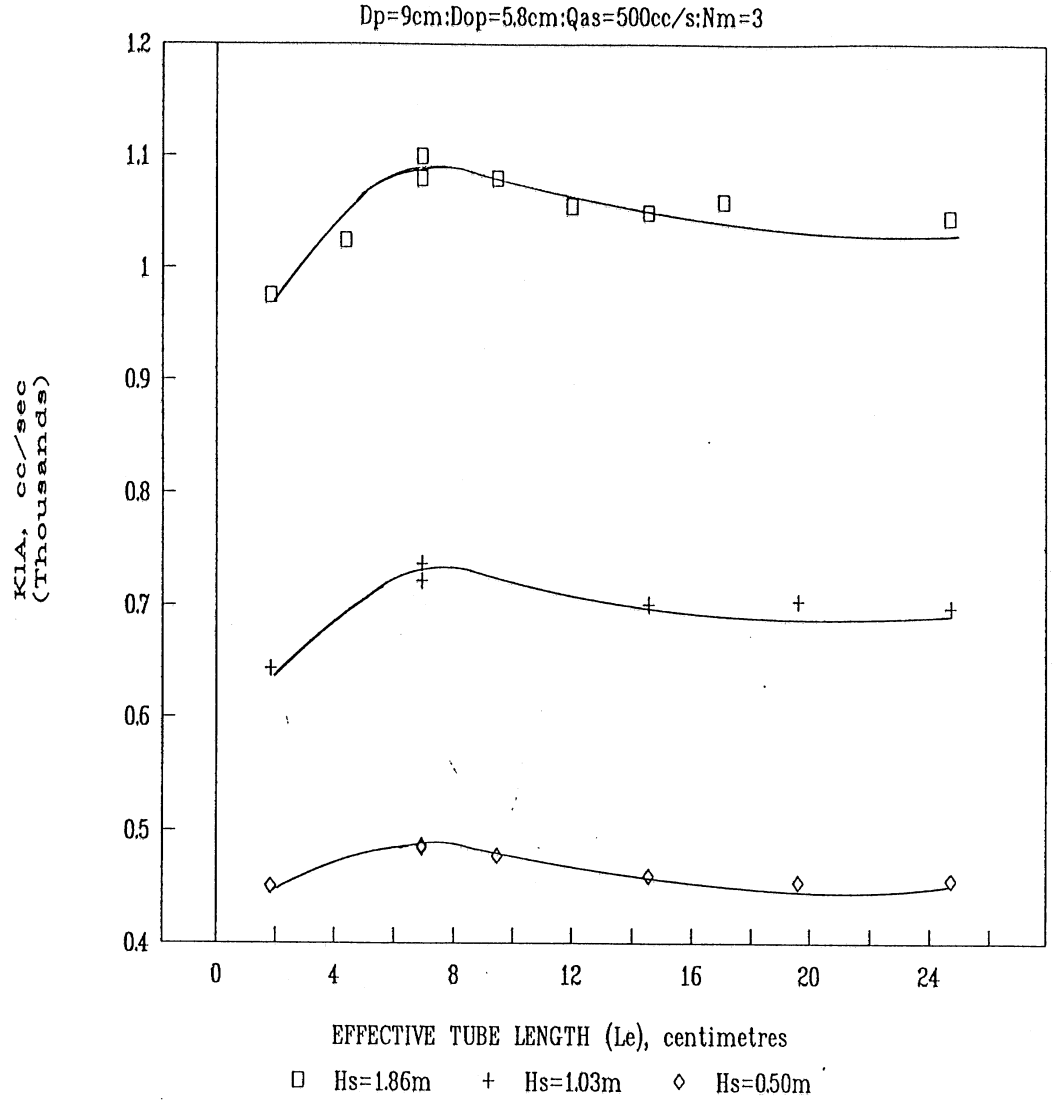

Fig. 4.16 Effect of diffuser submergence on K_1A

Saturation concentration

Figure 4.17 shows the variation of saturation concentration with the tube length and the diffuser submergence. The saturation concentration increased as the diffuser submergence was increased. This trend is normally expected as the increase in the diffuser submergence causes higher air pressures within the bubble and hence higher values of the saturation concentration. The saturation concentration did not show any appreciable variation with change in the tube length.

Figure 4.18 shows the effect of air flowrate on the saturation concentration. The saturation concentration remained practically constant over the range of air flowrates studied.

Non–dimensional correlation of the experimental data

As outlined in chapter 2, the experimental data was correlated in terms of non–dimensional parameters as below:

$$S_{tm} = f (F_s, G_a, L_r, D_r, H_r)$$

The non–dimensional parameters appearing in the above correlation are explained below.

$$S_{tm} = \frac{K_l A}{D_p^2 J_a} \tag{4.4}$$

where

K_lA = mass transfer coefficient (cm^3/s)
K_l = the liquid film coefficient (cm/s)
A = air–water interfacial area (cm^2)
D_p = tube diameter (cm)
J_a = superficial air velocity in the tube (cm/s)

S_{tm} is a modified Stanton number. The number represents the ratio of the mass transfer rate per unit concentration difference and the air flowrate through the device.

$$F_s = \text{Submergence Froude number}$$

$$= J_a/(gH_s)^{1/2} \tag{4.5}$$

where

H_s = the diffuser submergence (cm)
g = gravitational acceleration (cm/s^2)
G_a = Galileo number

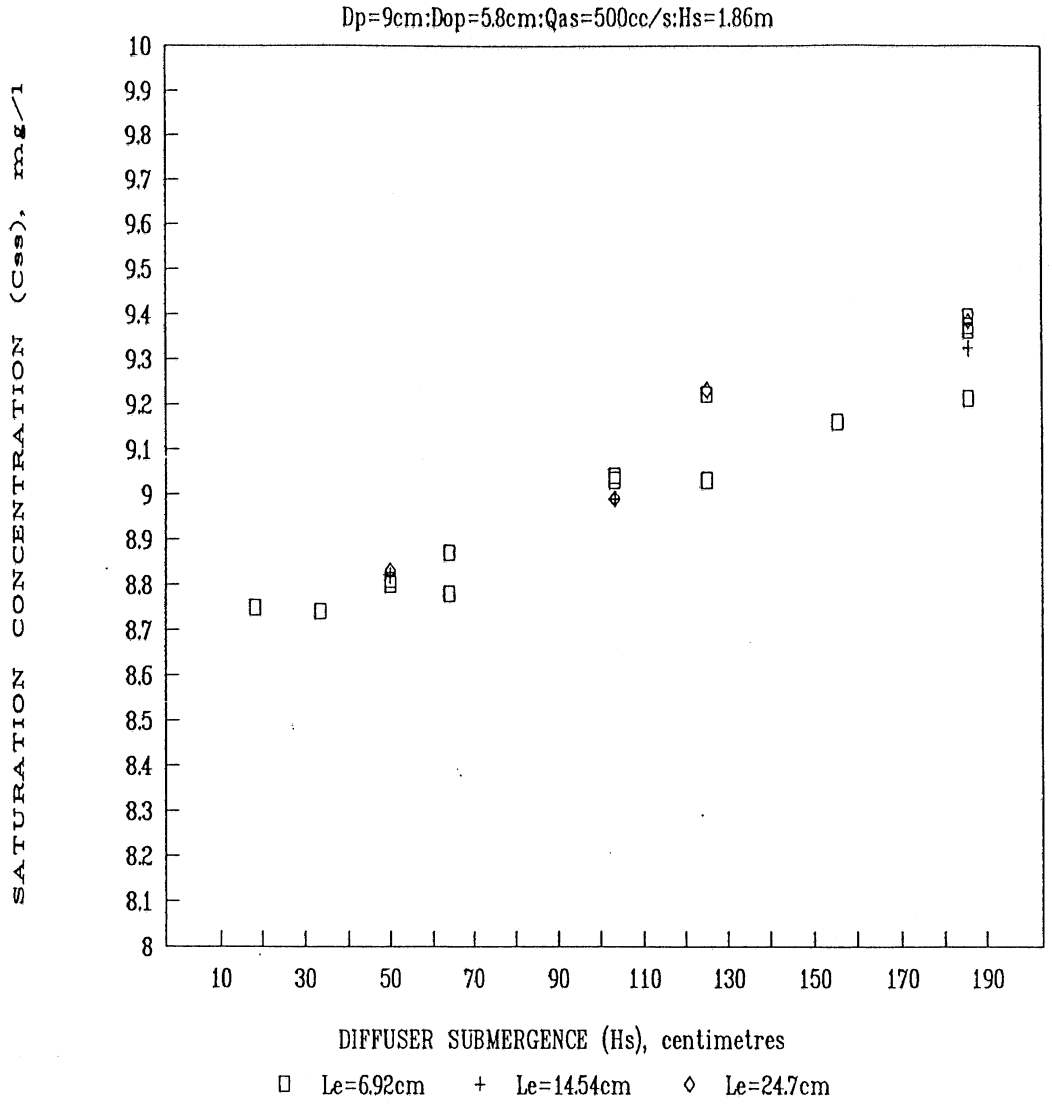

Fig. 4.17 Effect of diffuser submergence on saturation concentration

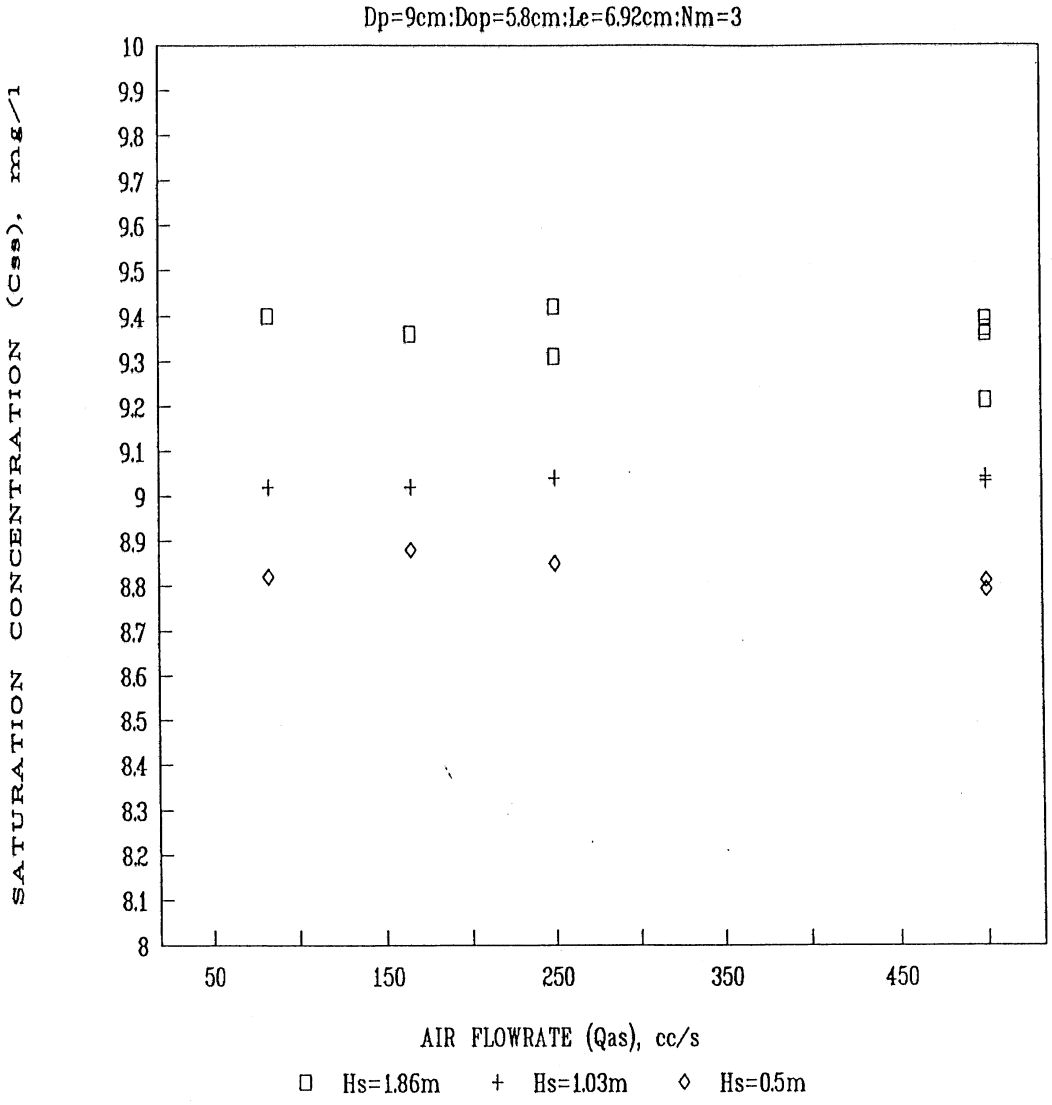

Fig. 4.18 Effect of air flowrate on saturation concentration

$$= \frac{g\ H_s^3}{\nu_w^2} \qquad (4.6)$$

ν_w = kinematic viscosity

The Galileo number represents the ratio of gravitational force to viscous force.

D_r and L_r are geometric parameters of the tube. H_r is the submergence ratio.

From figure 4.1 it is seen that the mass transfer coefficient does not vary monotonically with the tube length. As the tube length is increased, the mass transfer coefficient initially increases up to the optimum value and then decreases slightly with increase of the tube length. Hence two correlations were made, one for the range where the mass transfer coefficient increased with the tube length and the other for the range where the mass transfer coefficient decreased with the increase of the tube length. These correlations are given below.

K_1A decreasing with the increase in L_r (Upper range)

$$S_{tm} = 0.00526\ F_s^{-0.183}\ G_a^{0.1475}\ D_r^{-0.061}\ L_r^{-0.031}\ H_r^{0.162} \qquad (4.7)$$

K_1A increasing with the increase in L_r (Lower range)

$$S_{tm} = 0.0055\ F_s^{-0.187}\ G_a^{0.147}\ D_r^{-0.0295}\ L_r^{0.032}\ H_r^{0.141} \qquad (4.8)$$

The exponents of the terms in the two correlations are nearly the same except for the term L_r whose exponent has changed sign and the term D_r. These correlations are plotted in figures 4.19 and 4.20 alongwith the experimental values. The standard errors were 0.042 (number of observations = 75; degrees of freedom = 69) and 0.065 (number of observations = 55; degrees of freedom = 49) for the first and the second regression respectively. The coefficients of determination r^2 were 0.996 for the first regression and 0.995 for the second regression.

The range of applicability of the above two correlations depends on the diameter ratio. Figure 4.21 defines these ranges.

The correlations show that the mass transfer effected by the device in an air water system depends on both the Galileo and the Froude numbers through their effects on the liquid film coefficient and the air–water interfacial area.

The experimental results given by the above correlation (4.7) can be expressed in terms of the actual experimental parameters as below:

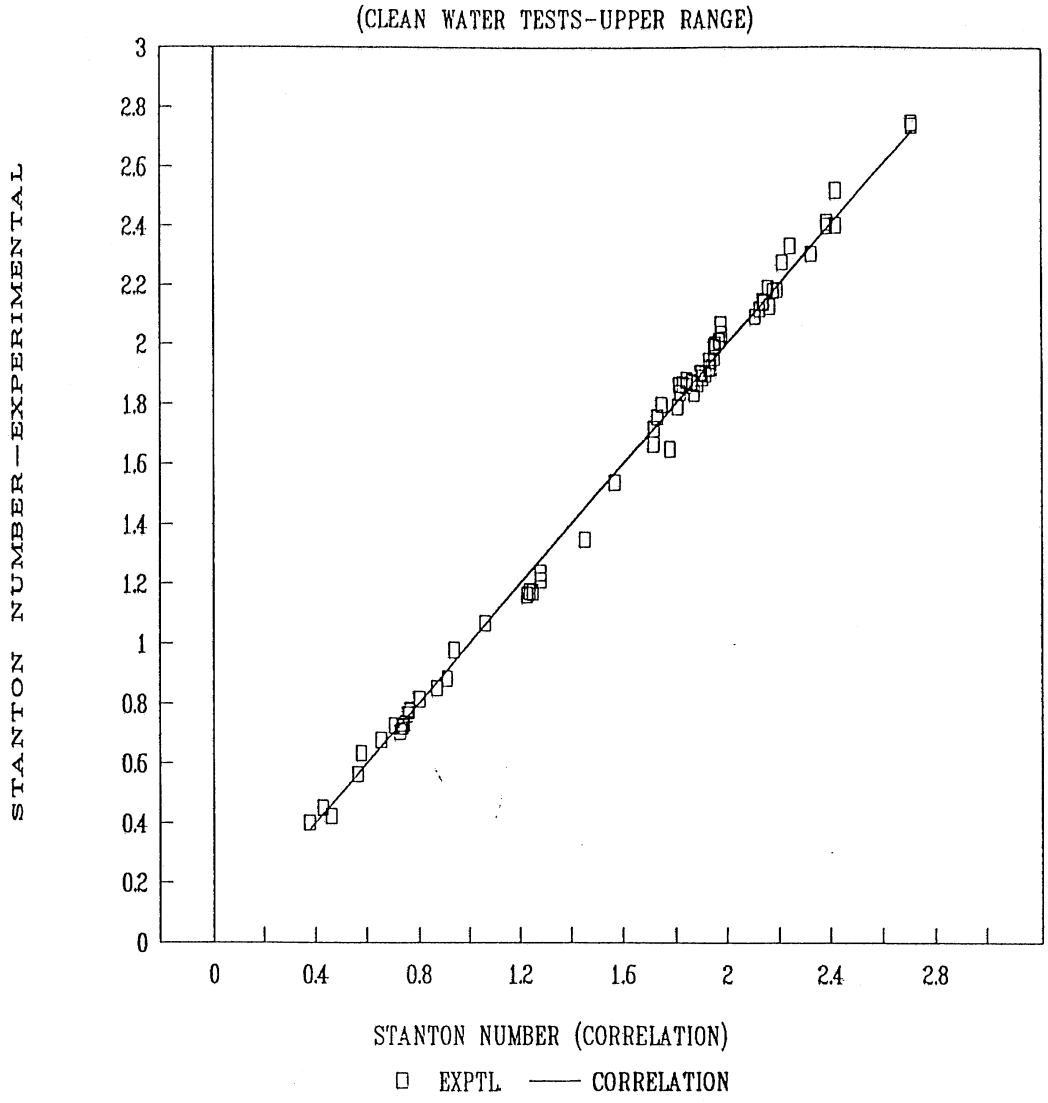

Fig. 4.19 Correlation for Stanton number (correlation 4.7)

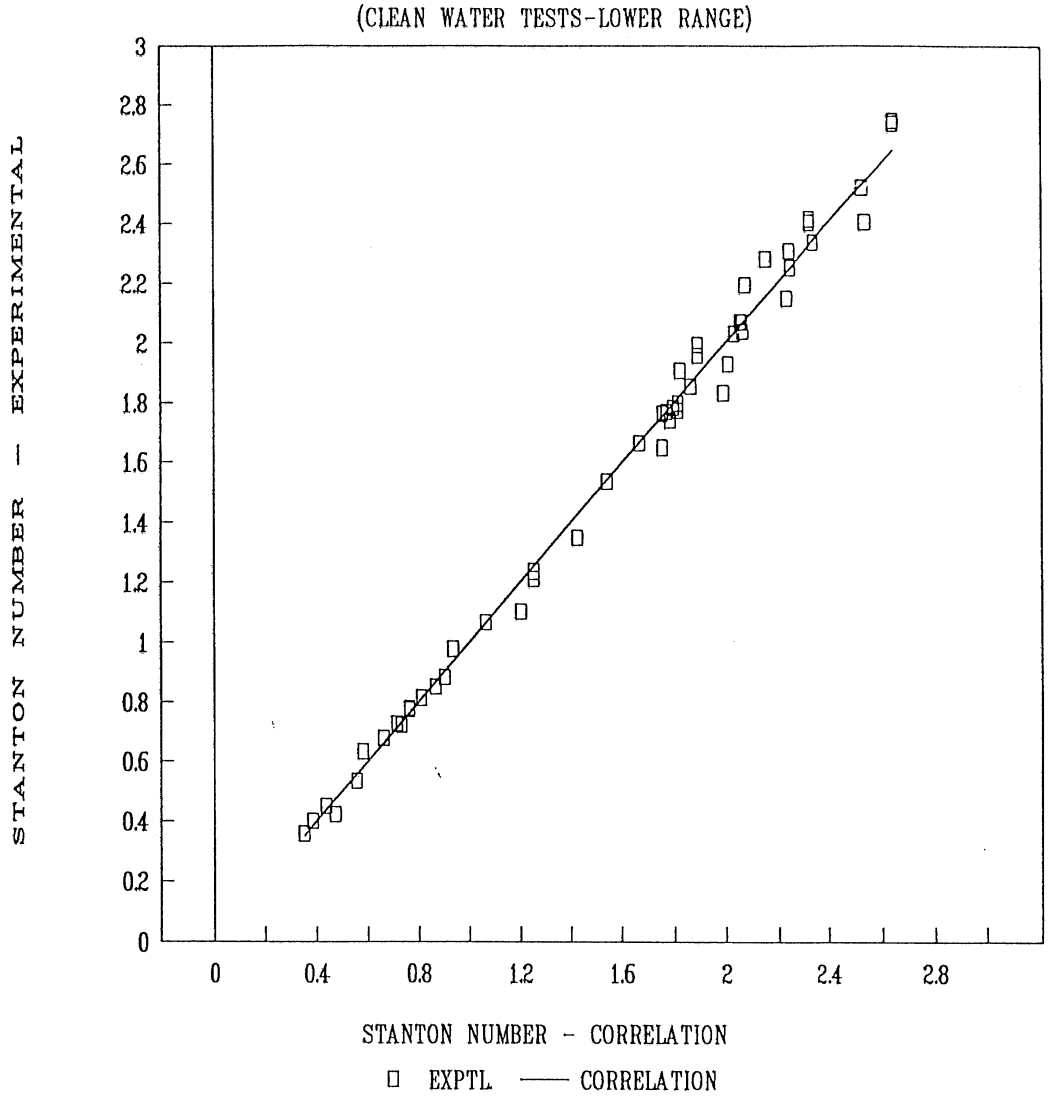

Fig. 4.20 Correlation for Stanton number (correlation 4.8)

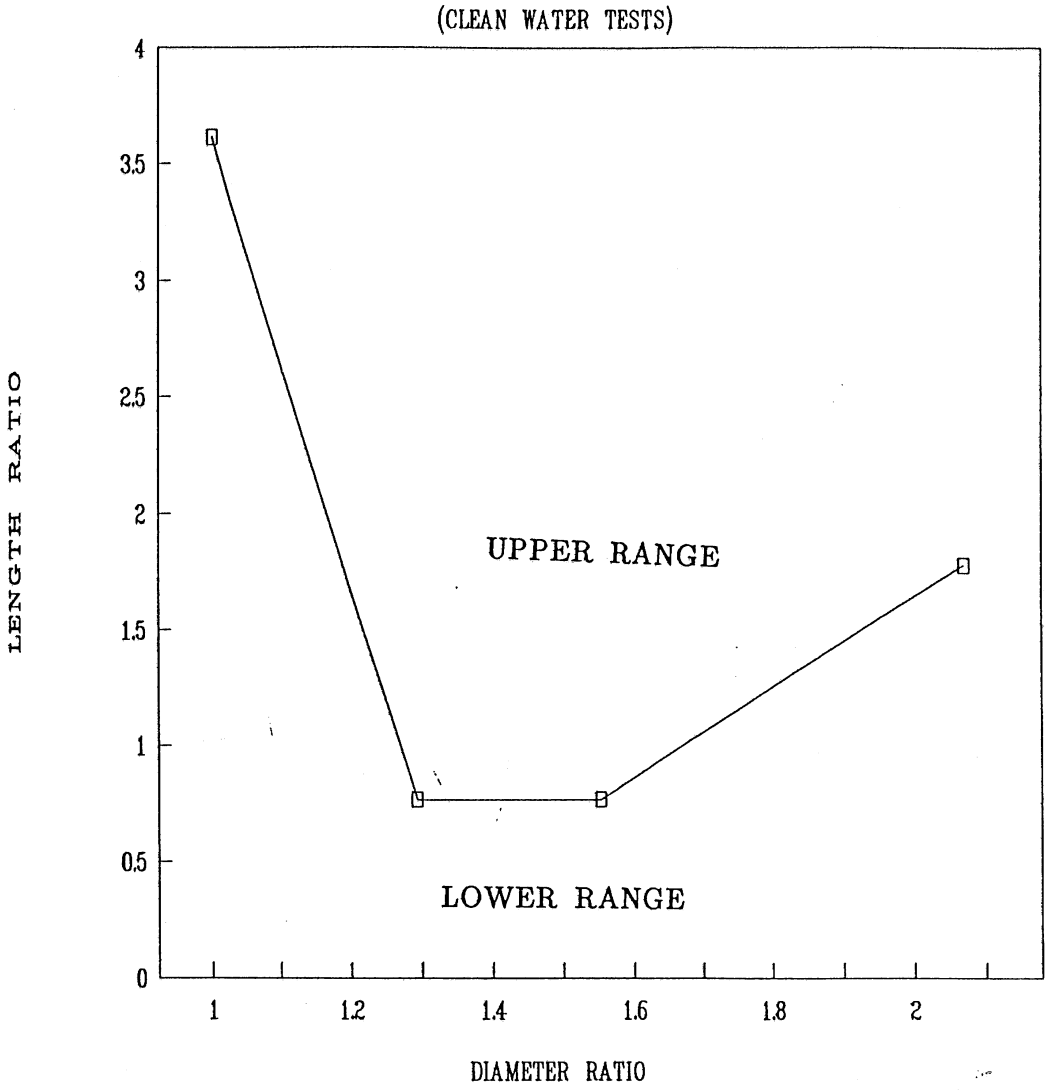

Fig. 4.21 Range of application of correlations

$$K_lA \propto H_s^{0.696} J_a^{0.817} D_p^{1.81} L_e^{-0.031} \quad (4.9)$$

$$\propto H_s^{0.696} Q_a^{0.817} D_p^{0.176} L_e^{-0.031} \quad (4.10)$$

The simple plume theory gave the following relationship for K_lA (equation 2.76):

$$K_lA \propto H_s^{2/3} J_a^{7/12} D_p^{7/6}$$

The exponent of H_s given by the simple plume theory agrees well with the experimental values given by equation (4.9). The other two exponents do not match with the experimental values.

Relationships (4.9) and (4.10) give the relative effects of the various parameters on the mass transfer coefficient which we have already seen from the experimental results. With sufficient number of the peripheral orifices, the effective tube lengths, larger than the optimum, do not significantly affect the mass transfer coefficient.

The correlation (4.7) was used to estimate the mass transfer contributions of the plume and the tube. This estimation was done on the assumption that the mass transfer within the tube for a given diffuser submergence (H_s) and air flowrate (Q_a) would be equal to the mass transfer in the bubble column for the same air flowrate and a submergence obtained with the water surface set at the elevation of the outlet end (top) of the tube. The value of K_lA_t, the mass transfer rate across the air–water interface lying within the tube, was obtained by substituting the value of diffuser submergence ratio corresponding to the top of the tube in the correlation (4.7). In this calculation, the volumetric air flowrate (Q_a) through the tube corresponding to the system submergence (H_s) was used. The value of K_lA_{pl}, the mass transfer rate within the plume outside the tube, was obtained by subtracting the value of K_lA_t from the value of the overall K_lA. The calculation was done for a diffuser diameter of 9 centimeters under a submergence of 1.86 m and for tube lengths varying from 6 to 30 centimetres. Figure 4.22 shows the results. These results show that as the tube length is increased, the mass transfer within the device increases whereas the mass transfer in the plume initially increases up to a maximum value and then decreases. The sum of these two variations result in the overall trend shown by the experimental results. With the optimum tube length, about 16 per cent of the total mass transfer occurred within the tube. The curves representing K_lA and K_lA_{pl} converge towards a value of about 800 cc/sec at zero effective tube length. This would be the value of the K_lA that would have been obtained without the tube. It can be seen from figure 4.22 that at the optimum tube length about 36 per cent increase in the value of K_lA has been achieved compared to the value obtained for zero tube length.

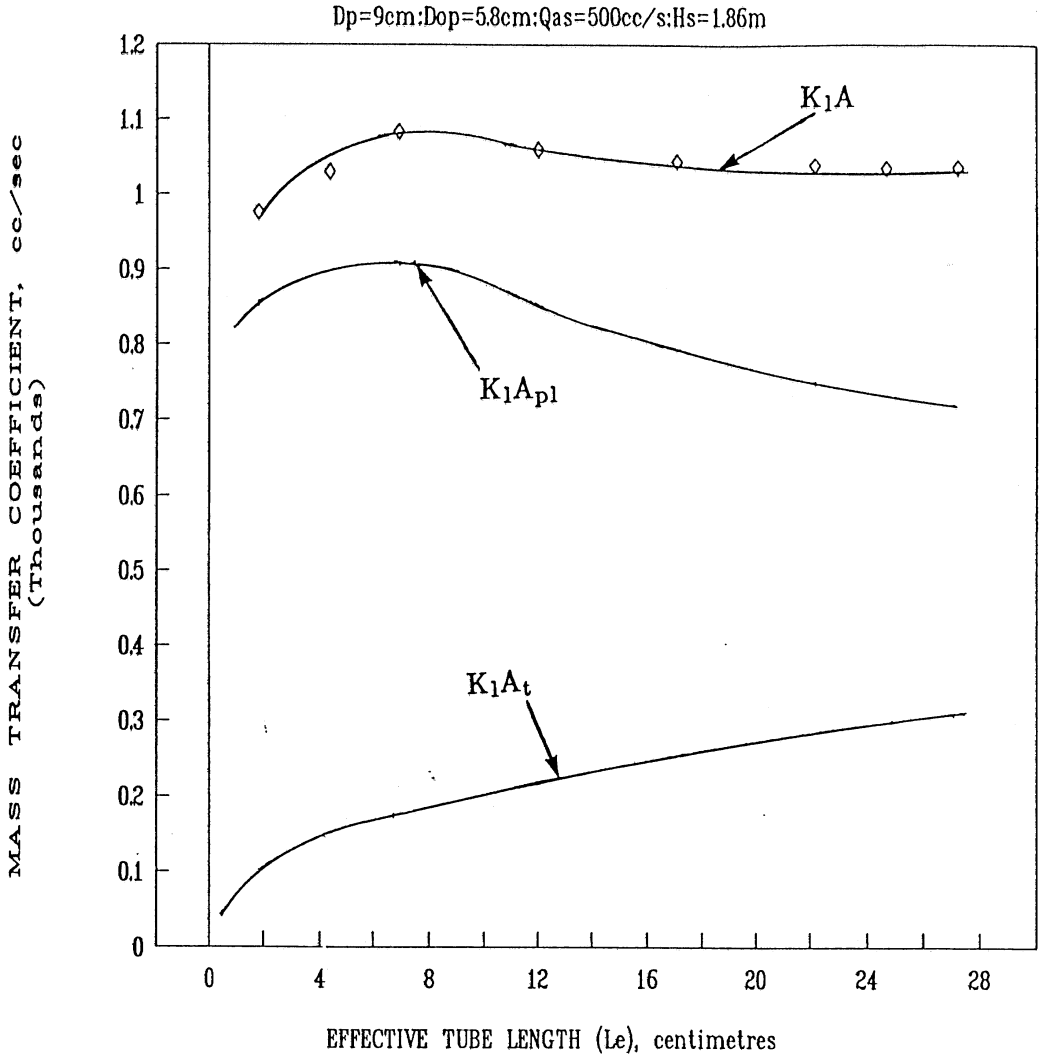

Fig. 4.22 Variation of K_lA_t and K_lA_{pl} with tube length (from correlation 4.7)

Performance comparison

As part of this research program, experiments were conducted to compare the mass transfer characteristics the SAF diffuser with those of a 17.8 cm dia. porous stone diffuser. The comparison is made in respect of the following parameters.

- Mass transfer coefficient
- Standard Aeration Efficiency

The SAF diffuser chosen had a tube diameter of 9 cm whereas the porous stone diffuser had a diameter of 17.8 cms. This meant that the porous stone diffuser had a plan area about 4 times that of the SAF design. Hence the comparison was made of the K_1A per unit area of the diffuser for the same air flux (air flowrate per unit area) through both the devices.

Figure 4.23 shows the comparison in respect of the mass transfer coefficient. It could be seen that the SAF design has nearly the same mass transfer coefficient per unit area as the porous stone for the same air flux. In this context, it may be noted that by increasing the number of the peripheral orifices, the K_1A of the SAF diffuser can be further increased by about 5 percent (see figure 4.5).

The mass transfer coefficients and the saturation concentration values were used to calculate the Standard Oxygen Transfer Rate (SOTR) through the device for different air flowrates. Figure 4.24 shows the SOTR of the SAF diffuser for different air flowrates.

The SOTR values were divided by the power input to obtain the Standard Aeration Efficiency. The input power was calculated from the measured air pressure upstream of the diffuser using the following relationship.

$$\text{Delivered power} = \frac{wRT_1}{K}\left[\left(\frac{P_2}{P_1}\right)^K - 1\right] \qquad (4.11)$$

where

w = weight flowrate of air
R = gas constant
T_1 = absolute temperature before compression
P_1 = absolute pressure before compression
P_2 = absolute pressure after compression
K = $(k-1)/k$
k = ratio of specific heats for air

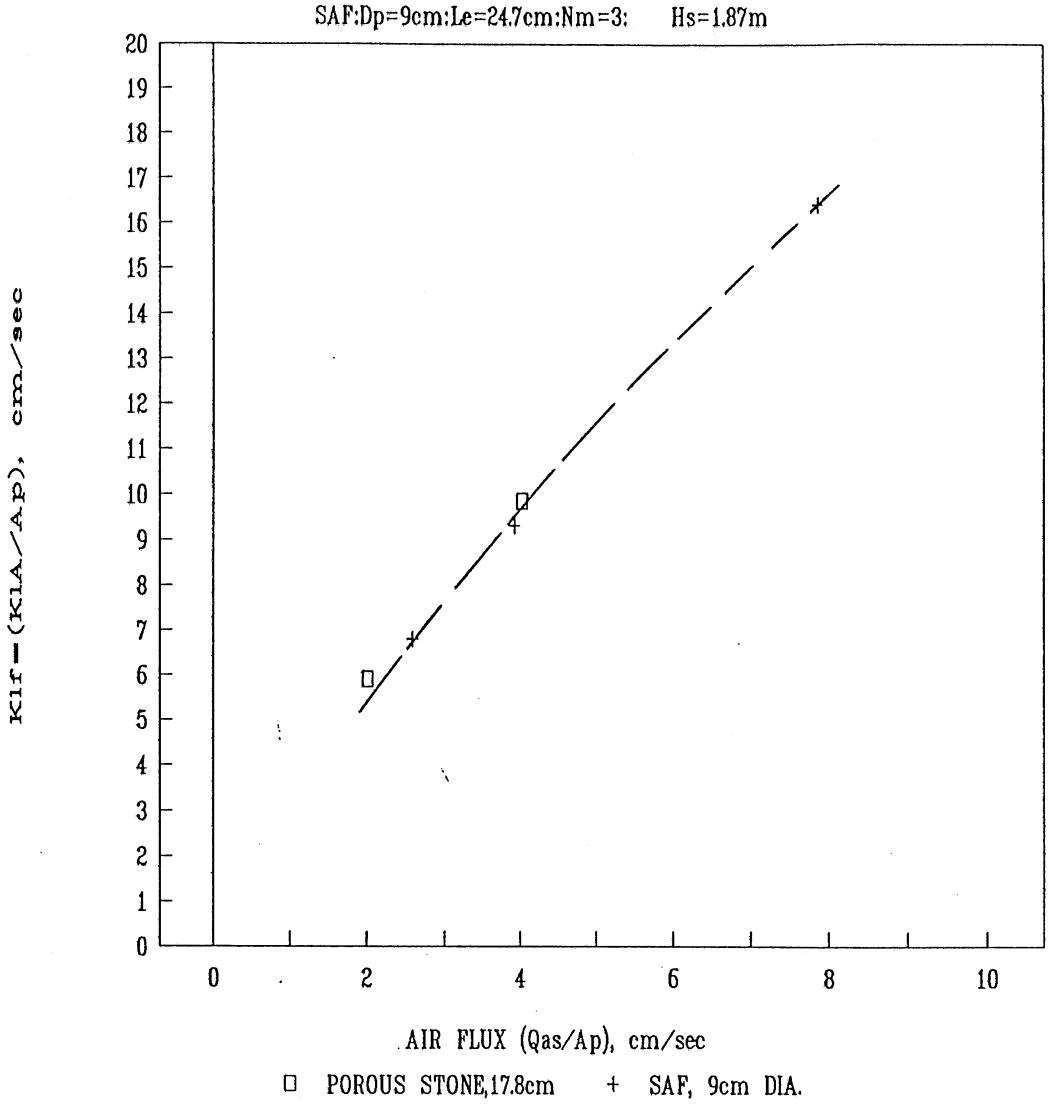

Fig. 4.23 Comparison of K_{lf}

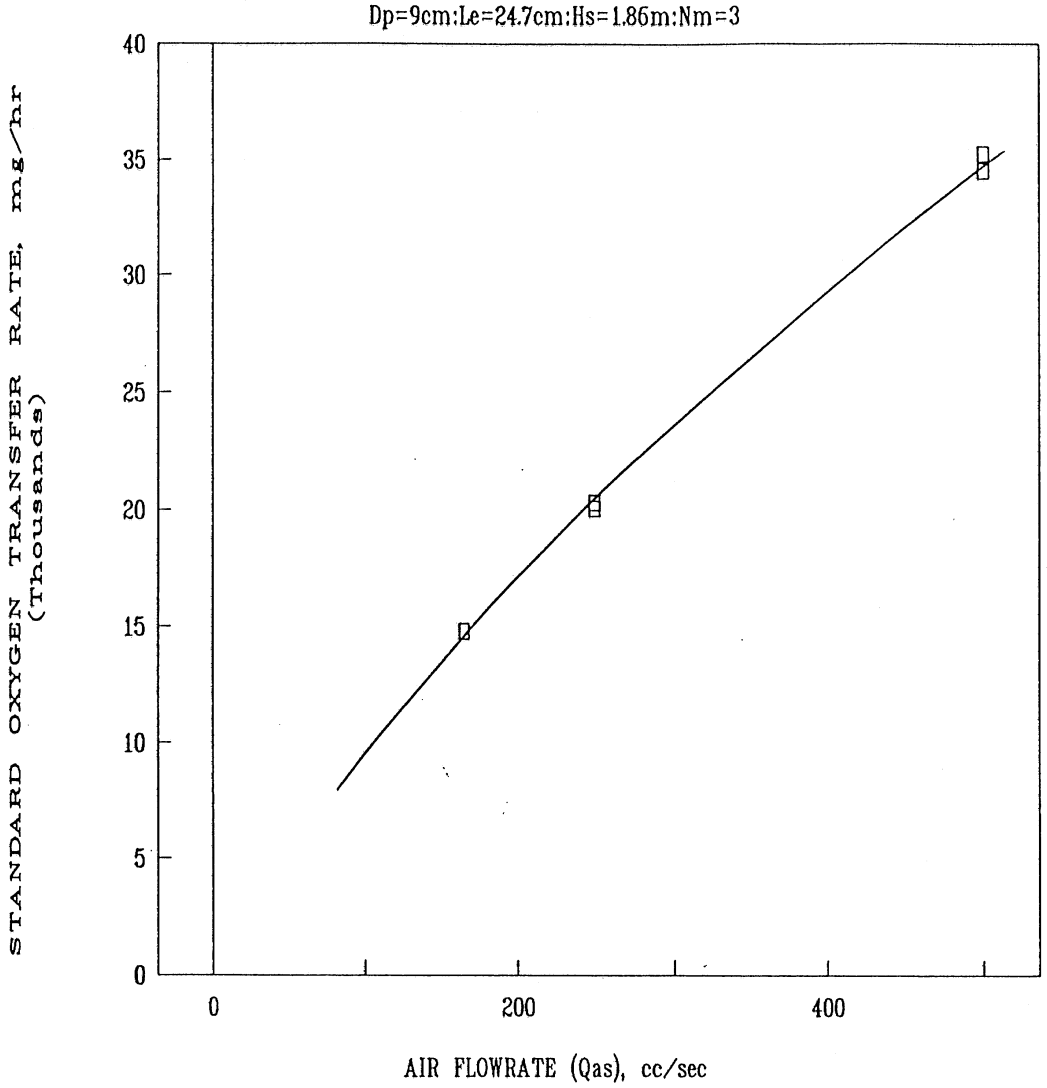

Fig. 4.24 Standard Oxygen Transfer Rate (SAF Diffuser)

The air pressures upstream of the SAF diffuser are shown in figure 4.25. As the air flowrate increased, the pressure upstream of the diffuser decreased. This decrease in pressure is due to the increase of the kinetic energy of water and consequent pressure drop within the tube as well as due to the density reduction of the liquid within the tube as a result of air injection. A comparison of the inlet air pressures upstream of the diffuser for the SAF diffuser and the porous stone diffuser is shown in figure 4.26. For a given air flux through the diffuser, the inlet air pressures of the SAF diffuser are much less than those of the porous stone diffuser. Also, with increase of the air flux, the upstream air pressure decreased in the case of the SAF diffuser and increased in the case of the porous stone diffuser.

Figure 4.27 shows comparison of the Standard Aeration Efficiencies (SOTR/delivered power) of the SAF and the porous stone diffusers operating in clean water. As could be seen from the results, the Standard Aeration Efficiencies of the SAF diffuser were about 10 to 20 per cent higher than those of the porous stone diffuser.

While comparing the efficiencies it should be noted that the air inlet arrangements of the SAF and the porous stone diffusers have some differences. In the SAF design, it is envisioned that the total air flow would branch equally into the three modules through air inlet tubes connected on the upstream side to a larger manifold tube such that the diffuser energy loss would essentially be that occurring in the air inlet tubes and downstream ie the manifold losses are small in comparison to the losses in the diffuser. Hence the air pressure used in the calculation of the energy requirement was that in the air inlet tube (7.1 mm dia) which passed one third of the total air flowrate. The porous stone diffuser had only one air inlet, 7.5 mm dia. This is an important difference in the design of the two devices.

As shown in the figure 4.23 the values of K_1A per unit area of the SAF and the porous stone diffusers are practically the same. The increased SAE values obtained with the SAF diffuser are due the low pressure losses associated with the device in comparison to the porous stone. Hence with higher diffuser submergences, the difference in the SAE values of the SAF and the porous stone diffusers would decrease and at sufficiently large submergences, the performance of the two devices would practically be the same. Thus the main advantage of the SAF diffuser in terms of the SAE is for low submergence applications. However, the SAF diffuser has additional advantage arising out of the large size orifices used. On account of the large size orifice (0.5 mm), the device is expected to be much less prone to clogging compared to the fine pore devices which have pore diameters of few microns. This would considerably decrease the maintenance costs. The extent of the savings can be quantified only after some field trials. Also, the SAF diffuser can be easily cleaned by increasing the inlet air pressure for short durations. The increased air flow would induce a high velocity air–water flow which would help cleaning of the tube.

Figure 4.28 shows the variation of the SAE of the SAF diffuser with diffuser submergence. As the diffuser submergence was increased, the SAE decreased. This trend is the consequence of the variation with depth of the

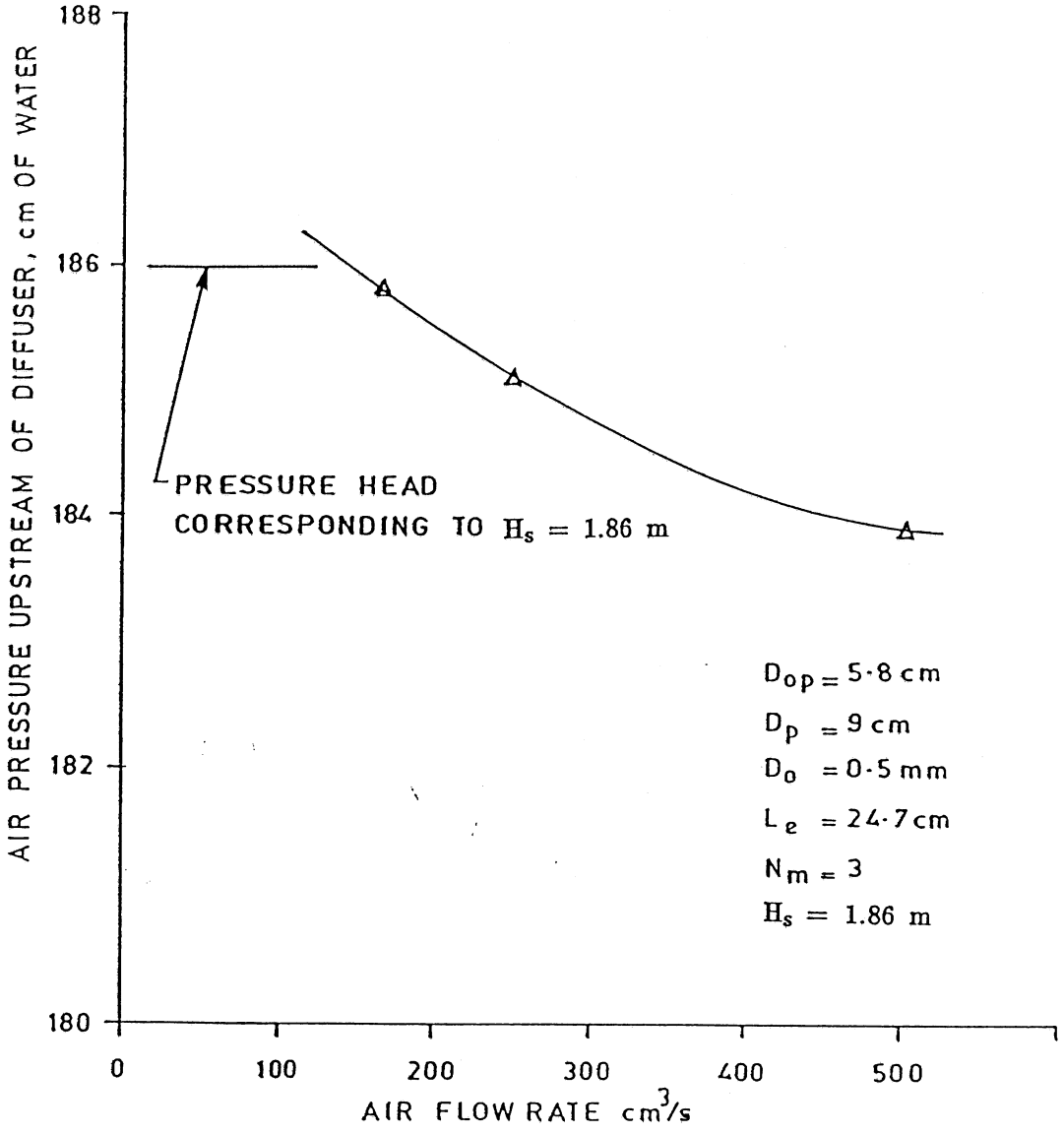

Fig. 4.25 Air pressure upstream of Diffuser (SAF)

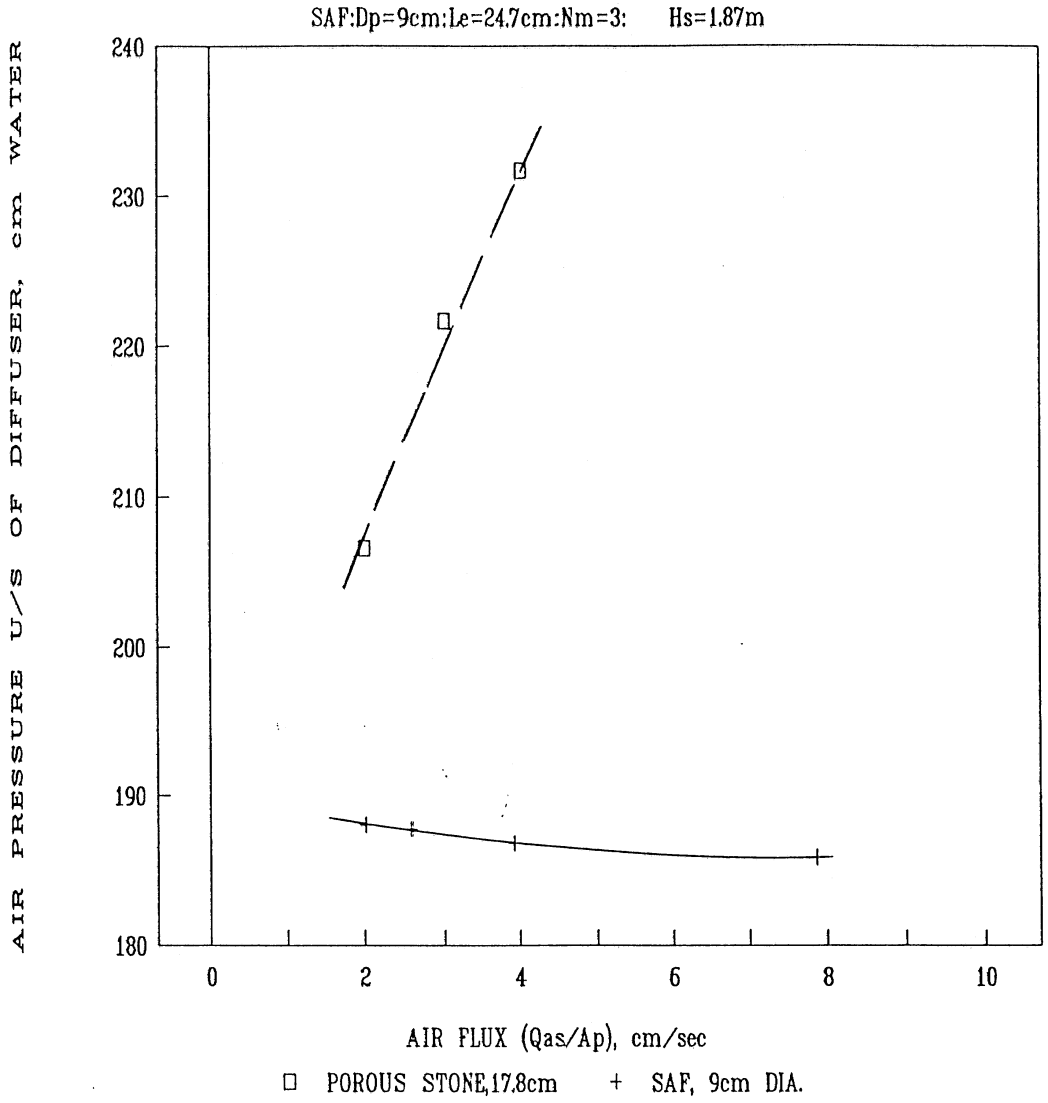

Fig. 4.26 Comparison of air pressure upstream of diffuser

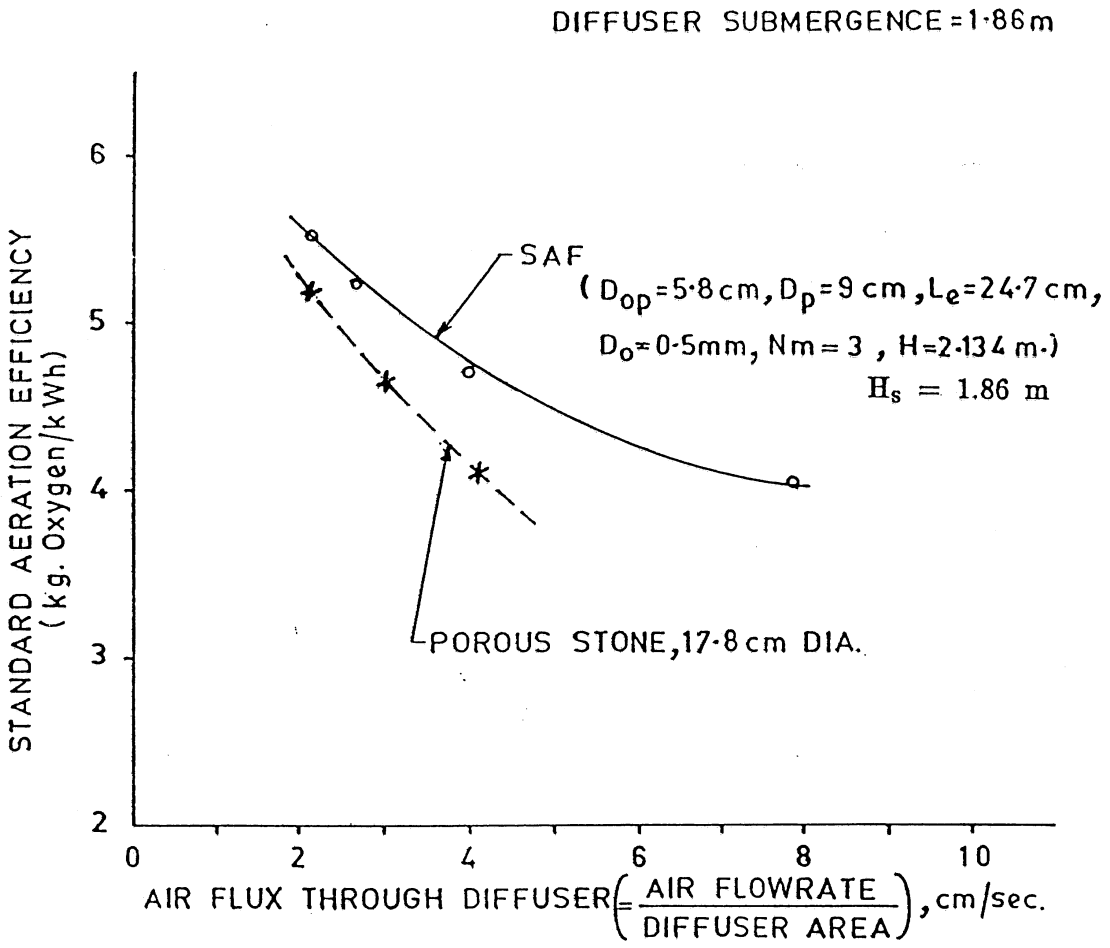

Fig. 4.27 Performance comparison in clean water

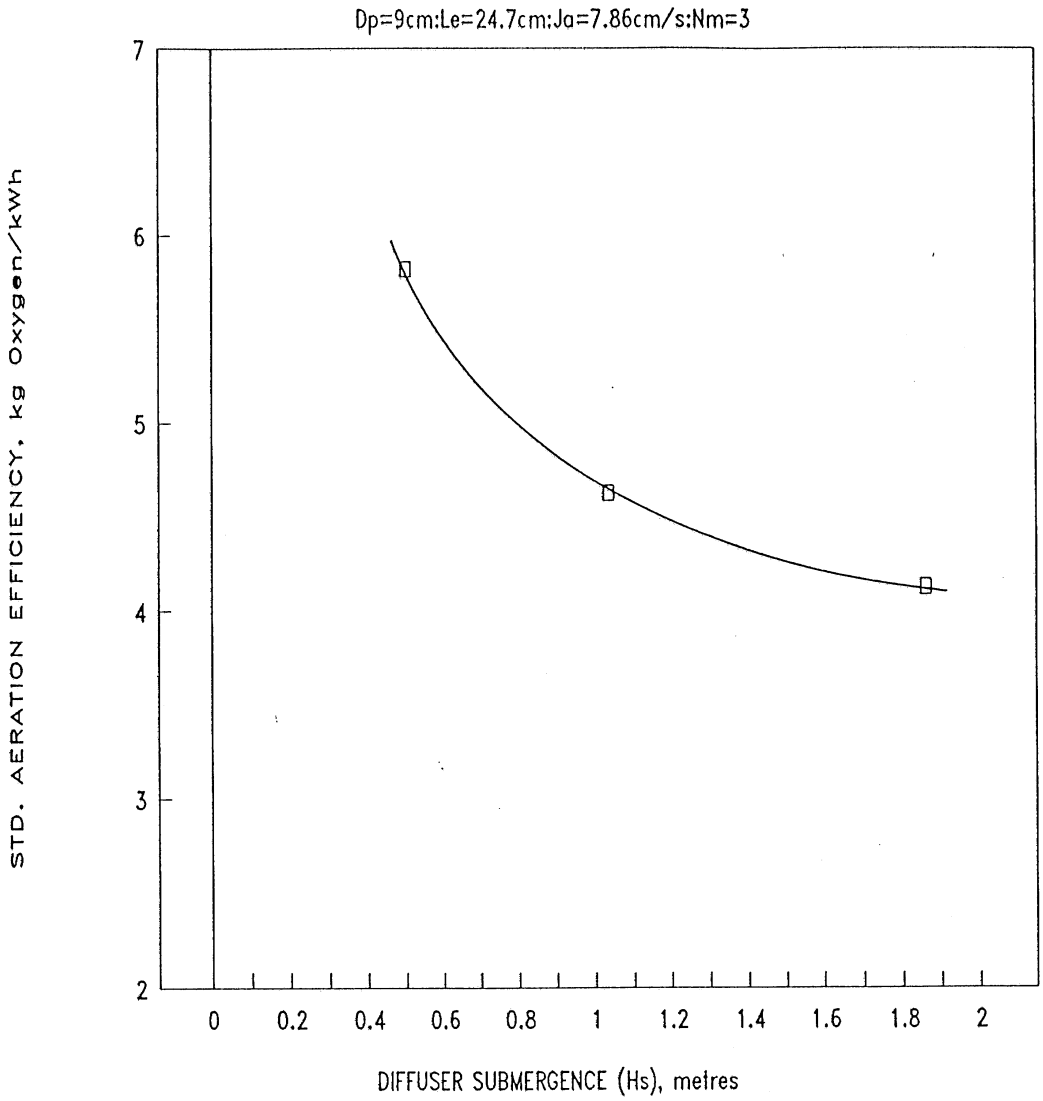

Fig. 4.28 Effect of diffuser submergence on SAE of SAF Diffuser

two parameters governing the SAE namely, the K_1A and the power input. As seen from equation (4.9), the value of K_1A increased with the increase of submergence as $H_s^{0.69}$ whereas the input power increased as $\left[\left(\frac{P_2}{P_1}\right)^K - 1\right]$ (equation 4.11). The rate of increase of the power input with increase of the diffuser submergence is more than that of the K_1A and hence the reduction of the SAE with increase of the diffuser submergence.

4.6 EFFECT OF SURFACTANT ON PERFORMANCE CHARACTERISTICS

Few experimental studies were undertaken to assess the effect of surfactants on the mass transfer characteristics of the SAF diffuser. These studies were conducted by adding 7 mg/l of household detergent to the water at the beginning of the test as recommended in the ASCE Standard for the Measurement of Oxygen Transfer in Clean Water, July 1984.

Figure 4.29 shows the effect of the tube geometry on the mass transfer coefficient. As seen with the experimental results obtained with clean water, the mass transfer coefficient for a given tube diameter increased initially as the effective tube length was increased, reached maximum value over a range of tube lengths and thereafter decreased with further increase of the tube length. The trend was the same for all the tube diameters though the effective tube length corresponding to the maximum mass transfer coefficient differed for different tube diameters. For a given tube diameter, the maximum mass transfer coefficient occurred at an effective tube length that was greater than the length obtained in clean water (see figures 4.7, 4.29 and 4.30). Figure 4.31 shows a comparison of the optimum effective tube lengths for different tube diameters for performance in clean water and in water with detergent addition. These results indicate that the optimum tube length for a given tube diameter varies with the water quality.

Figure 4.32 shows the effect of air flowrate on the mass transfer coefficient. As in the case of the clean water tests, the mass transfer coefficient increased with the increase in the air flowrate. The trend of variation of the mass transfer coefficient with effective tube length was the same for the two air flowrates studied.

Figure 4.33 shows the effect of diffuser submergence on the mass transfer coefficient. The mass transfer coefficient increased as the diffuser submergence was increased. The trend of variation of the mass transfer coefficient with the effective tube length was the same for all the submergences. Results presented in figures 4.32 and 4.33 show that the optimum length ratio of the diffuser does not vary with the variations in the air flowrate and diffuser submergence.

Figure 4.34 shows the variation of the maximum areal specific mass transfer coefficient with the diameter ratio. The trend is similar to the one

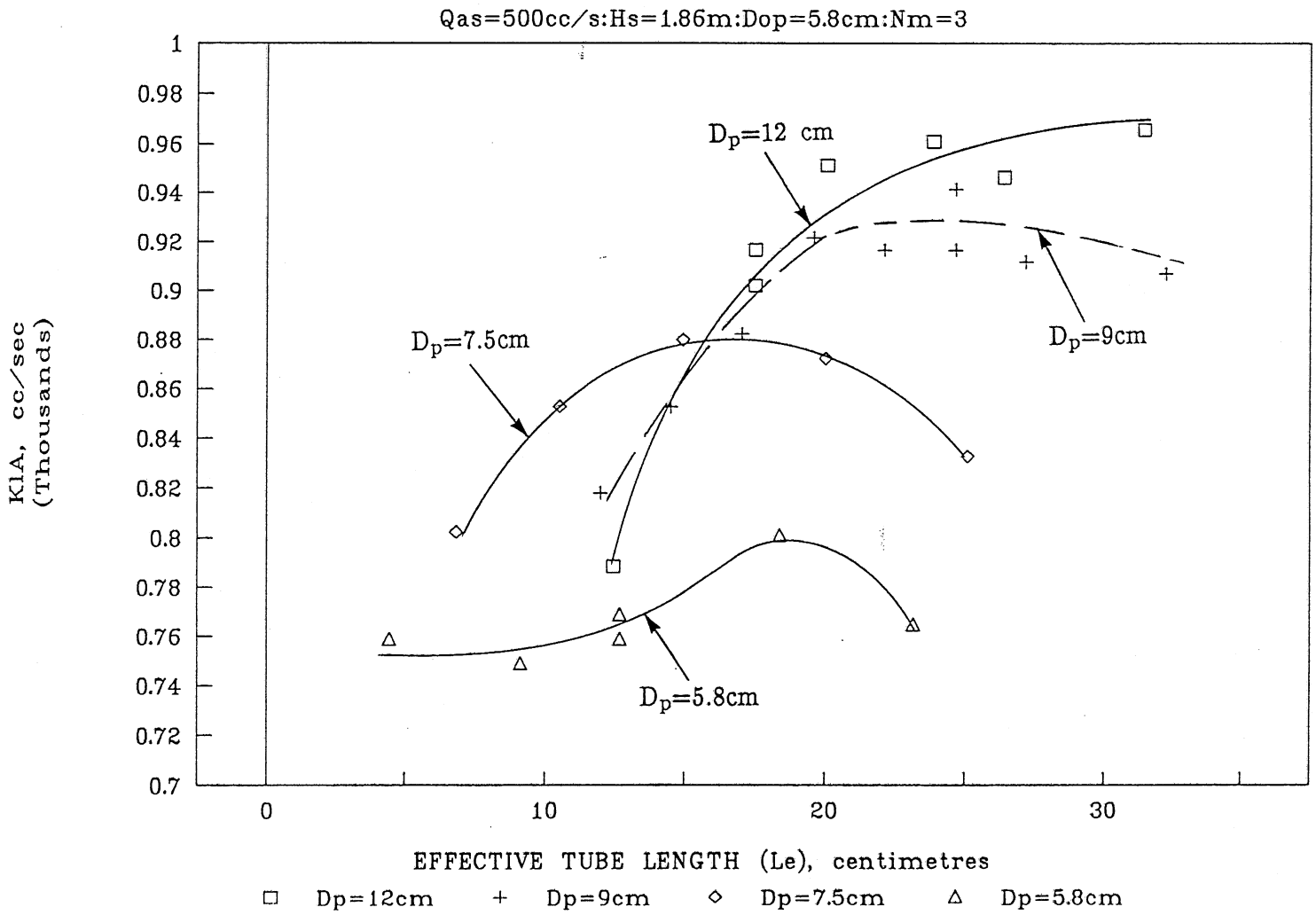

Fig. 4.29 Effect of tube geometry on K_1A
(Water + Detergent)

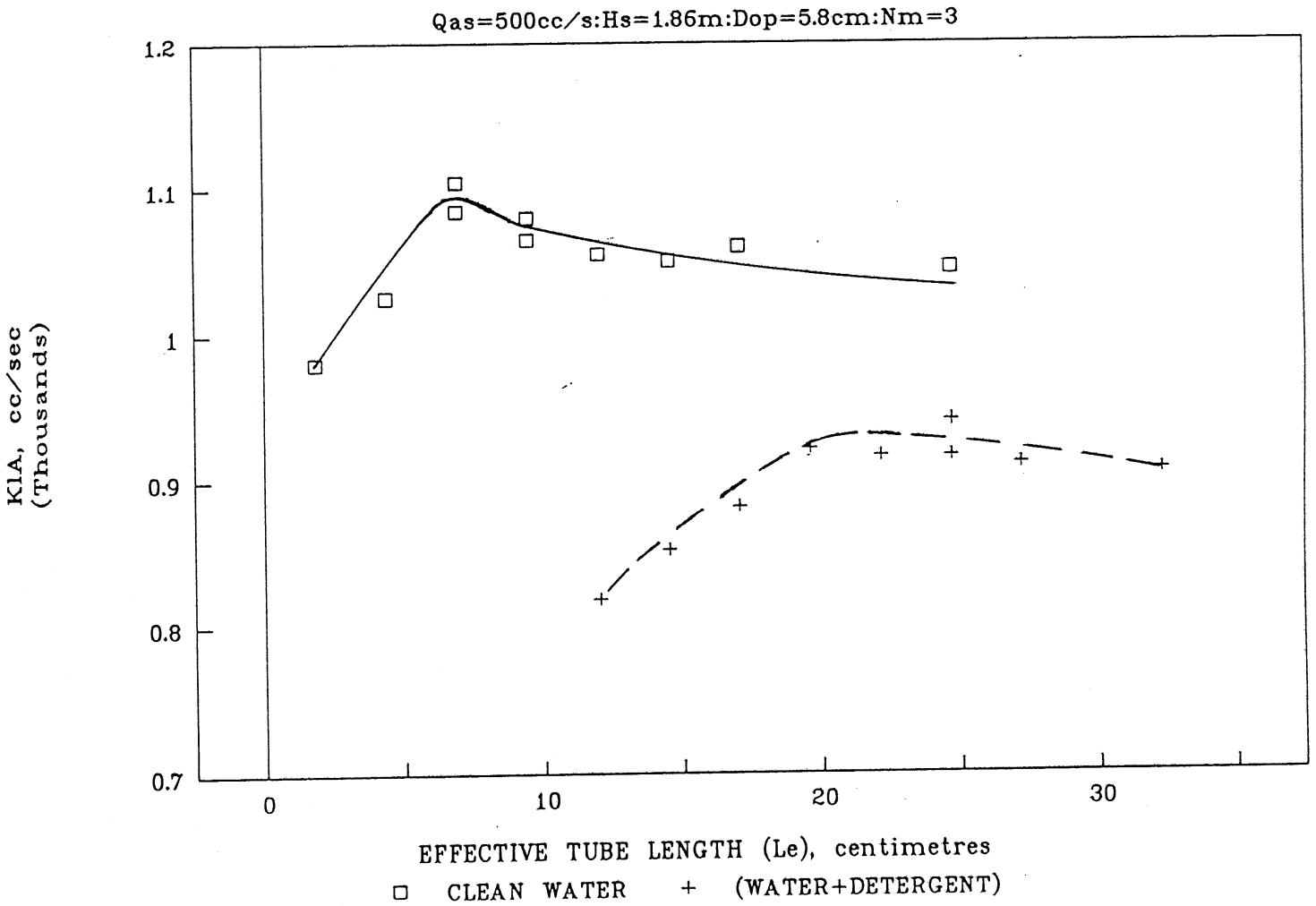

Fig. 4.30 Comparison of K_1A (D_p = 9 cm)

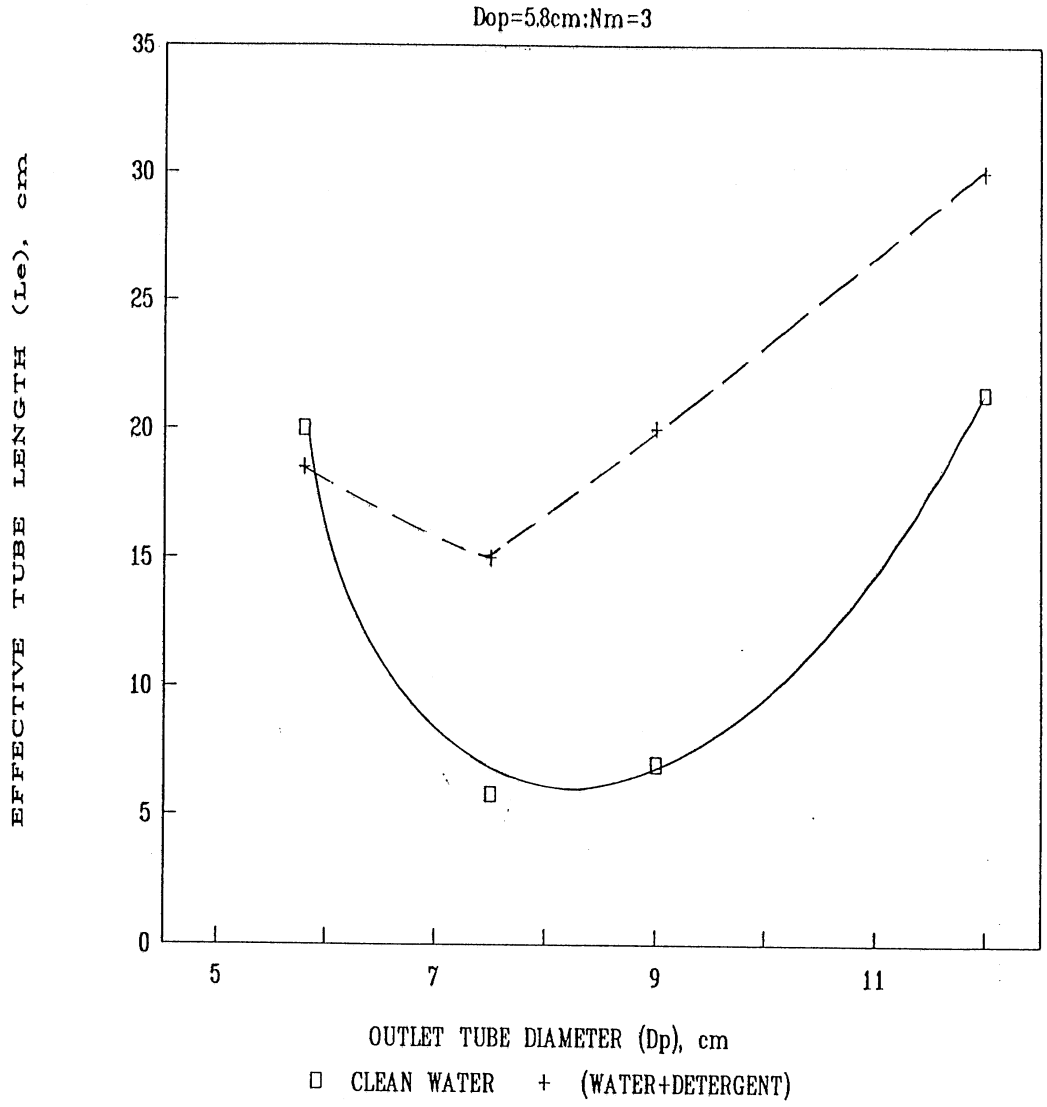

Fig. 4.31 Comparison of optimum tube lengths

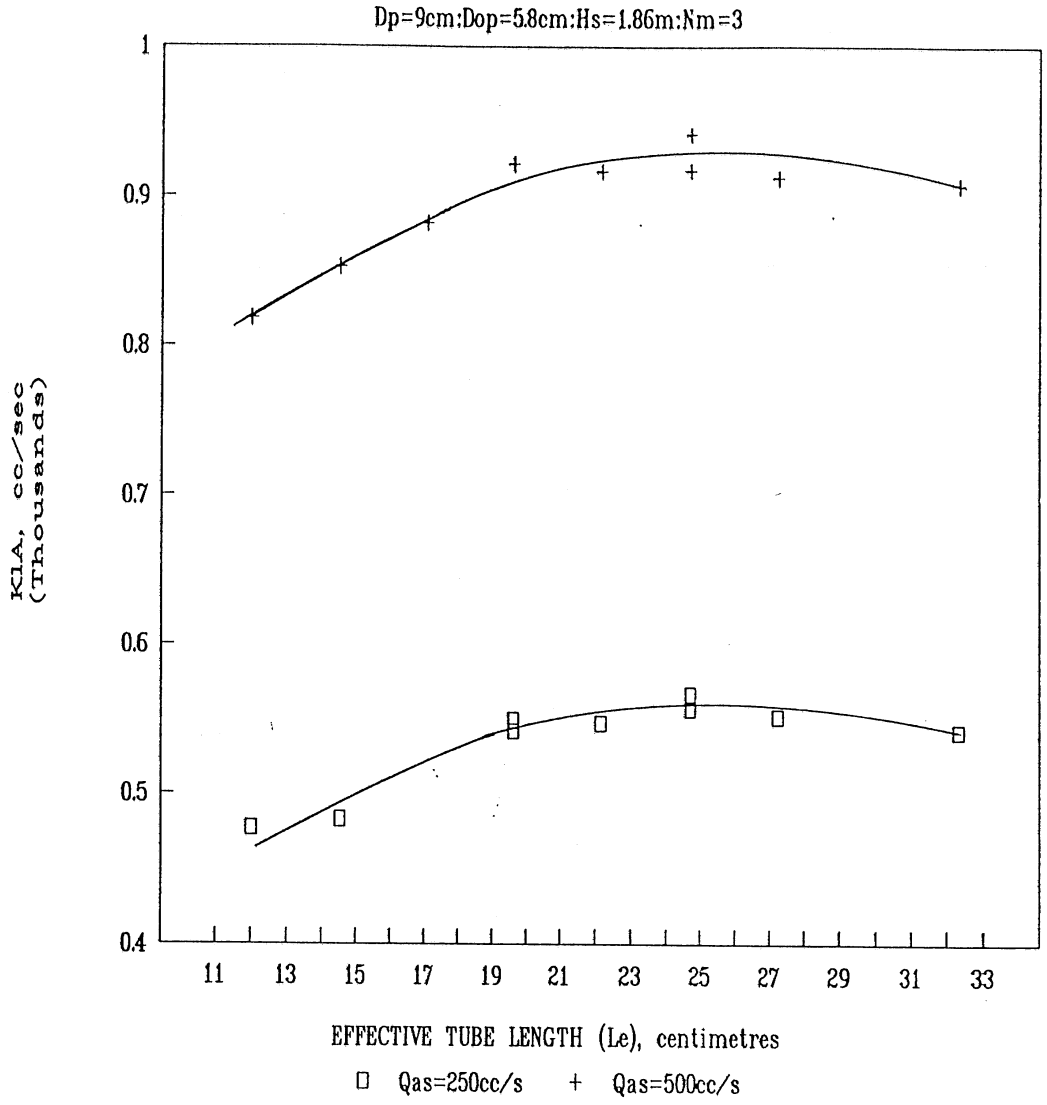

Fig. 4.32 Effect of air flowrate on K_1A (Water + Detergent)

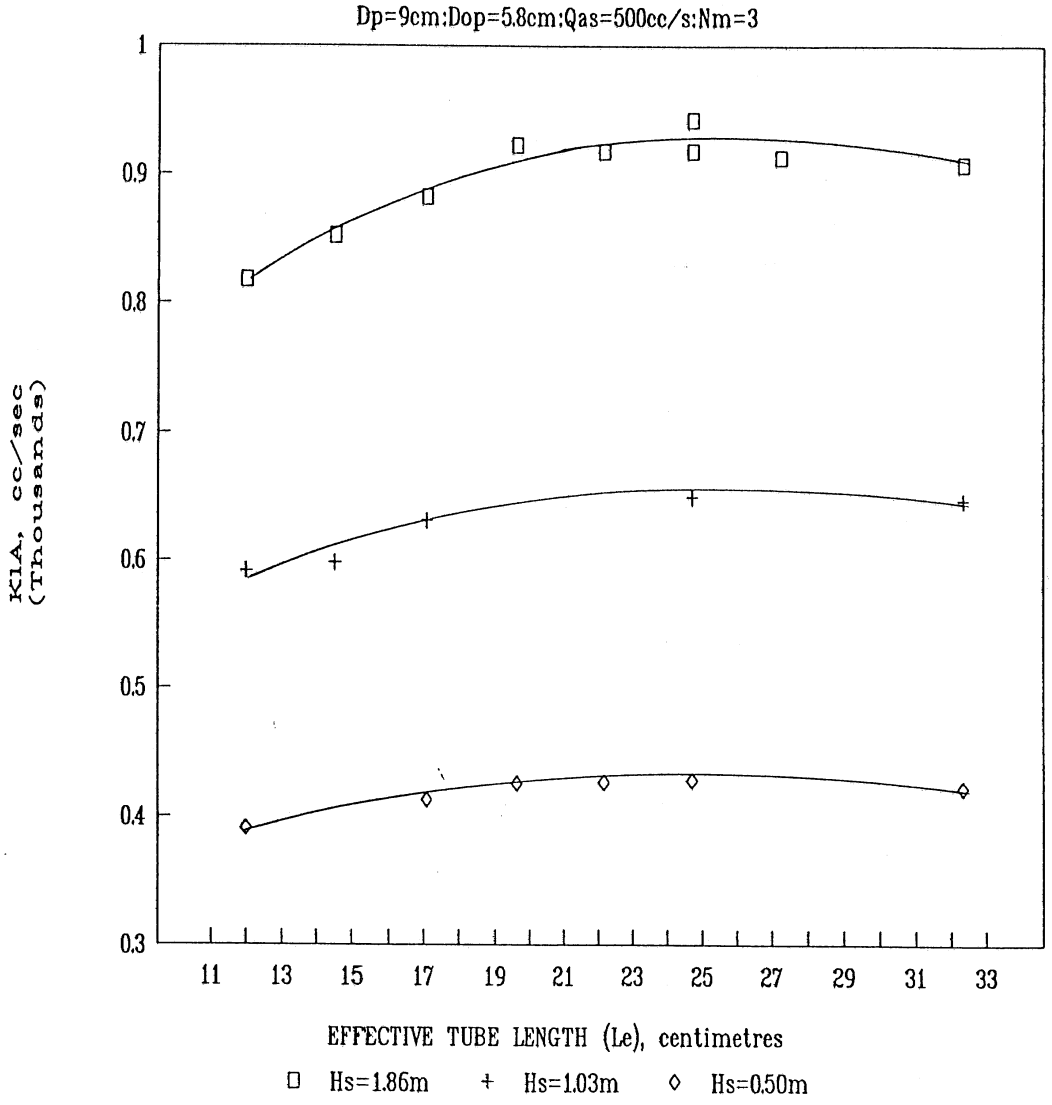

Fig. 4.33 Effect of diffuser submergence on K_1A (Water+Detergent)

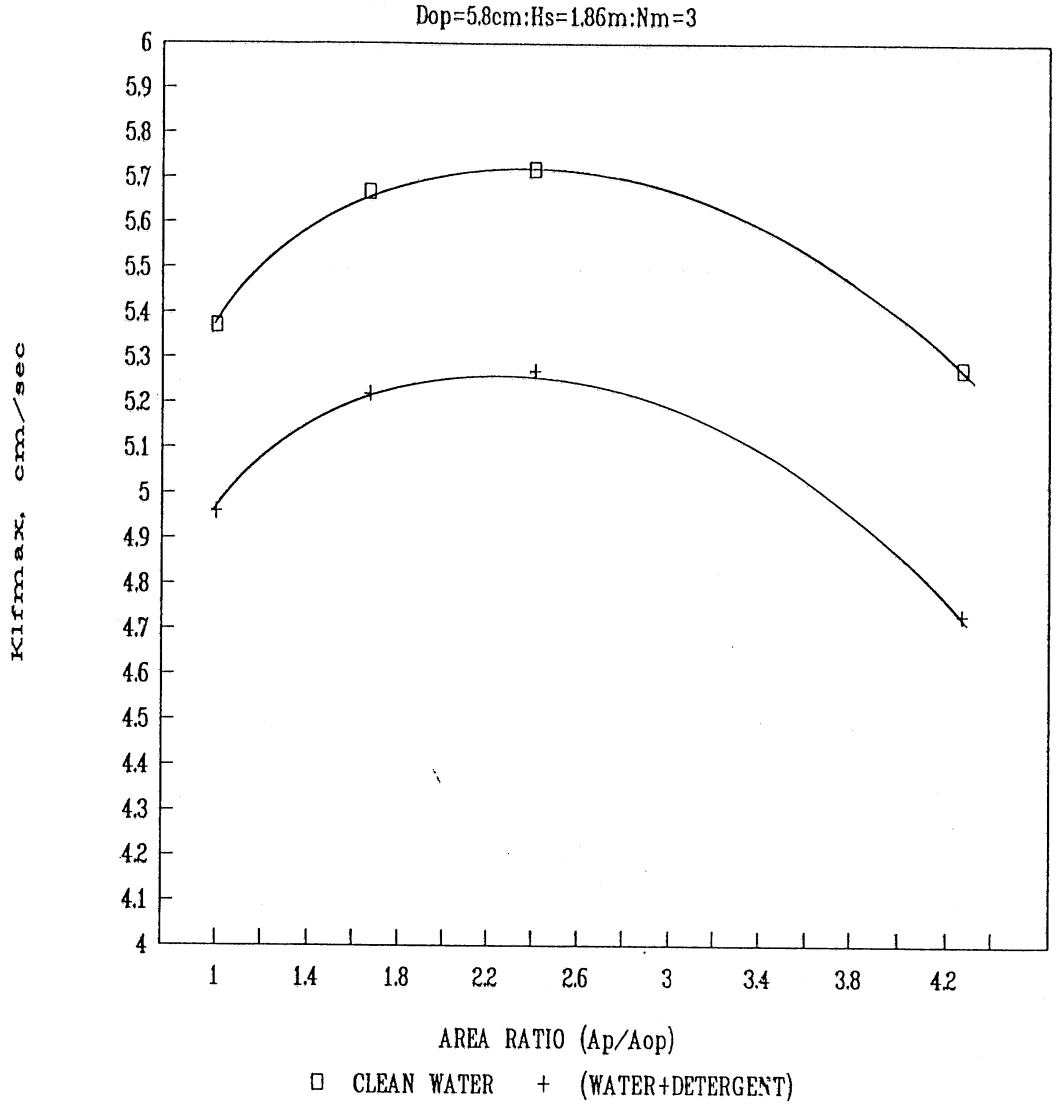

Fig. 4.34 Comparison of K_{lfmax} (diffuser air flux = 2 cc/s)

obtained in the studies with clean water though the magnitudes of the mass transfer coefficients are lower due to the effect of the surfactant.

The ratio of the mass transfer coefficient in process water (water with detergent addition in this study) to that of the mass transfer coefficient in clean water of a new diffuser is usually expressed as an alpha factor (5). The results presented in the figure 4.34 show an alpha value of about 0.92 for all the optimum tube configurations irrespective of the differences in the tube diameter. However, comparison of the variation of the K_1A values given in figures 4.7 and 4.29 show that the alpha value of the SAF diffuser varies with the tube length (see also figure 4.30). Alpha increases as the effective tube length is increased, reaches a maximum and then decreases. This dependence of alpha on the effective tube length calls for taking into account the water quality while optimizing the device configuration for a particular application. The fact that the optimum tube length is greater for the diffuser performance in water with detergent addition indicates that the optimum bubble size in this case would probably be less than the size for performance in clean water. In such a case, it might be possible to improve the diffuser performance and at the same time decrease the optimum tube length by increasing the number of the peripheral orifices or the modules further. To examine this possibility, experiments were conducted by varying the number of modules. The results of these studies are shown in figure 4.35. From the results it is seen that on increasing the number of modules from 1 to 3, the K_1A increased linearly whereas in the results of clean water tests shown in figure 4.6, with three modules, K_1A approached an asymptotic maximum. The clean water tests showed that increasing the number of modules increased the K_1A up to a maximum value and at the same time decreased the effective tube length corresponding to the maximum K_1A. In the case of clean water, the optimum effective tube length did not decrease any further after reaching an absolutely minimum value with two modules (see figure 4.2). Assuming a similar variation for the water with the detergent addition or the process water, it is prudent to expect that by increasing the number of the modules from three to a sufficiently higher value , say, four or five, the mass transfer coefficient would further increase and the optimum effective tube length would reach an absolute minimum value and would not change with water quality thereafter. This aspect needs further experimental verification. However, for tube lengths greater than the optimum, the variation of the mass transfer coefficient K_1A with increase of the tube length is quite small in clean water (correlation 4.7). Hence the tube optimized for operation in process water would perform well in clean water as well.

A detailed study of the variation of the surfactant concentration during the tests was not conducted. However, to get an idea of the variation of the detergent concentration, the surface tension of the test water was measured at the beginning, middle and end of one of the experimental runs. The surface tension increased from 59 dynes/cm at the beginning of the experiments to 64 dynes/cm at the middle of the experiment (after a time lapse of 1.5 hours from the beginning of the experiment) and further to 65.5 dynes/cm at the end of the experiment (after 3 hours from the start). This corresponded to a

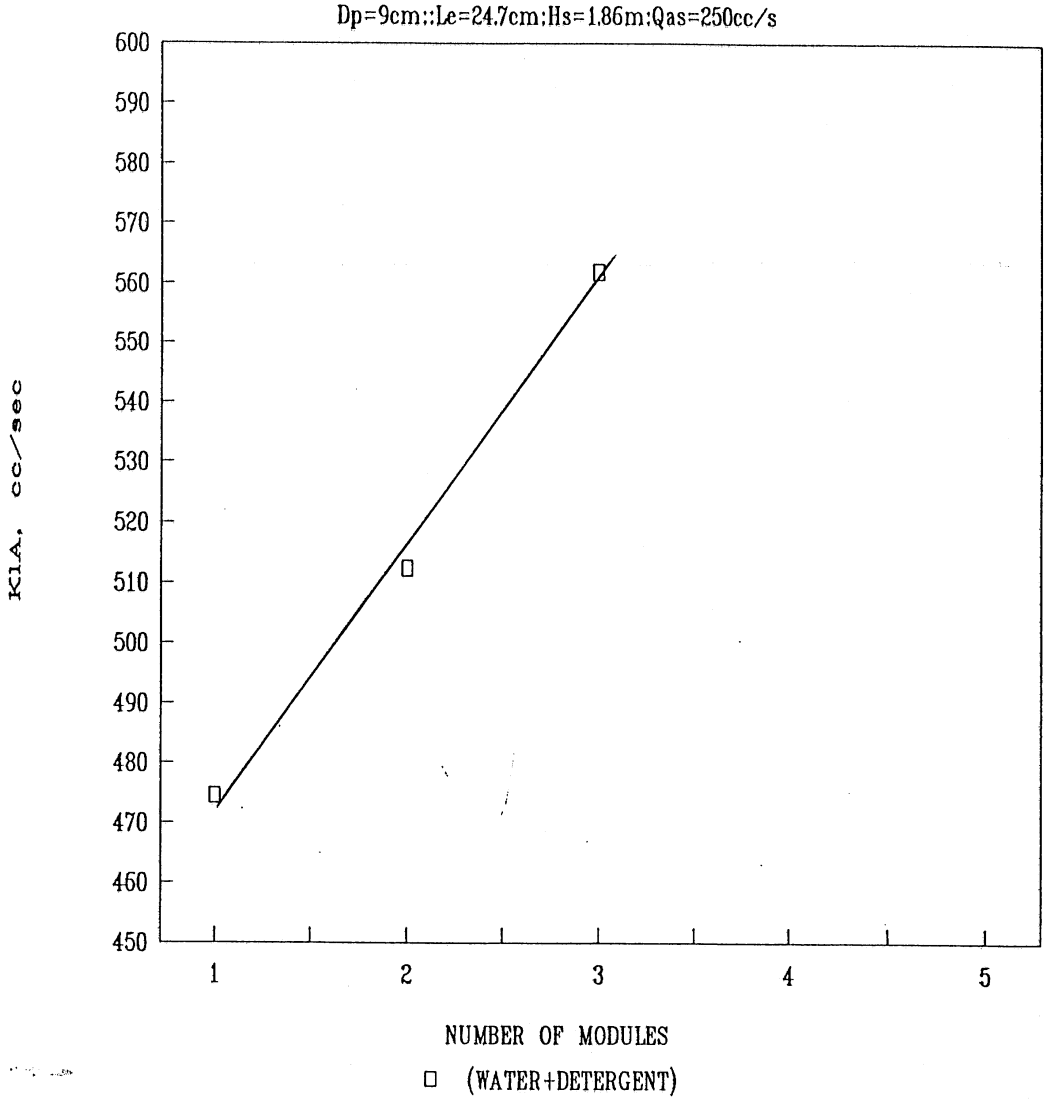

Fig. 4.35 Effect of number of modules (Water+Detergent)

time averaged surface tension of 63 dynes/cm. Assuming that the surface tension varied linearly with the detergent concentration, the mean detergent concentration worked out to about 4.75 mg/l.

4.7 MEASUREMENT ERRORS

An estimate of the errors associated with the measurement of each parameter is given below.

4.7.1 Mass Transfer Coefficient, K_1A

The mass transfer coefficient K_1A was determined from the values of the overall mass transfer coefficient K_1a using the the following relationship.

$$K_1A = K_1a \; \forall \tag{4.12}$$

where

$\forall$ = volume of water in the test tank.

The errors associated with K_1A would be those arising out of the determination of K_1a and $\forall$.

K_1a was determined by analysing the DO concentration versus time data using a non linear regression routine to fit equation (4.3) to the data. The program provides a least square estimate of the parameters K_1a, C_s and C_o. Since the values of C_s and C_o are obtained from C through regression and since K_1a depends on the values of the these concentration differences, any systematic error in the concentration would not affect the values of K_1a. The error in K_1a would be that arising out of the regression.

The standard error of the computed K_1A varied between 0.2 and 0.8 per cent. Mean of the standard error taken from twenty random sets of experiments gave a value of 0.45 per cent. Multiplying this value by the corresponding Student t value of 2.1, the error corresponding to 95 per cent confidence limit is obtained as 0.95 per cent, say 1 per cent.

The error in the measurement of the diameter of the tank (D_t) is estimated as 0.2 per cent taking into account the least count of the scale used for the measurement and the human errors that could occur during such a measurement. Similarly the error in the measurement of the water depth (H) in the tank for the minimum depth for which the experiment was done is estimated as 0.7 per cent. From these errors, the error in the volume measurement is obtained:

$$\frac{d\forall}{\forall} = \left[\left[\frac{2 \; dD_t}{D_t} \right]^2 + \left[\frac{dH}{H} \right]^2 \right]^{1/2} \tag{4.13}$$

$$= 0.8 \text{ per cent}$$

Combining the errors in K_1a and $\forall$ we get the error in K_1A (assuming that the error estimated for the volume measurement has also the 95 per cent confidence limit):

$$\frac{d(K_1A)}{K_1A} = \left[(1)^2 + (0.8)^2 \right]^{1/2}$$

$$= 1.28 \text{ per cent}$$

4.7.2 Saturation Concentration

The error in the determination of the saturation concentration would comprise the error in the concentration measurement and the error associated with the regression of the experimental data.

Based on the data given by the probe manufacturer, the measurement related uncertainty in the determination of the saturation concentration was estimated as 1.7 per cent.

From twenty random experimental results, the regression error in the saturation concentration corresponding to the 95 per cent confidence limit was calculated as 0.26 per cent.

Combining the above two errors, assuming that both the errors belong to the 95 per cent confidence level, the error in the saturation concentration is obtained as

$$\frac{dC_s}{C_s} = \left[(1.7)^2 + (0.26)^2 \right]^{1/2}$$

$$= 1.72 \text{ per cent}$$

4.7.3 Standard Oxygen Transfer Rate (SOTR)

The SOTR is given by,

$$SOTR = K_1A \; C_{ss} \tag{4.14}$$

Hence the error in SOTR can be obtained by combining the errors in the values of K_1A and C_{ss}. This gives

$$\frac{d(SOTR)}{SOTR} = \left[(1.28)^2 + (1.72)^2 \right]^{1/2}$$

$$= 2.15 \text{ per cent}$$

4.7.4 Standard Aeration Efficiency (SAE)

The SAE is the ratio of the SOTR to the power input. The power input is determined by the air flowrate and the absolute pressure upstream of the diffuser. The measurement error of the pressure upstream of the diffuser is very small compared to the actual absolute pressure and hence is neglected. The error associated with the measurement of the air flowrate is 2 per cent. Hence the error in the SAE can be obtained by combining the errors associated with the SOTR and the air flowrate.

$$\frac{d(SAE)}{SAE} = \left[(2.15)^2 + (2)^2 \right]^{1/2}$$

$$= 2.94 \text{ per cent} \quad \text{say} \quad 3 \text{ per cent}$$

4.8 CONCLUSIONS

i) The number of peripheral orifices is an important parameter affecting the mass transfer coefficient K_1A and also the optimum effective length of the tube. Increasing the number of peripheral orifices increased the K_1A until it reached an asymptotic maximum and at the same time decreased the effective tube length for optimum performance.

ii) The K_1A increased with increase of the diffuser submergence H_s and the air flowrate Q_a. K_1A varied as $H_s^{0.69}$ and $Q_a^{0.82}$. The optimum tube geometry did not vary with either the diffuser submergence or the air flowrate.

iii) The mass transfer coefficient per unit area of the diffuser (K_{1f}) was found to be maximum for tubes with area ratios in the range of 1.5 to 3. The optimum tube lengths were found to be minimum for the area ratios in the range of 1.5 to 2.4.

iv) The mass transfer coefficient associated with the operation of the device in clean water can be expressed in terms of a modified Stanton number, the submergence Froude number, the Galileo number, the submergence ratio and the tube geometric parameters (L_r and D_r) using the correlations (4.7) and (4.8) over a wide range of air flowrates, diffuser submergences and tube geometries.

v) An analysis using the above correlations showed that by introducing the tube, the mass transfer coefficient increased by about 36 per cent compared to the value obtained for zero tube length.

vi) For given air flux through the device, the Standard Aeration Efficiencies of an optimum SAF diffuser configuration were about 10 to 20 percent higher than those of the porous stone diffuser under a diffuser

submergence of 1.86 m. The increased efficiencies were due to the reduced pressures upstream of the SAF diffuser necessary to pump a given air flowrate as compared to those upstream of the porous stone diffuser. With increase of diffuser submergence, the difference in the SAE values of the SAF and the porous stone diffusers would decrease. Thus the main advantage of the SAF diffuser in terms of SAE is for low submergence applications.

vii) The inlet air pressure upstream of the SAF diffuser decreased with the increase of the air flowrate whereas in the case of the porous stone the air pressure increased with the air flowrate. This is a significant advantage of the SAF design which makes it relatively more efficient than other devices for low depth applications under large air flowrates.

viii) The optimum effective length of the tube for operation in water with detergent addition was found to be greater than the value obtained in clean water. Thus the water quality needs consideration while optimizing the device for a particular application. The experimental results indicate the possibility of achieving further reduction in the optimum tube lengths and increase in K_1A by increasing the number of the peripheral orifices for operation in process water. In clean water, for tube lengths greater than the optimum, the variation of K_1A with increase of the tube length is quite small, K_1A decreasing as $L_e^{-0.032}$. Hence the tube optimized for operation in the process water would perform well in clean water as well.

ix) The alpha factors for the optimum configurations of tubes of different diameter ratios were the same ($\simeq$ 0.92) irrespective of the differences in the tube diameters.

Chapter 5

Overall Conclusions

The main conclusions of this study are summarized below:

5.1 The conceptual design of a new aeration device named the SAF Diffuser has been developed. The application of the new device is for diffused aeration which forms a major energy consuming component in several water quality improvement processes pertaining to aquaculture, wastewater treatment and lake water quality enhancement.

5.2 The design of the SAF Diffuser is based on the *air lift* principle. The diffuser essentially comprises a vertical composite draft tube. A buoyancy induced water flow field is created inside the tube by injecting air through 0.5 mm to 1 mm diameter peripheral orifices located near the inlet end. The induced water velocity exerts a drag on the bubbles that are being formed at the peripheral orifices. This additional drag force causes the bubble to detach from the orifice much before it grows to the normal size which it would have otherwise attained in a stagnant water body. For a given air flowrate, the induced water velocity and hence the bubble size would depend upon the tube dimensions. This dependence provides a unique way of controlling the bubble size.

5.3 Through simple theoretical considerations and extensive experimentation, empirical correlations were developed to predict the induced velocities and void fractions within the tube in the bubbly flow regime (equations (3.6), (3.7) and (3.8)). The results of these studies indicate the following:

- The tube Froude number based on the induced water velocity and the tube length is a function of the mean void fraction and the energy losses in the tube. The energy losses depend on the tube geometry and the mean void fraction. Hence the tube Froude number can be expressed as a function of the mean void fraction and the parameters defining the tube geometry namely, the length ratio and the diameter ratio. This functional relationship is given by equations (3.6) and (3.7).

- The void fraction in the tube depends on the tube Froude number based on the superficial air velocity and the geometry of the tube. Equation (3.8) expresses the mean void fraction in the tube in terms of the tube Froude number based on the superficial air velocity, the length ratio and the diameter ratio.

- Using the equations (3.6), (3.7) and (3.8), the induced water velocities and the mean void fractions in the tube can be calculated for given values of air flowrate and geometric parameters of the tube.

5.4 Analysis of flow using the above correlations in a tube with an inlet diameter of 5.8 cm proposed for the mass transfer studies indicated that with an air flowrate of 500 cc/s, induced orifice water velocities of 50 to 80 cm/s could be achieved with tube lengths in the range of 8 to 35 cm. The analysis also indicated that the orifice velocities would be maximum at diameter ratios in the range of 1.3 to 1.6.

5.5 According to Barnhart (2) the optimum bubble size for mass transfer in an air water system is on the order of 2.2 mm. Analysis of bubble formation in flowing water indicated that the bubble size would depend on the orifice diameter, the air flowrate through the orifice and the water velocity (equations (2.16) and (2.18)). Thus for a given orifice size, the bubble size at formation can be controlled by controlling the air flowrate through the orifice as well as the water velocity. In the SAF Diffuser, both these parameters are controlled to achieve optimum performance. The air flowrate per orifice is controlled by changing the number of the peripheral orifices. The induced water velocity is controlled by changing the tube dimensions.

5.6 The analysis of bubble formation showed that the induced water velocity required to produce 2.2 mm diameter air bubbles over a 0.5 mm diameter orifice, for an air flowrate of 1 cc/s through the orifice, would be about 50 cm/s. The flow analysis, mentioned under 5.4 above, indicated that orifice velocities of 50 to 80 cm/s could be induced with reasonable tube lengths (8 to 35 cm). The analysis prima facie indicated that the concept might be feasible.

5.7 Having established the feasibility through the study of the induced flow in the tube, a detailed study of the mass transfer characteristics was undertaken. The effects of the number of the peripheral orifices, the tube geometry and the system submergence were the main focus of the study.

5.8 A theoretical analysis of mass transfer in the bubble column using the simple plume theory showed that the mass transfer characteristics of the device under varying air flowrates, diffuser submergences, and tube geometries could be expressed in non–dimensional form in terms of a modified Stanton number, the submergence Froude number, the Galileo number, the submergence ratio, and the length and the diameter ratios of the tube (equations (2.88) and (2.89)).

5.9 The theoretical analysis was followed by detailed experimental studies on mass transfer characteristics of the device. The main conclusions of these studies are the following.

- For a given air flowrate and diffuser submergence, the mass transfer characteristics of the device would be influenced by the number of the peripheral orifices, the length ratio and the diameter ratio of the tube.

- For a given air flux, the mass transfer coefficient per unit area of the diffuser was found to be maximum for tubes with area ratio in the range of about 1.5 to 3. The optimum tube lengths were found to be minimum for area ratios in the range of 1.5 to 2.4 (figures 4.10 and 4.11).

- The optimum tube length was found to be dependent on the number of peripheral orifices. Increasing the number of peripheral orifices increased the K_1A until it reached an asymptotic maximum and at the same time decreased the optimum tube length. The reason for this is the reduction in the air flowrate per orifice as the number of the orifices is increased. The induced velocity required to produce a given bubble size decreases as the air flowrate per orifice is decreased. Since the induced velocity decreases with the decrease of the tube length, the decrease of the required induced velocity results in the decrease of the required tube length. Thus the number of the peripheral orifices and the tube length can be combined for optimum performance for a given application.

- The K_1A values increased with increase of the diffuser submergence H_s and the air flowrate Q_a. K_1A varied as $H_s^{0.69}$ and $Q_a^{0.82}$. The exponent of H_s is close to the value of $^2/_3$ obtained from theoretical analysis using simple plume theory. The exponent of Q_a differed much from the theoretical value of $^7/_{12}$. The optimum tube geometry did not vary with either the diffuser submergence or the air flowrate.

- Analysis of the experimental data showed that as shown by the simplified theoretical study, the mass transfer coefficient associated with the operation of the device in clean water could be expressed in terms of the modified Stanton number, the submergence Froude number, the Galileo number and the tube geometric parameters (the length ratio and the diameter ratio) over a wide range of air flowrates, diffuser submergences, and tube geometries (equations (4.7) and (4.8)).

- The results showed that by the introduction of the tube, the mass transfer coefficient increased by about 36 per cent as compared to the value for zero tube length.

- For a given air flux through the device, the Standard Aeration Efficiencies of an optimum SAF diffuser configuration were 10 to 20 per cent higher than those of a porous stone diffuser under a diffuser submergence of 1.86 m. The increased efficiencies were due to the reduced pressures upstream of the SAF diffuser necessary to pump a given air flowrate as compared to the corresponding pressure upstream of the porous stone diffuser. With an increase of the diffuser submergence, the difference in the SAE values of the SAF and the porous stone diffusers would decrease. Thus the main advantage of the SAF diffuser in terms of SAE is for low submergence applications.

- The inlet air pressure upstream of the SAF diffuser decreased with an increase of the air flowrate whereas in the case of the porous stone diffuser the air pressure increased with the air flowrate. This significant advantage of the SAF diffuser makes it relatively more efficient than other devices for low depth applications under large air flowrates.

- The optimum tube length was found to depend on the water quality. The optimum tube length for operation in water with detergent addition was found to be greater than the value obtained in clean water. The optimum K_1A values obtained in the water with detergent addition were about 92 per cent of the values obtained in clean water. The studies indicated the possibility of achieving further increase in the K_1A and further reduction in the optimum tube length for operation in process water (in this case, water with detergent addition) by increasing the number of the peripheral orifices.

Additional remarks:

The diameter of the tube used in this study was 9 cm. For a practical application, many such tubes would have to be provided in an aeration tank. The number of the tubes required could be decreased by designing the tube (the inlet and the outlet) with a rectangular planform (see figure 1.7 (b)) rather than a circular planform. The rectangular planform has the advantage that by increasing the length of the planform, the rangeability of the device can be increased. Alternatively several of the circular inlet tubes can be attached to a common outlet tube which could be either circular or rectangular in planform. These configurations need further study.

The results presented in Chapter 4 show that the Aeration Efficiency would increase with the decrease of the diffuser submergence. Hence placing the diffuser at higher elevations rather than close to the basin floor may result in increased Aeration Efficiencies provided the diffuser can still maintain the liquid as well-mixed. The reductions in the mixing and the

saturation concentration values would set an upper limit up to which the diffuser can be raised to achieve increase in the Aeration Efficiency. In the SAF diffuser, the length of the inlet tube can be increased to maintain the mixing and at the same time to raise the air inlet elevation. Figures 5.1 and 5.2 show two configurations of the diffuser with several air inlets and a common extended inlet tube. Such a possibility needs further study.

In addition to the increased SAE values associated with the device for low depth applications, the SAF diffuser can also result in considerably reduced maintenance costs on account of the relatively large orifice sizes. At this juncture it a reasonable surmise. Field studies are required to assess the performance of the device under actual site conditions.

In the foregoing discussions, the performance of the device was compared only with that of a porous stone diffuser and it was concluded that the device is most suited for low depth applications from the point of view of the Aeration Efficiency values. While this is true, the Aeration Efficiency is not the only criteria for the diffuser selection for an application. Coarse bubble diffusers are used in many applications on account of their relatively clogging free operation despite their low Aeration Efficiencies. The concept of the SAF diffuser can be used for such applications to obtain a balanced performance in respect of the Aeration Efficiency as well as reduced diffuser clogging.

With further developmental work, which should include laboratory as well as field studies of the several possible configurations, the concept could develop into a viable aeration technology.

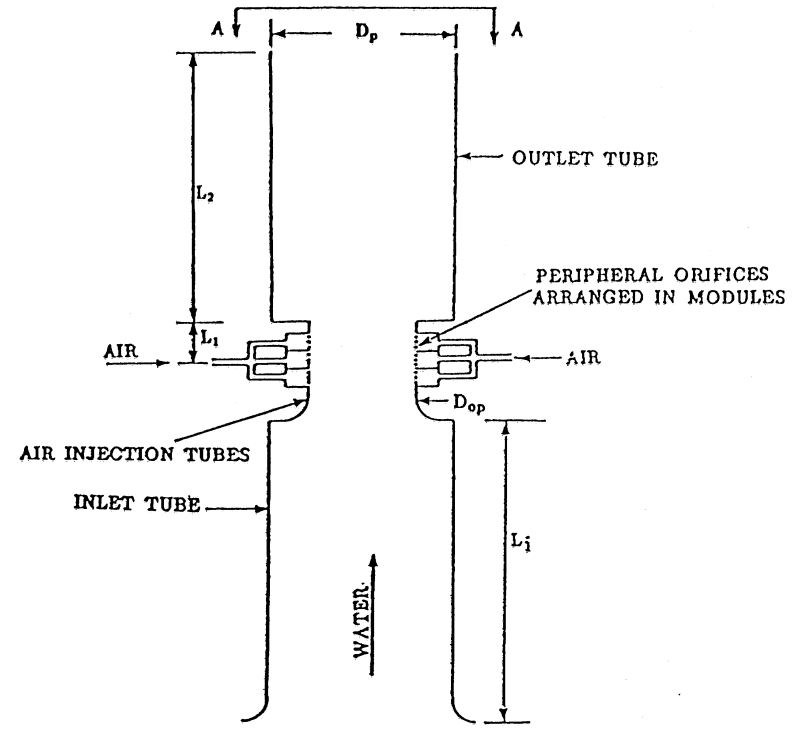

SECTIONAL ELEVATION (VIEW BB)

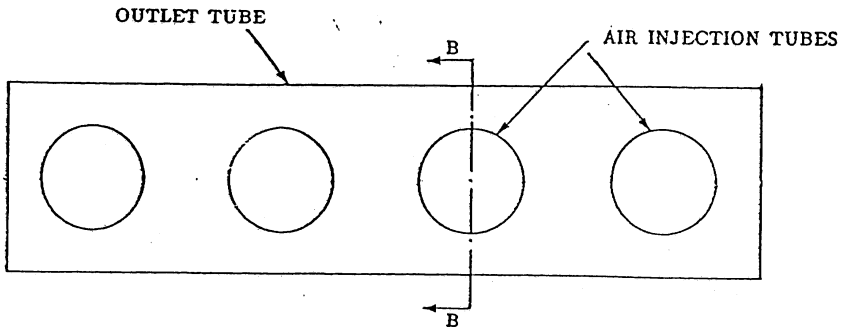

PLAN (VIEW AA)

Fig. 5.1 The SAF Diffuser with Extended Inlet Tube (Rectangular)

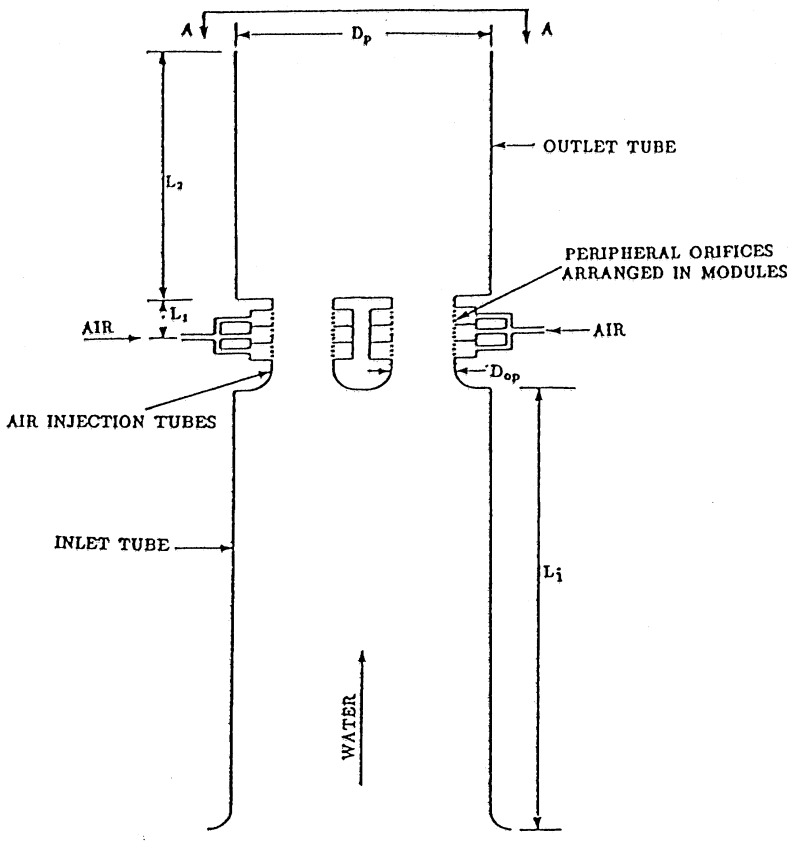

SECTIONAL ELEVATION (VIEW BB)

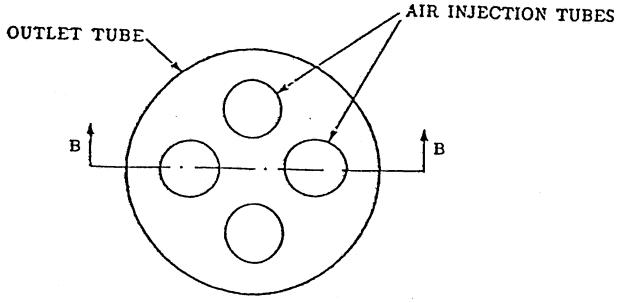

PLAN (VIEW AA)

Fig. 5.2 The SAF Diffuser with Extended Inlet Tube (Circular)

References

1. U.S. Environmental Protection Agency, "Fine pore aeration systems," EPA/625/8–85/010, October, 1985.
2. Barnhart, E. L., "Transfer of oxygen in aqueous solutions," ASCE *Jl. Sanitary Engg. Div.*, June, 1969.
3. Ashley, K. L., et al., "Effects of orifice size and surface conditions on oxygen transfer in a bench scale diffused aeration system," *Environmental Technology*, Vol.11, 1990.
4. U.S. Environmental Protection Agency, "Design manual – fine pore aeration systems," EPA/625/1–89/023, September, 1989.
5. Water Pollution Control Federation and American Society of Civil Engineers, "Aeration – a wastewater treatment process," Manual of Practice FD – 13, 1988.
6. Metcalf and Eddy, Inc., *Waste Water Engineering*, McGraw–Hill, Inc., 1991.
7. Davidson, J. F., et al ., "Bubble formation at an orifice in an inviscid liquid," *Trans. Inst. Chem. Engrs.*, Vol. 38, 1960.
8. Hooper, A. P., "A study of bubble formation at a submerged orifice using the boundary element method," *Chemical Engineering Science,* Vol. 41, No. 7, 1986.
9. McCann, D. J and Prince, R. G. H., "Bubble formation and weeping at a submerged orifice," *Chemical Engineering Science*, Vol. 24, 1969.
10. Miyahara, T., et al., "The size of bubbles generated from perforated plates," *International Chemical Engineering,* Vol. 23, July, 1983.
11. Satyanarayan, A., et al., "Bubble formation under constant pressure conditions," *Chemical Engineering Science,* Vol. 24, 1969.
12. Kumar, R., Kuloor N. R., "The formation of bubbles and drops," *Int. Chem. Eng.*, 255, 1970.
13. Gaddis, E. S., et al., "Bubble formation in quiescent liquids under constant flow conditions," *Chem. Eng. Sci.*, 1986, Vol.41, No.1.
14. Ramakrishnan, S., et al., "Bubble formation under constant flow conditions," *Chem. Eng. Sci.*, 1969, Vol.24.
15. Davidson, J. F and Harrison H., "Fluidised particles," Cambridge University Press, Cambridge 1963.
16. Silberman, E., "Gas jets in liquids," St. Anthony Falls Hydraulic Laboratory, Technical Paper No.12, Series A, 1957.
17. Van Krevelen, D. W and Hoftijzer P. J., "Studies of gas bubble formation," *Chemical Engineering Science,* Vol. 46, No. 1, 1950.
18. Sada, E., et al., "Bubble formation in Flowing Liquid," *The Canadian Jl. of Chem Eng.*, Dec., 1978.
19. Lockhart, P. W., Martinelli, R. C., "Proposed correlation of data for isothermal two phase two component flows in pipes," *Chemical Engineering Progress,* Vol.45, 1949.
20. Armand, A. A., "Pressure drop in two phase mixture in horizontal pipes," Izv. VTI I, 1950.
21. Aoki, S., Inoue, S., "Fundamental studies in pressure in an air water two phase flow in vertical pipes," 2nd Japan Heat Transfer Symposium, 1965.
22. Nakoryakov, V. E., et al., "Local characteristics of upward gas liquid flows," *International Journal of Multiphase Flow,* Vol. 7, 1981.

23. Kytomaa, H. K., Brennen, C. E., "Measurements of friction pressure drops in vertical slurry and bubbly flows," ASME Cav. and Multiphase Flow Forum, FED – Vol.36, 1986.
24. Bertodano, M. L., et al., "The prediction of two phase turbulence and phase distribution phenomenon using a Reynolds stress model", *Journal of Fluids Engineering,* March, 1990.
25. Merchuk, J. C., "Gas hold–up and liquid velocity in a two dimensional air lift reactor," *Chemical Engineering Science,* Vol41, 1986.
26. Merchuk, J. C., "Local hold–up and liquid velocity in air lift reactors," *AIChE Journal,* May, 1981.
27. Radovcich, N. A and Moissis, R., "The transition from two–phase bubble flow to slug flow," Rep #7–7673–22, MIT., 1962 (from ref. 44)
28. ASCE Standard "Measurement of Oxygen Transfer in Clean Water," July, 1984.
29. Lewis, W. K., and Whitman, W. G., "Principles of gas adsorption," *Industrial and Engineering Chemistry,* Vol. 16., 1924.
30. Mavinic D. S and Bewtra J. K., "Mass transfer of oxygen in diffused aeration systems," *Canadian Journal of Civil Engineering,* Vol. 1, 1974.
31. Higbie, R., "On the adsorption of of a pure gas into a still liquid during short period of exposure," *Trans. American Inst. of Chem. Engrs.*,Vol. 31., 1935.
32. Dankwerts, P. V., "Significance of liquid film coefficients in gas adsorption," *Industrial and Engineering Chemistry,* Vol.43., 1951.
33. Takeli, S and Maxwell, W. H. C., "Behaviour of bubble screens," Report No. UILU–ENG–79–2019, University of Illinois at Urbana–Champaign, September, 1978.
34. Milgram, J. H ., "Mean flow in round bubble plumes," *Journal of Fluid Mechanics,* Vol. 133, 1983.
35. Morton, B. R., et al., "Turbulent gravitational convection from maintained and instantaneous sources," *Proc. Roy. Soc. (London),* A 234, 1956.35.
36. Azbel, D., *Two phase flows in Chemical Engineering,* Cambridge University Press, 1981.
37. Akita, K and Yoshida, F., "Bubble size, interfacial area and liquid phase mass transfer coefficient in bubble columns," *Ind. Eng. Chem.,* Process Des. Develop., Vol. 13, No. 1, 1974.
38. Motarjemi, M., et al., "Mass transfer from very small bubbles– the optimum bubble size for aeration," *Chem. Eng. Sci.,* Vol.33., 1978.
39. Gulliver J. S., "Introduction to air–water mass transfer," Second International Symposium on Gas Transfer at Water Surfaces, Univ. of Minnesota, Minneapolis, September, 1990.
40. Cussler E. L., *Diffusion: Mass transfer in fluid systems,* Cambridge University Press, 1991.
41. Yoshida, F and Akita, K., "Performance of gas bubble columns," *A.I.Ch.E.Jl,* 11:9, 1965.
42. Murphy, D., et al., "Aeration in tower type fermentors," *Can. J. Chem. Eng.,* 157, 1959.
43. Blanco, J., et al., "Hold–up and mass transfer in a highly expanded gas liquid sparged reactor," I and E. C. Research Result Service, 1970 (from Ref. 44).
44. Hatch, T. R., "Experimental and theoretical studies of Oxygen Transfer in the airlift fermentor," Ph D Thesis., Massachusetts Institute of Technology, February, 1973.

45. Ramanathan, V and Arndt R. E. A., "An experimental study of buoyancy driven air–water flow through vertical tubes," ASME Cavitation and Multiphase Flow Forum, Los Angeles, June, 1992.
46. *American Society of Mechanical Engineers, Flowmeters Computation Handbook*, 1961.
47. YSI Inc., "YSI Model 58 Operating Instructions," Yellow Springs Instrument Company Inc., Yellow Springs, Ohio, 1989.
48. Blevins, R. D., *Applied Fluid Dynamics Handbook*, Van Nostrand Reinhold Co., 1984.

Appendix A

The Chimney Equation

Consider the straight vertical tube shown in figure A.1. Applying energy equation between points 1 and 2, neglecting the energy losses in the tube, the surface tension energy of the bubbles and also the energy transfer from the air at the air inlet section, we get

$$p_1 = p_2 + \rho_m \frac{V_m^2}{2} + g\ \rho_m\ L_e \tag{A.1}$$

or

$$\rho_m \frac{V_m^2}{2} = (p_1 - p_2) - g\ \rho_m\ L_e \tag{A.2}$$

where

p_1 = pressure at 1

p_2 = pressure at 2

V_m = velocity of the air–water mixture in the tube

ρ_m = density of the air–water mixture in the tube

L_e = tube length

g = gravitational acceleration

Assuming that the pressure outside the plume is hydrostatic and its variations in the plume are small (33), the pressure at the point 2 would be equal to the hydrostatic pressure. With this assumption, we get

$$(p_1 - p_2) = \rho_w\ g\ L_e \tag{A.3}$$

where

ρ_w = density of water

Substituting for (p_1-p_2) from equation (A.3) into equation (A.2),

$$\rho_m \frac{V_m^2}{2} = L_e\ g\ (\rho_w - \rho_m) \tag{A.4}$$

To express the mixture velocity V_m in terms of the water velocity V_w and the air velocity V_a, consider the mass flux of the mixture at any cross section of the tube.

$$\rho_m\ V_m = \rho_w\ V_w\ (1-\alpha) + \rho_a\ V_a\ \alpha \tag{A.5}$$

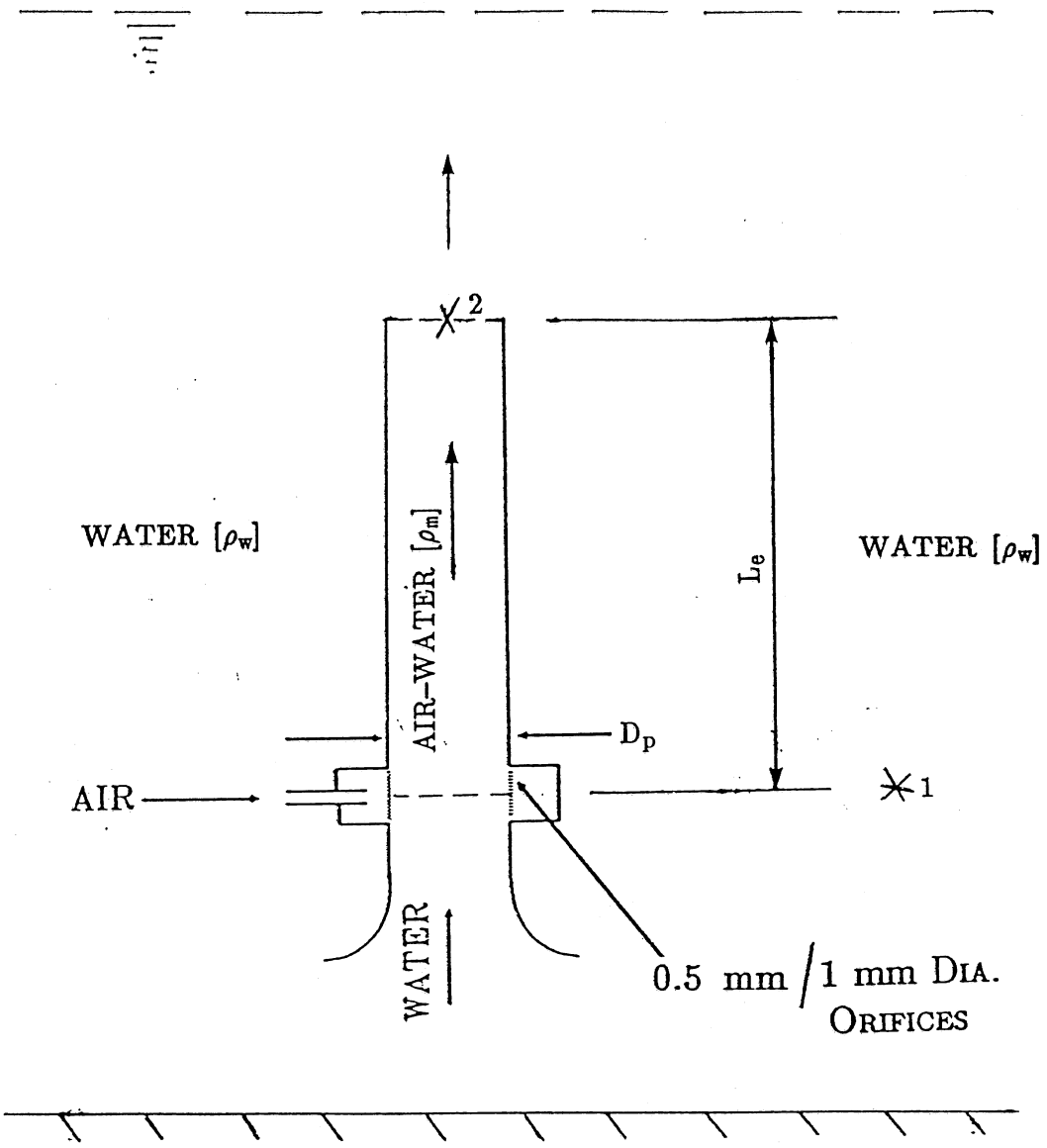

Fig. A.1 The SAF Diffuser – Straight Tube

where

α = mean void fraction in the tube

Equation (A.5) can be written as

$$V_m = \frac{\rho_w V_w (1-\alpha)}{\rho_m} + \frac{\rho_a V_a \alpha}{\rho_m} \quad (A.6)$$

The density of the mixture can be expressed in terms of the void fraction as below (33):

$$\rho_m = (1-\alpha) \rho_w + \alpha \rho_a \quad (A.7)$$

Since $\rho_a <<< \rho_w$, the above equation can be written as

$$\rho_m = (1-\alpha) \rho_w \quad (A.8)$$

Substituting for ρ_m from equation (A.8) into equation (A.6),

$$V_m = V_w + \frac{\rho_a V_a \alpha}{\rho_w} \quad (A.9)$$

Again, since $\rho_a <<< \rho_w$, the above equation can be approximated as

$$V_m = V_w \quad (A.10)$$

Substituting for V_m from equation (A.10), equation (A.4) becomes

$$(1-\alpha) \rho_w \frac{V_w^2}{2} = g L_e (\rho_w - \rho_m) = g L_e \alpha \quad (A.11)$$

or

$$F_{rw} = \frac{V_w}{\sqrt{L_e g}} = \left[\frac{2\alpha}{(1-\alpha)}\right]^{1/2} \quad \text{[Chimney Equation]} \quad (A.12)$$

where

F_{rw} = the tube Froude number based on water velocity

Now, considering the composite draft tube and taking into account the energy losses occurring in the tube, equation A.11 becomes

$$(1-\alpha) \rho_w \frac{V_w^2}{2} + p_l = g L_e \rho_w \alpha \quad (A.13)$$

where

p_l = pressure losses in the tube

Expressions for the various energy losses occurring in the tube are derived in terms of the water velocity V_w in the tube:

Entrance loss

The pressure loss at the bellmouthed entrance is given by (48)

$$p_e = k_e \rho_w (V_o^2/2) \tag{A.14}$$

where

V_o = entrance water velocity at the tube inlet

k_e = entrance loss coefficient

Applying the continuity equation, V_o can be expressed in terms of V_w as below:

$$V_o = \frac{D_p^2}{D_{op}^2} (1-\alpha) V_w \tag{A.15}$$

where

D_p = diameter of the tube

D_{op} = diameter of the tube inlet (see figure A.2)

Substituting for V_o from equation (A.15) into equation (A.14), we get

$$p_e = \frac{V_w^2}{2} (1-\alpha) \rho_w K_e \tag{A.16}$$

where

$$K_e = k_e (D_p/D_{op})^4 (1-\alpha) \tag{A.17}$$

The entrance bellmouth used in the studies had a radius equal to 0.6 times the diameter of the tube inlet. For this ratio of the bellmouth radius to pipe diameter, $k_e = 0.01$ (48).

Expansion loss

The pressure loss occurring at the sudden expansion between the tube inlet and the tube can be expressed in terms of the water velocity in the tube as below:

$$p_{ex} = \rho_m \frac{V_m^2}{2} \left[\frac{D_p^2}{D_{op}^2} - 1 \right]^2 \tag{A.18}$$

Substituting for ρ_m and V_m from equations (A.8) and (A.10), equation (A.18) becomes

$$p_{ex} = (1-\alpha) \rho_w \frac{V_w^2}{2} K_{ex} \tag{A.19}$$

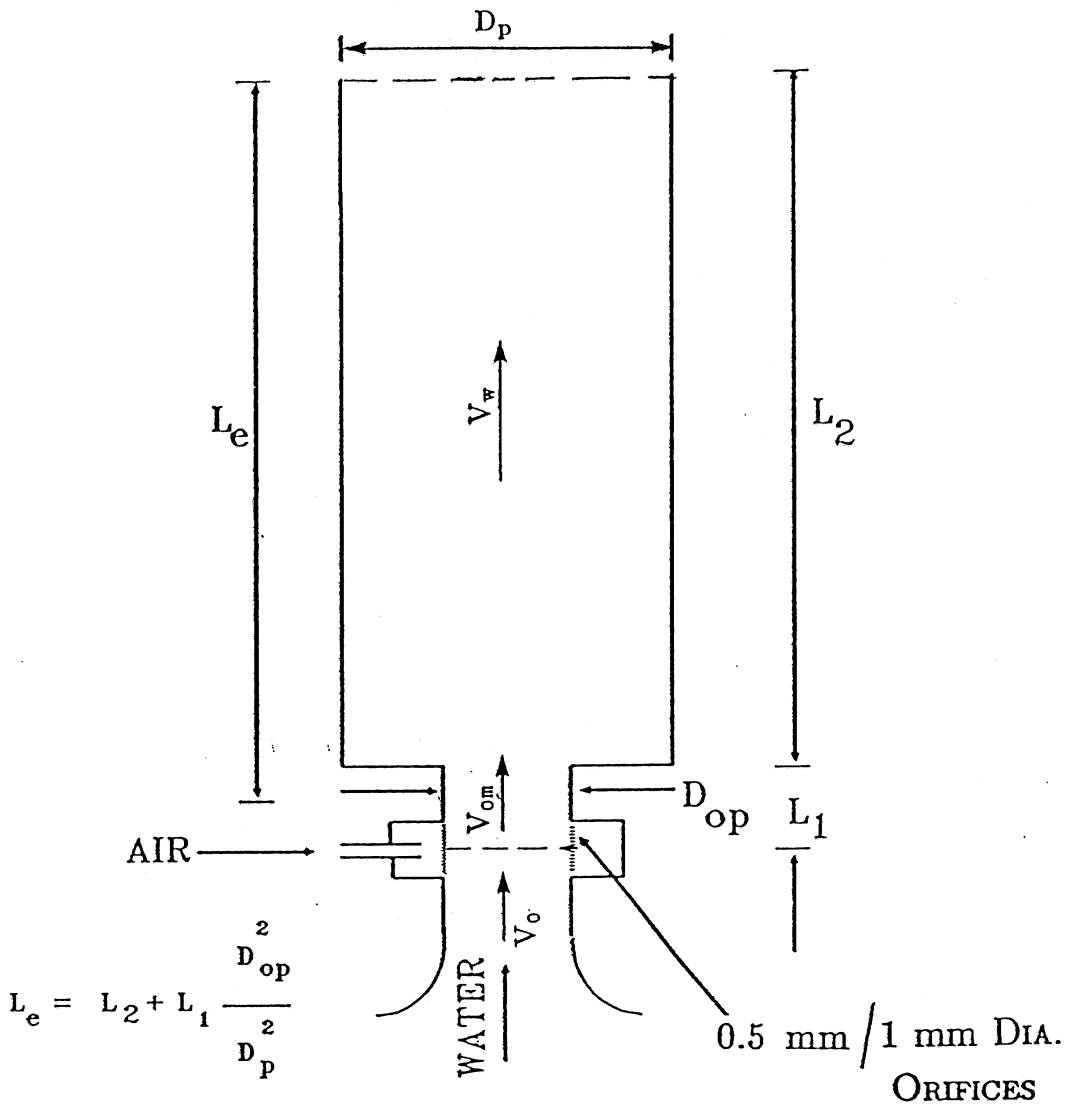

Fig. A.2 The SAF Diffuser – Composite Tube

where

$$K_{ex} = \left[\frac{D_p^2}{D_{op}}_2 - 1 \right]^2$$

$$= (D_r^2 - 1)^2 \quad \text{(A.20)}$$

$$D_r = (D_p/D_{op}) \quad \text{(A.21)}$$

$$= \text{diameter ratio}$$

Friction loss

The friction loss in the tube can be expressed in terms of the mean water velocity in the tube (23).

$$p_f = \rho_w \, f \, (L_e/D_p) \, \frac{J_w^2}{2} \quad \text{(A.22)}$$

where

f = friction coefficient for the air–water bubbly flow in the tube

L_e = effective tube length

$$= L_2 + [L_1 \, (A_{op}/A_p)] \quad \text{(A.23)}$$

J_w = superficial water velocity in the tube

$$= V_w \, (1-\alpha) \quad \text{(A.24)}$$

A_p = cross sectional area of the tube

A_{op} = cross sectional area of the tube inlet

Substituting for J_w from equation (A.24), the expression (A.22) for the friction loss becomes

$$p_f = (1-\alpha) \, \rho_w \, \frac{V_w^2}{2} \, K_f \quad \text{(A.25)}$$

where

$$K_f = f \, L_r \, (1-\alpha) \quad \text{(A.26)}$$

L_r = length ratio

$$= (L_e/D_p) \quad \text{(A.27)}$$

Loss due to the lateral entry of the bubbles at the air inlet

It is assumed that there would be a contraction loss at the air inlet section due to the lateral entry of the bubbles into the tube. This contraction loss can be expressed in terms of an appropriate contraction loss coefficient k_c as

$$p_c = k_c \, \rho_w \, (V_{om}^2/2) \quad \text{(A.28)}$$

where

V_{om} = velocity of water in the air–water flow region in the tube inlet

Assuming the void fraction to be the same in the tube inlet and the tube, applying continuity equation we get

$$V_{om} D_{op}^2 = V_w D_p^2 \tag{A.29}$$

Substituting for V_{om} from equation (A.29) into equation (A.28),

$$p_c = (1-\alpha) \rho_w \frac{V_w^2}{2} K_b$$

where

$$K_b = k_c D_r^4/(1-\alpha) \tag{A.30}$$

Other losses

In addition to the above losses, there are other secondary losses which are to be accounted for. These losses are dealt with in Chapter 2. It is assumed that all these losses can be expressed by a single loss coefficient K_s.

Substituting for the pressure loss p_l in equation (4.13) in terms of the loss terms derived above, we get

$$F_{rw} = \frac{V_w}{\sqrt{L_e g}} = \left[\frac{2\alpha}{(1-\alpha)K}\right]^{1/2} \tag{A.31}$$

where

K = overall loss coefficient

$$K = 1 + K_e + K_{ex} + K_f + K_b + K_s \tag{A.32}$$

K_e = entrance loss term

$= k_e D_r^4 (1-\alpha)$

K_{ex} = expansion loss term

$= (D_r^2 - 1)^2$

K_f = friction loss term

$= f (L_e/D_p) (1-\alpha)$

$= f L_r (1-\alpha)$

K_b = term representing the losses due to the lateral entry of air bubbles into the tube at the air inlet

$= k_c D_r^4/ (1-\alpha)$

f = friction factor for the air–water bubbly flow

k_c = appropriate contraction loss coefficient at the bubble entrance region

K_s = coefficient of the secondary losses not considered by the above loss coefficients

D_p = diameter of the tube

D_{op} = diameter of the tube inlet

L_r = length ratio of the tube

= L_e/D_p

D_r = diameter ratio = D_p/D_{op}

APPENDIX B

Experimental Results of Tube Flow Characteristics

Dop (cm)	Dp (cm)	Le (cm)	Qa (cc/s)	Qw (cc/s)	α	Vw (cm/s)
1.10	1.10	18.92	6.36	35.00	0.15	43.08
1.10	1.10	18.92	14.93	42.00	0.24	58.30
1.10	1.10	18.92	24.24	44.58	0.33	70.01
1.10	1.10	18.92	33.55	45.83	0.40	80.38
1.10	1.10	18.92	43.19	45.83	0.45	88.16
1.10	1.10	26.54	6.73	39.30	0.14	48.20
1.10	1.10	26.54	14.93	46.66	0.23	64.10
1.10	1.10	26.54	24.24	50.01	0.32	77.39
1.10	1.10	26.54	33.56	51.33	0.38	87.12
1.10	1.10	26.54	43.19	52.00	0.44	97.71
1.10	1.10	26.54	52.00	52.00	0.50	109.00
1.10	1.27	26.58	6.73	46.20	0.11	41.31
1.10	1.27	26.58	14.93	56.33	0.20	55.77
1.10	1.27	26.58	24.24	61.17	0.26	65.90
1.10	1.27	26.58	33.56	63.67	0.32	74.50
1.10	1.27	26.58	43.19	65.00	0.38	82.75
1.10	1.27	26.58	52.90	65.33	0.42	90.15
1.10	1.27	19.05	6.73	41.00	0.11	36.60
1.10	1.27	19.05	14.93	51.33	0.20	50.75
1.10	1.27	19.05	24.24	55.50	0.27	60.69
1.10	1.27	19.05	33.56	57.16	0.34	69.12
1.10	1.27	19.05	43.19	57.83	0.40	76.75
1.10	1.27	19.05	52.90	57.83	0.45	83.95
1.10	1.61	18.49	6.73	43.33	0.09	23.48
1.10	1.61	18.49	14.93	56.33	0.16	33.05
1.10	1.61	18.49	24.24	64.50	0.22	40.98
1.10	1.61	18.49	33.56	67.04	0.27	45.33
1.10	1.61	18.49	43.19	72.66	0.33	53.51
1.10	1.61	18.49	52.90	74.33	0.37	58.47
1.10	1.61	26.10	6.73	49.80	0.08	26.85
1.10	1.61	26.10	14.93	64.50	0.15	37.29
1.10	1.61	26.10	24.24	71.83	0.20	44.53
1.10	1.61	26.10	33.56	76.00	0.25	50.11
1.10	1.61	26.10	43.19	78.75	0.30	55.30
1.10	1.61	26.10	52.90	80.33	0.34	60.40
5.17	5.17	29.72	57.00	780.76	0.05	39.07
5.17	5.17	29.72	122.50	962.91	0.08	49.86
5.17	5.17	29.72	190.00	1120.28	0.11	60.23
5.17	5.17	29.72	256.67	1206.16	0.14	66.65
5.17	5.17	29.72	323.33	1273.10	0.16	72.20
5.17	5.17	29.72	391.66	1335.93	0.18	77.61

Contd....

Dop (cm)	Dp (cm)	Le (cm)	Qa (cc/s)	Qw (cc/s)	α	Vw (cm/s)
5.17	5.79	25.00	122.50	1025.76	0.08	42.30
5.17	5.79	25.00	190.00	1176.05	0.11	50.24
5.17	5.79	25.00	256.67	1302.14	0.14	57.31
5.17	5.79	25.00	323.33	1389.68	0.15	62.39
5.17	5.79	25.00	391.66	1447.46	0.18	66.64
5.17	5.79	36.20	36.42	790.54	0.04	31.11
5.17	5.79	36.20	57.00	893.94	0.04	35.37
5.17	5.79	36.20	76.17	1032.23	0.05	41.40
5.17	5.79	36.20	82.66	1037.18	0.06	41.77
5.17	5.79	36.20	105.83	1142.92	0.07	46.52
5.17	5.79	36.20	156.33	1300.18	0.08	53.85
5.17	5.79	36.20	203.33	1404.35	0.10	59.26
5.17	5.79	36.20	256.66	1504.72	0.12	65.09
5.17	5.79	36.20	330.00	1616.33	0.14	71.71

APPENDIX C

Experimental Results of Mass Transfer Studies

Qas = air flowrate corresponding to standard atmosphere
Qa = air flowrate corresponding to pressure at tube centre
Css = saturation concentration corresponding to standard atmosphere
Dop = 5.8 cm : Do = 0.5 mm: (Clean water)

Dp (cm)	Le (cm)	Hs (cm)	Qas (cc/s)	Qa (cc/s)	Nm	KlA (cc/s)	Css (mg/l)
9.00	6.92	33.53	500	499.2	3	402.6	8.74
9.00	6.92	64.01	500	485.0	3	544.8	8.88
9.00	6.92	49.99	500	491.4	3	484.6	8.81
9.00	6.92	103.33	500	467.7	3	736.9	9.04
9.00	6.92	155.45	500	446.6	3	946.1	9.16
9.00	6.92	185.93	500	435.2	3	1084.1	9.39
9.00	6.92	33.53	250	249.6	3	215.4	8.81
9.00	6.92	49.99	250	245.7	3	266.4	8.85
9.00	6.92	103.33	250	233.9	3	401.7	9.04
9.00	6.92	185.93	250	217.6	3	630.8	9.31
9.00	6.92	33.53	165	164.8	3	152.0	8.80
9.00	6.92	49.99	165	162.2	3	202.1	8.88
9.00	6.92	103.33	165	154.3	3	302.0	9.02
9.00	6.92	185.93	165	143.6	3	438.6	9.36
9.00	6.92	33.53	83	82.9	3	85.9	8.81
9.00	6.92	49.99	83	81.6	3	110.9	8.82
9.00	6.92	103.33	83	77.6	3	163.1	9.02
9.00	6.92	185.93	83	72.2	3	251.3	9.40
9.00	6.92	18.29	500	506.7	3	257.6	8.75
9.00	6.92	18.29	250	253.4	3	145.7	8.89
9.00	6.92	18.29	165	167.2	3	89.8	8.85
9.00	14.54	185.93	500	436.6	3	1049.6	9.34
9.00	12.00	185.93	500	436.1	3	1054.5	9.34
9.00	9.46	185.93	500	435.6	3	1079.2	9.32
9.00	24.70	185.93	500	438.5	3	1044.7	9.38
9.00	17.08	185.93	500	437.0	3	1059.5	9.27
9.00	9.46	185.93	500	435.6	3	1064.4	9.28
9.00	6.92	185.93	500	435.2	3	1084.1	9.20
9.00	6.92	185.93	500	435.2	3	1103.8	9.35
9.00	9.46	185.93	250	217.8	3	606.1	9.47
9.00	14.54	185.93	250	218.3	3	591.3	9.41
9.00	19.62	185.93	250	218.8	3	596.3	9.47
9.00	24.70	185.93	250	219.2	3	591.3	9.47
9.00	32.32	185.93	250	219.9	3	586.4	9.44
9.00	6.92	185.93	250	217.6	3	630.8	9.42
9.00	6.92	185.93	165	143.6	3	440.5	9.36
9.00	6.92	185.93	83	72.2	3	252.3	9.40
12.00	21.35	185.93	500	438.0	3	1153.1	9.31
12.00	24.53	185.93	500	438.6	3	1123.5	9.37
12.00	37.86	185.93	500	441.1	3	1079.2	9.39
12.00	30.24	185.93	500	439.6	3	1118.6	9.35
12.00	21.35	185.93	250	219.0	3	650.5	9.44
12.00	21.35	185.93	165	144.5	3	463.2	9.35

Contd....

Dp (cm)	Le (cm)	Hs (cm)	Qas (cc/s)	Qa (cc/s)	Nm	KlA (cc/s)	Css (mg/l)
5.80	20.96	185.93	500	437.3	3	1000.3	9.33
5.80	27.62	185.93	500	438.5	3	979.1	9.35
5.80	35.71	185.93	500	440.0	3	960.9	9.28
5.80	20.96	185.93	250	218.6	3	566.7	9.25
5.80	20.96	185.93	165	144.3	3	394.2	9.25
5.80	20.96	185.93	83	72.6	3	221.8	9.34
7.50	5.77	185.93	500	434.9	3	1054.5	9.47
7.50	15.52	185.93	500	436.7	3	1044.7	9.46
7.50	20.60	185.93	500	437.6	3	1039.8	9.44
7.50	25.68	185.93	500	438.6	3	1039.8	9.43
7.50	28.30	185.93	500	439.0	3	1000.3	9.23
7.50	23.52	185.93	500	438.2	3	1025.0	9.25
7.50	15.93	185.93	500	436.8	3	1034.8	9.27
7.50	10.85	185.93	500	435.8	3	1039.8	9.25
7.50	7.34	185.93	500	435.2	3	1034.8	9.28
7.50	5.77	185.93	250	217.4	3	606.1	9.44
7.50	5.77	185.93	165	143.5	3	421.3	9.32
9.00	24.70	103.33	500	471.5	3	697.6	8.99
9.00	14.54	103.33	500	469.3	3	700.6	8.99
9.00	19.62	103.33	500	470.4	3	703.7	8.96
9.00	6.92	103.33	500	467.7	3	721.8	9.03
9.00	6.92	103.33	500	467.7	3	736.9	9.03
9.00	6.92	49.99	500	491.4	3	484.5	8.80
9.00	14.54	49.99	500	493.2	3	459.5	8.83
9.00	19.62	49.99	500	494.4	3	454.2	8.84
9.00	24.70	49.99	500	495.6	3	456.0	8.83
9.00	32.32	49.99	500	497.4	3	446.1	8.82
9.00	6.92	49.99	500	491.4	3	486.4	8.81
9.00	9.46	49.99	500	492.0	3	477.4	8.84
9.00	24.70	185.93	500	438.5	3	1025.0	9.34
9.00	1.84	185.93	500	434.2	3	980.6	9.39
9.00	1.84	185.93	250	217.1	3	571.6	9.43
9.00	4.38	185.93	500	434.7	3	1025.0	9.44
12.00	9.92	185.93	500	435.9	3	1069.3	9.40
12.00	15.00	185.93	500	436.8	3	1128.5	9.38
12.00	7.38	185.93	500	435.4	3	1015.1	9.31
5.80	9.21	185.93	500	435.1	3	979.6	9.25
5.80	11.75	185.93	500	435.6	3	965.8	9.27
5.80	6.99	185.93	500	434.7	3	975.7	9.37
5.80	15.24	185.93	500	436.2	3	990.5	9.46
9.00	1.84	103.33	500	466.6	3	655.3	9.25
9.00	1.84	49.99	500	490.2	3	450.6	8.80
9.00	1.84	33.53	500	498.0	3	340.0	8.78
9.00	9.46	185.93	500	436.0	2	1015.1	9.43
9.00	14.54	185.93	500	436.9	2	995.4	9.36
9.00	19.62	185.93	500	437.9	2	980.6	9.36
9.00	24.70	185.93	500	438.8	2	965.8	9.35
9.00	1.84	185.93	500	434.6	2	911.6	9.36
9.00	6.92	185.93	500	435.5	2	1044.7	9.42
9.00	4.38	185.93	500	435.0	2	985.6	9.45

Contd....

Dp (cm)	Le (cm)	Hs (cm)	Qas (cc/s)	Qa (cc/s)	Nm	KlA (cc/s)	Css (mg/l)
9.00	14.54	185.93	500	436.9	1	828.4	9.39
9.00	24.70	185.93	500	438.8	1	862.4	9.33
9.00	32.32	185.93	500	440.2	1	891.9	9.36
9.00	39.94	185.93	500	441.7	1	911.6	9.34
9.00	9.46	185.93	500	436.0	1	813.1	9.37
9.00	1.84	185.93	500	434.6	1	709.6	9.36
7.50	28.29	185.93	500	439.5	1	818.0	9.27
7.50	18.47	185.93	500	437.6	1	783.5	9.28
7.50	33.70	185.93	500	440.5	1	788.4	9.25
7.50	10.85	185.93	500	436.2	1	763.8	9.24
7.50	2.26	185.93	500	434.7	1	709.6	9.24
5.80	9.21	185.93	500	435.9	1	709.6	9.22
5.80	14.92	185.93	500	437.0	1	737.2	9.26
5.80	19.05	185.93	500	437.8	1	758.9	9.23
5.80	27.31	185.93	500	439.3	1	763.8	9.24
5.80	36.83	185.93	500	441.1	1	754.0	9.24
5.80	43.82	185.93	500	442.4	1	744.1	9.26
19.00 (Dop=12)	15.00	185.93	500	436.7	3	1250.0	9.33
19.00 (Dop=12)	48.26	185.93	500	443.3	3	1230.1	9.32